Macromolecular crowding effects on multi-scale diffusion of fluorescent probes

A Thesis
SUBMITTED TO THE FACULTY OF
UNIVERSITY OF MINNESOTA
BY

Megan M. Currie

IN PARTIAL FULFILLMENT OF THE REQUIREMENTS
FOR THE DEGREE OF
MASTER OF SCIENCE

Thesis Advisor: Dr. Ahmed A. Heikal

May 2017

Acknowledgements

I would like to express my sincerest appreciation to my research advisor and mentor, Dr. Ahmed Heikal. He truly has a passion for science and life, and I will be forever indebted to him for all the guidance he has given me throughout my time at UMD. He is truly one of the most influential people I have ever had the opportunity to know and I admire his enthusiasm, character and excellent sense of humor.

I would also like to thank Dr. Erin Sheets for sharing her wealth of knowledge with me and for all the help with the biochemistry aspects of this project.

I would like to thank the members of my committee, Dr. Steve Berry, Dr. Paul Siders and Dr. Zhihua Xu for their help along the way.

I would like to acknowledge my fellow graduate students Hannah Leopold and Jacob Schwarz for their extensive work on the purification, characterization, and assessment of the FRET sensor. Hannah and Jacob have contributed a significant amount of knowledge, time and dedication to this project and I am forever grateful for all the help they have provided me.

I would also like to acknowledge the work of former students Chang Thao and Dhanushka Wickramasinghe and current student Ryan Leighton who contributed to various aspects of this project. As well as the entire Heikal/Sheets group of students for all their help along the way, especially Rochelle Warner for making my lab experience full of laughs.

I would like to thank the Department of Chemistry & Biochemistry and the staff and faculty for all the support and opportunities I was afforded while at UMD. I would especially like to acknowledge Carrie, Christine, and Dawna in the department office for answering every question I have ever had and for always giving me a reason to smile.

I would like to thank all of my fellow graduate students for all the memories, especially all the members of the intramural team and the office.

I would like to thank my grandparents for their unwavering support.

Finally, I would like to thank my friends Kate, Melissa and John for being amazing. I do not think I would be the person I am today without their support through good times and bad. I owe them a tremendous amount of recognition for always being there when I needed them, for always providing comic relief, and for making every day an adventure.

Dedication

I would like to dedicate this thesis to Melissa and John Clark, without them I would be a lost cow on this Earth.

Abstract

Living cells are crowded with a diverse population of macromolecules and organelles. It is not clear how macromolecular crowding affects the myriad of biochemical reactions, transport and structural stability of biomolecules that are essential to cellular function and survival. These molecular processes, with or without electrostatic interactions, in living cells are therefore expected to be distinct from those carried out in a test tube of dilute solutions where excluded volumes are absent. Thus there is an urgent need to understand the macromolecular crowding effects on cellular and molecular biophysics towards quantitative cell biology. The goal of this project is to investigate how biomimetic crowding affects both the rotational and translation diffusion of three size-dependent probes: RhG110 (507 Da), eGFP (32.7 kDa) and a FRET sensor (64 kDa). For biomimetic crowding agents, we used glycerol (homogeneous viscosity), Ficoll-70 (synthetic polymer), as well as bovine serum albumin and ovalbumin (proteins) at variable concentrations in a buffer at room temperature. The corresponding bulk viscosity was measured independently to test the validity of the Stokes-Einstein model of a diffusing species undergoing a random walk. For rotational diffusion (ps–ns time scale), we used time-resolved anisotropy measurements to examine interactions between our molecular probe and crowding agent a function of the crowding agents (surface structure and size). For translational diffusion (μs–s time scale), we used fluorescence correlation spectroscopy for single-molecule fluctuation analysis. Our results allow us to examine the diffusion model of a molecular probe in crowded environments as a function of concentration, length scale, homogeneous versus heterogeneous viscosity, size, and surface structures. These biomimetic crowding studies using non-invasive fluorescence spectroscopy methods represent an important step towards understanding cellular biophysics and quantitative cell biology.

Table of Contents

List of Tables

List of Figures

List of Abbreviations

APD	Avalanche photodiode
BSA	Bovine serum albumin
CFP	Cyan fluorescent protein
eGFP	Enhanced green fluorescent protein
FCS	Fluorescence correlation spectroscopy
FRET	Förster resonance energy transfer
IPTG	Isopropyl β-D-1-thiogalactopyranoside
MCP	Mircrochannel plate
PMSF	Phenylmethylsulfonyl fluoride
PBS	Phosphate-buffered saline
RhG110	Rhodamine green carboxylic acid, succinimidyl ester, hydrochloride (5(6)-CR 110, SE), mixed isomers
TCSPC	Time-correlated single-photon counting
TIRF	Total internal refraction fluorescence microscopy
YFP	Yellow fluorescent protein

List of Symbols

α_i	Amplitude fraction
β_i	Amplitude of anisotropy decay
$r(t)$	Anisotropy
G	Anisotropy geometrical factor
$G(t)$	Autocorrelation of fluorescence fluctuation
ω_z	Axial extension of the observation volume
k_B	Boltzmann's constant
τ	Correlation lag time
E	Energy transfer efficiency
k_{ET}	Energy transfer rate
$\delta F(t)$	Fluorescence fluctuation
$F(t)$	Fluorescence intensity
τ_i	Fluorescence lifetime
τ_D	Fluorescence lifetime of the donor in the FRET pair
τ_{DA}	Fluorescence lifetime of the donor in the presence of the acceptor in the FRET pair
ϕ_D^{fl}	Fluorescence quantum yield of the donor in FRET pair
k_{fl}	Fluorescence rate constant
R_0^6	Förster distance at which energy transfer efficiency is 50%
f_j	Fraction of molecular population undergoing intersystem crossing
a	Hydrodynamic radius
R_{Rot}	Hydrodynamic radius for rotational diffusion
V_{Rot}	Hydrodynamic volume for rotational diffusion
r_0	Initial anisotropy

τ_r^{-1}	Inverse of excited state fluorescence lifetime
ω_{xy}	Lateral extension of the observation volume
k_{nr}	Non-radiative rate constant
N	Number of molecules
κ^2	Orientation parameter between donor-acceptor dipole moments
$I_{\parallel}$	Parallel polarized fluorescence intensity
$I_{\perp}$	Perpendicular polarized fluorescence intensity
k_r	Radiative rate constant
n	Refractive index
r_{∞}	Residual anisotropy
D_R	Rotational diffusion coefficient
φ_i	Rotational diffusion time
$J(\lambda)$	Spectral overlap
T	Temperature
R_{DA}^6	The 6th power of the donor-acceptor distance
t	Time
D_T	Translational diffusion coefficient
τ_D	Translational diffusion time
τ_j	Triplet or blinking time associated with photophysical processes
η	Viscosity

1. Chapter 1: Introduction

Disclosure: This chapter has been published, in part, in the following:

(*1*): Currie, M., Thao, C., Timerman, R., Welty, R., Berry, B., Sheets, E.D., and Heikal, A.A. (2015) Multiscale diffusion of a molecular probe in a crowded environment: a concept. pp. 95840E-95840E-95816.
(*2*): Currie, M., Leopold, H., Schwarz, J., Boersma, A., Sheets, E.D., Heikal, A.A. (2017) "Fluorescence Dynamics of a FRET Probe Designed for Crowding Studies" *Journal of Physical Chemistry (B)*. (*In review*).

Living cells are crowded by macromolecules such as proteins, DNA, microtubules, and a number of organelles (*3, 4*). It is estimated that intracellular environments are crowded with macromolecules that occupy approximately 20-30% of the total volume of cells, which translates to approximate concentrations of 200-300 g/L (*3*). Such macromolecular crowding is believed to influence protein folding (*5, 6*), diffusion and transport (*7, 8*) and the kinetics of biochemical reactions (*5, 9-11*). In addition, emerging evidence suggests a correlation between compartmentalized cellular crowding and cell pathophysiology and diseases (*4*). Yet, macromolecular crowding effects on cellular processes remain far from being fully understood.

The effects of crowded environments on biochemical reactions and transport (e.g., diffusion) have been treated theoretically (*11-14*). Recent studies have explored the role of crowding in regulating diffusion, protein folding, and protein activities (*11, 13-15*), using synthetic polymers (e.g., Ficoll, polyethylene glycol) as crowding agents. The results from these studies were modeled in terms of an excluded volume effect due to hard-sphere repulsions. It was shown that the excluded volume may also depend on soft (or weak) chemical interactions (e.g., electrostatics, hydrogen bonding) between protein-based crowding agents (e.g., bovine serum albumin, ovalbumin) and the molecule of interest (*16-19*). Thus, crowding consists of both physical (hard spheres) and chemical (intermolecular) interactions between the crowding agents and the molecule of interest. Such complexity requires the acquisition of single-molecule information along with bulk

studies to understand the length- and time-scale dependence associated with crowding effects on protein association kinetics, conformational changes, and biological activities.

To date, the effects of macromolecular crowding have been assessed experimentally using a variety of techniques. Aqueous two-phase systems have been used to assess the effects of crowding on intermolecular interactions (*20, 21*). Current experimental techniques for investigating the effects of crowding include: NMR spectroscopy (*22, 23*), fluorescence resonance energy transfer (FRET) (*24-26*), time-resolved anisotropy measurements (*27-30*), and fluorescence correlation spectroscopy (FCS) (*31*). Each of these approaches has its own advantages and limitations with respect to sample preparation, molecular sensitivity, spatial and temporal constraints, and degree of invasiveness of the technique. Part of the challenges towards understanding macromolecular crowding is the multidimensional nature of crowding effects, which requires novel molecular sensors that are sensitive to crowding. In addition, different experimental approaches are needed to elucidate the extended nature of spatial and temporal scaling associated with crowding.

Additionally, fluorescence resonance energy transfer (FRET) can be a powerful tool to investigate how crowding may influence conformational changes in biomolecules (*32*) and intermolecular interactions (*24-26*). The energy transfer efficiency between a donor and acceptor (i.e., FRET pair) depends on (*i*) the spectral overlap between the donor's emission and the acceptor's absorption, (*ii*) the intermolecular donor-acceptor distance, and (*iii*) the relative orientation of the dipole moments of the FRET pair (*33, 34*). FRET methods have been used successfully for intermolecular interactions in both solution and living cells (*35*). The energy transfer efficiency in FRET studies can be determined using steady-state spectroscopy of a solution in a cuvette (*35*), multichannel confocal microscopy (*36*) or total-internal refraction fluorescence (TIRF) microscopy (*37*) for intracellular investigations. Fluorescence lifetime measurements have also been used to quantify FRET in both controlled environments (*35*) and in living cells (*38, 39*).

Recently, Boersma *et al.* have developed a novel, genetically-encoded sensor for macromolecular crowding (**Figure 1.1**) (*24*). This sensor consists of mutated (A206K) mCerulean (a donor) and mCitrine (an acceptor) fluorophores that are separated by a flexible linker (—$(GSG)_6A(EAAAK)_6A(GSG)_6A(EAAAK)_6A(GSG)_6$—). Importantly, this FRET probe can be genetically encoded into different cellular compartments towards site-specific crowding studies (*24*). The authors demonstrated the sensitivity of this FRET sensor to biomimetic crowding and when expressed in living cells (*24*). In those studies, steady-state spectroscopy was used to indicate the energy transfer from the donor to the acceptor. The A206K mutation minimizes self-association (i.e., aggregation) between the two fluorophores; however it is not clear how the A206K mutations of mCerulean and mCitrine may influence the corresponding excited state dynamics in this FRET probe as compared with the parent CFP and YFP. Steady-state spectroscopy approach for determining the energy transfer efficiency in a FRET pair is known to suffer from complications due to spectral overlap as well as the sensitivity to the donor *versus* donor-acceptor concentrations (*40-43*). To overcome these challenges, a complementary fluorescence lifetime approach is needed to determine the energy transfer efficiency in this novel FRET probe.

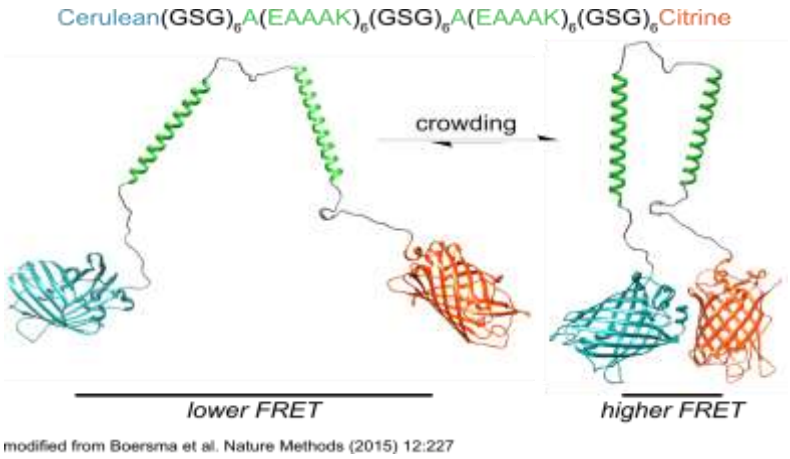

Figure 1.1: Design and concept of the FRET sensor (*mCerulean—linker—mCitrine*). As the environment becomes more crowded, the fluorophores are pushed together, which can lead to higher FRET (*24*).

To address the inherent complexity of diffusion in crowded environments, we are using laser-based fluorescence spectroscopy for both quantitative and noninvasive studies. Time-resolved fluorescence anisotropy is used to assess fast (ps–ns) conformational changes, which would be reflected as changes in the rotational diffusion (*44*). In the context of crowding, we can determine whether crowding agents impose intermolecular interactions (e.g., specific or non-specific binding) upon the molecular probe of interest, which would decrease the corresponding rotational time. For larger molecular tracers, however, crowding agents may induce a compaction of the molecule of interest and lead to faster rotational times than those measured in the absence of crowding. Using a similar approach, the corresponding fluorescence lifetime is also measured as a means to determine the effects of crowding on the excited-state dynamics. The fluorescence lifetime of a given molecular tracer represents the time window during which the rotational diffusion is measured (anisotropy) and variations in the lifetime also reflect structural changes of the probe within its local microenvironment. For translational diffusion (μs–s time scale), we use fluorescence correlation spectroscopy (FCS) to assess the effects of crowding on a molecular probe. FCS allows us to measure the translational diffusion on longer spatial length scales than those measured with time-resolved anisotropy (*45*). At sufficiently high concentrations of crowding agent, the translational diffusion of the tracer will be impeded and be reflected in a slower diffusion coefficient as compared with the absence of crowding agents.

We hypothesize that the effects of macromolecular crowding on diffusion will depend upon the chemical structure and size of both the molecular tracer and the crowding agents (polymers or proteins). Critically, the spatial and temporal resolution as well as the molecular sensitivity of the experimental techniques used will make a difference in probing different aspects of the diffusion processes in the presence of the crowding agents. **Figure 1.2** depicts different scenarios of the proposed model describing macromolecular crowding effects on the diffusion of a molecular probe. Our hypothesis is that the validity of the Stokes-Einstein model for a diffusing spherical molecule in crowded environments will be limited by (*i*) the viscosity range in a homogeneously

viscous environment, (*ii*) the concentration and type of the crowding agents, and (*iii*) the spatio-temporal resolution of the experimental technique used.

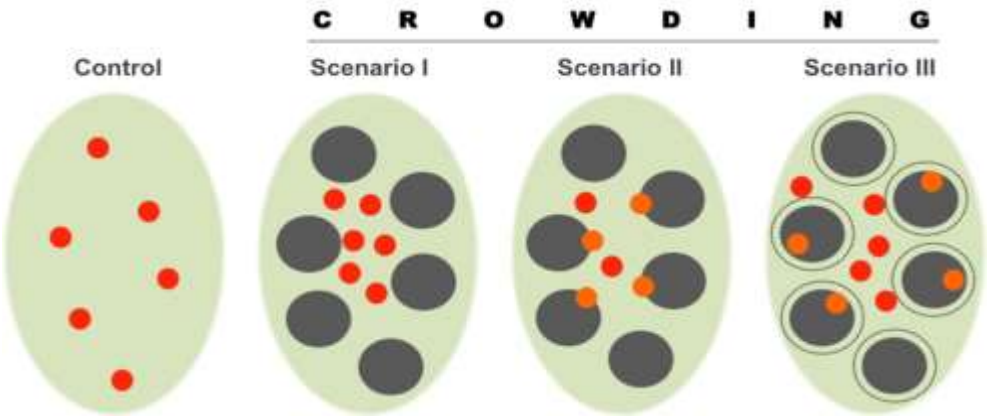

Figure 1.2: A sketch describing possible scenarios for how macromolecular crowding agents (black circles) may influence the diffusion of a molecular tracer (red dot). The dotted circles represent an excluded volume region of weak (or electrostatic) interactions that extends beyond the hard-sphere volume. Binding events (Scenarios II & III) are represented by the changed orange color of the molecular tracer.

Based on the nature of the crowding agents, particularly with respect to the surface charges and size, we hypothesize that different factors may influence the diffusion processes of a molecular tracer. For the excluded volume effect by crowding agents, for example, the diffusion processes will reflect a buffer-like environment as well as caging (or confinement) by the crowding agents. Our rationale is that although molecules may encounter buffer-like environments, they will also undergo a reduction in the apparent diffusion coefficient as compared with that in dilute solutions due to hard spheres causing the confinement (**Scenario I**). This confinement by the crowding agents will be detected by differences in the spatial and temporal resolution of the techniques used. It is worth noting that the cage formed by the crowding agent may also be mobile on a much slower time scale. In **Scenario II**, there is a potential for binding (specific or non-specific) between the molecular tracer and the crowding agent. These binding interactions may be transient or long-lived, based on the chemical structure of both the tracer and the crowding agents. For example, this scenario is likely to be observed in a crowded

environment of proteins or cell extracts where a plethora of weak interactions may be present. **Scenario III** describes the presence of electrostatic interactions due to the potential surface charges of both the molecular probe and the crowding agents. These scenarios are likely to be present in complicated crowded environments such as those found in living cells. In controlled environment studies, however, different scenarios may be in play at a given time based on the selection of the crowding agents and/or molecular tracer. Importantly, the length scaling associated with crowding can also be investigated using different experimental methods with diverse spatial, temporal, and molecular sensitivities.

In the work described here, we examined these scenarios in the context of how crowding may influence the rotational and translation diffusion of three size-dependent probes. We used rhodamine green 110 (RhG110), enhanced green fluorescent protein (eGFP) and a novel FRET sensor in homogeneous (glycerol-enriched buffer) and heterogeneous (Ficoll-70, ovalbumin and bovine serum albumin [BSA]) environments. We used laser-based fluorescence spectroscopy for both quantitative and noninvasive studies to elucidate how the diffusion mechanisms of our probes are affected by the various crowded environments. Our results allow us to examine the effects of crowding as a function of concentration, length scale, homogeneous versus heterogeneous viscosity, size and surface structure. The fluorescence spectroscopy methods we are using represent an important step towards understanding cellular biophysics and quantitative cell biology.

Accordingly, you will find the topics described above in the following chapters of this thesis: in **Chapter 2**, the materials and methods used for these studies are described in detail; including information on the fluorescence spectroscopy methods that were used, sample preparation, and equations relevant to all techniques. **Chapter 3** will focus on the effects that crowding has on the rotational diffusion of the three probes as it relates to their size. We will use fluorescence lifetime measurements along with time-resolved anisotropy to assess the effects of crowding on the rotational diffusion of our probes. Next, **Chapter 4** will investigate the effects that crowding has on the translational

diffusion and fluorescence fluctuation of our size-dependent probes. Finally, in **Chapter 5**, I will give my conclusions and provide a future outlook for this project.

2. Chapter 2: Materials and Methods

Disclosure: This chapter has been published, in part, in the following:

(*1*): Currie, M., Thao, C., Timerman, R., Welty, R., Berry, B., Sheets, E.D., and Heikal, A.A. (2015) Multiscale diffusion of a molecular probe in a crowded environment: a concept. pp. 95840E-95840E-95816.
(*2*): Currie, M., Leopold, H., Schwarz, J., Boersma, A., Sheets, E.D., Heikal, A.A. (2017) "Fluorescence Dynamics of a FRET Probe Designed for Crowding Studies" *Journal of Physical Chemistry (B)*. (*In review*).

2.1 *Rationale for sample choices*

The effects of macromolecular crowding on diffusion will depend upon the chemical structure and size of both the molecular tracer and the crowding agents (polymers, proteins or cell extracts). Critically, the spatial and temporal resolution, as well as the molecular sensitivity of the experimental techniques used, will make a difference in probing different aspects of the diffusion processes in the presence of crowding agents.

To differentiate between homogeneous and heterogeneous (crowding) viscosity, a control experiment is done in glycerol-enriched buffer under the same experimental conditions. This control allows us to distinguish among diffusion in viscous solution, confinement in a cage created by the hard-sphere crowding agents, weak interactions, and association reactions (long-lived or transient) that a molecular probe may experience in the crowded milieu of living cells.

We examined these scenarios in the context of how crowding may influence the rotational and translation diffusion of rhodamine green (RhG110), enhanced green fluorescent protein (eGFP) and a FRET probe in homogeneous (glycerol-enriched buffer) and heterogeneous (Ficoll-70, bovine serum albumin and ovalbumin) environments.

2.2 *Fluorescent probes*

Rhodamine Green carboxylic acid, succinimidyl ester, hydrochloride (5(6)-CR 110,SE) (RhG110; Invitrogen) is a small fluorescent molecule with a molecular weight of approximately 507 Da (**Figure 2.1**). The diffusion and fluorescence properties are well documented (*32, 33, 46*) and therefore RhG110 can be used as a control to calibrate both FCS and time-resolved anisotropy systems in our studies. Concentrations of 4 nM and 4 μM were prepared without further purification using phosphate-buffered saline (PBS; pH 7.4) for FCS and time-resolved anisotropy techniques respectively.

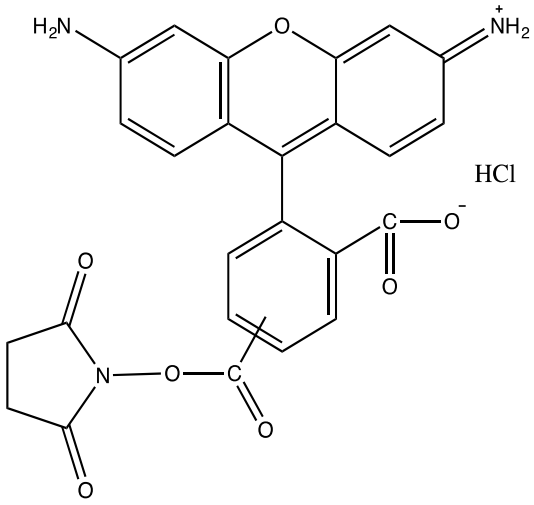

Figure 2.1: Chemical structure of rhodamine green 110 (RhG110).

Enhanced green fluorescent protein (eGFP; BioVision) is a 32.7 kDa derivative of wt GFP, which is isolated from the jellyfish *Aequorea victoria* (*47*). The mutation allows for greater folding efficiency, and therefore enhanced fluorescence properties as compared with the wild type (*47*). eGFP (**Figure 2.2**) was used as received, without further purification at concentrations of 6 nM and 6 μM for FCS and time-resolved anisotropy measurements respectively.

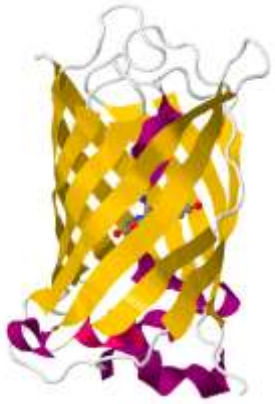

Figure 2.2: Biological assembly of enhanced green fluorescent protein (eGFP) (*48*).

The genetically-encoded FRET-based sensor is a 64 kDa protein with the fluorescent proteins mCerulean (31.3 kDa) and mCitrine (26.4 kDa) held together via a flexible linker. The design of this probe is described in detail elsewhere (*24*). Briefly, mCerulean (cyan fluorescent protein) and mCitrine (yellow fluorescent protein) serve as a donor and acceptor (i.e., FRET pair) respectively (**Figure 2.3**). The mCerulean is located at the N terminus of a flexible linker (—$(GSG)_6A(EAAAK)_6A(GSG)_6A(EAAAK)_6A(GSG)_6$—), while mCitrine is attached to the corresponding C terminus. α-helical peptides were included as part of the flexible linker as a means to induce larger changes in donor-acceptor distance as compared with a random coil. In addition, CFP and YFP in this senor were mutated (A206K) to minimize self-association.

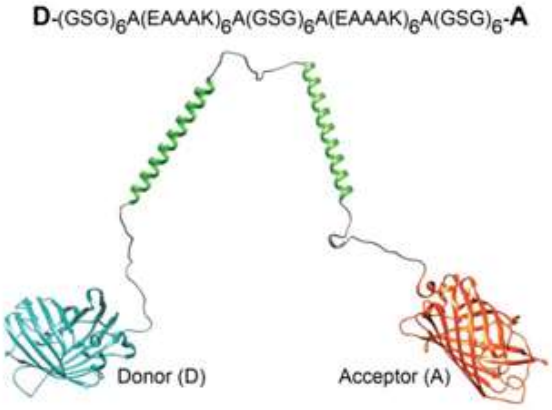

Figure 2.3: Chemical structure of the FRET probe, which consists of mutated (A206K) CFP and YFP attached with a flexible linker (*24*).

The absorption and emission spectra of the FRET probe was determined using a Beckman Coulter DU800 spectrophotometer and Horiba Jobin Yvon Fluorolog, respectively. In **Figure 2.4**, the absorption band at 280 nm (ε = 54000 $M^{-1}cm^{-1}$) was used to calculate the concentration of the isolated FRET sensor (*24*). While the donor-to-acceptor ratio is 1:1 in the FRET sensor, the absorption band of the mutated CFP (454 nm) is 59.1% smaller than that of the corresponding acceptor (514 nm) due to differences in the extinction coefficient in the PBS buffer. The main emission peaks of the donor (475 nm) and acceptor (530 nm) are in agreement with previous studies (*24*).

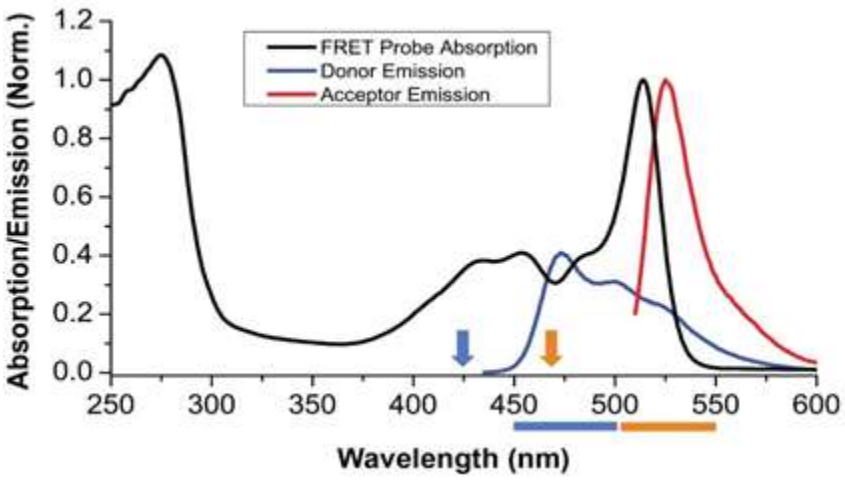

Figure 2.4: The absorption spectrum of the FRET probe (black curve) as well as the emission spectra of both the donor (excited at 425 nm) and acceptor (excited at 500 nm) is shown in buffer (PBS; pH 7.4). The arrows indicate the excitation wavelengths used in the reported fluorescence lifetime and anisotropy measurements in this thesis. The horizontal lines indicate the width of the bandwidth of the emission filters for the donor (blue curve) and acceptor (red curve) fluorescence detections. The absorption and emission bands are normalized for both the donor and acceptor.

Purification of the FRET probe

For purification, the *E. coli* strain BL21(DE)pLysS was transformed with the FRET sensor plasmid, which was in a pRSET host vector, and grown to an OD_{600} of 0.6 in terrific broth supplemented with 0.4% (v/v) glycerol and 1 mg/mL ampicillin at 30°C (*24*). The cells were then incubated overnight with 0.1 mM isopropyl β-D-1-thiogalactopyranoside (IPTG) at 25°C to induce protein expression. Following

centrifugation, the cells were re-suspended in lysis buffer (10 mM sodium phosphate, pH 7.4, 100 mM sodium chloride, 0.1 mM phenylmethylsulfonyl fluoride (PMSF), 1 mg/mL lysozyme) and then lysed with sonication. The lysate was again clarified (i.e., the supernatant was isolated) through centrifugation to which imidazole was added to a final concentration of 10 mM. The sensor was then purified using ProBond™ nickel-chelating resin (Life Technologies). The binding buffer was 10 mM sodium phosphate, pH 7.4, 100 mM sodium chloride, 10 mM imidazole; the wash buffer was 50 mM sodium phosphate, pH 8.0, 300 mM sodium chloride, 20 mM imidazole; and the elution buffer was 50 mM sodium phosphate, pH 8.0, 300 mM sodium chloride, 250 mM imidazole. The purified fractions were then dialyzed against phosphate-buffered saline (pH 7.4). Fractions were stored at 4°C and used within a two-week period of preparation.

FRET probe cleavage

As a control for energy transfer studies, the flexible linker region of the FRET sensor was cleaved using proteinase K, as described elsewhere (*24*). For this sensor cleavage, 0.56 ng of proteinase K (Sigma Aldrich) was added per μmol of the purified FRET sensor. After one minute incubation at 25°C, 20 μmol PMSF per mg proteinase K was added to terminate the cleavage reaction. The extent of cleavage was analyzed using SDS-PAGE and compared with intact protein.

2.3. ***Buffer, crowding agents, and sample preparation***

Phosphate-buffered saline (PBS; pH 7.4) was used as a buffer in the preparation of all samples used in this thesis. PBS was prepared with potassium phosphate dibasic (K_2HPO_4; VWR) and potassium phosphate monobasic (KH_2PO_4; VWR). The pH was adjusted to pH 7.4 with 1 M HCl and stored at 4 °C.

Proteins and synthetic polymers were used as crowding agents in these studies. Bovine serum albumin (BSA; Sigma Aldrich) and ovalbumin (Sigma Aldrich) are globular

proteins with molecular weights of ~66 kDa and ~45 kDa respectively. Both proteins were used as received without further purification as a means to mimic the heterogeneity in cellular environments. Protein samples were prepared up to 300 g/L as reported to match the projected macromolecular crowding in living cells (*49, 50*). For RhG110 experiments, BSA and ovalbumin samples were prepared using the following concentrations: 30, 60, 90, 120, 150, 180, 210, 240, 270 and 300 g/L. For eGFP experiments, samples were prepared using concentrations of 50, 100, 200 and 300 g/L.

Ficoll-70 (Santa Cruz Biotechnology) is a 70 kDa nonionic synthetic polymer of sucrose. Ficoll-70 was used without further purification at concentrations up to 400 g/L to mimic heterogeneous cellular environments (*49, 50*). For RhG110 and eGFP experiments, samples were prepared using the following concentrations: 20, 40, 80, 120, 160, 200, 240, 280, 320, 360 and 400 g/L. For FRET probe studies samples of 100, 200 and 300 g/L were used.

As a control for homogeneous viscosity, glycerol-enriched PBS was used under the same experimental conditions. Concentrated glycerol (≥99.5%; Fisher Scientific) samples were extended up to 900 g/L to cover a wide range of the viscosity that might be found in cellular compartments. For RhG110 and eGFP experiments, samples were prepared using the following concentrations: 270, 340, 410, 480, 550, 620, 690, 760, 830, and 900 g/L. For FRET probe studies, samples of 480, 620, 760 and 900 g/L were used.

According to the Stokes-Einstein model, the diffusion coefficient of a spherical molecule depends inversely on the viscosity of the surrounding medium. Here we independently measured the bulk viscosity of crowded solution using Ubbelohde viscometers. As shown in **Figure 2.5** our results show that the viscosity depends nonlinearly on the concentration of the crowding agents. The concentration and viscosity range shown here allow us to use fluorescence spectroscopy methods to determine if diffusion in crowded environments follows the Stokes-Einstein model. It must be noted that the Stokes-Einstein model is based on the assumption of homogeneous bulk viscosity.

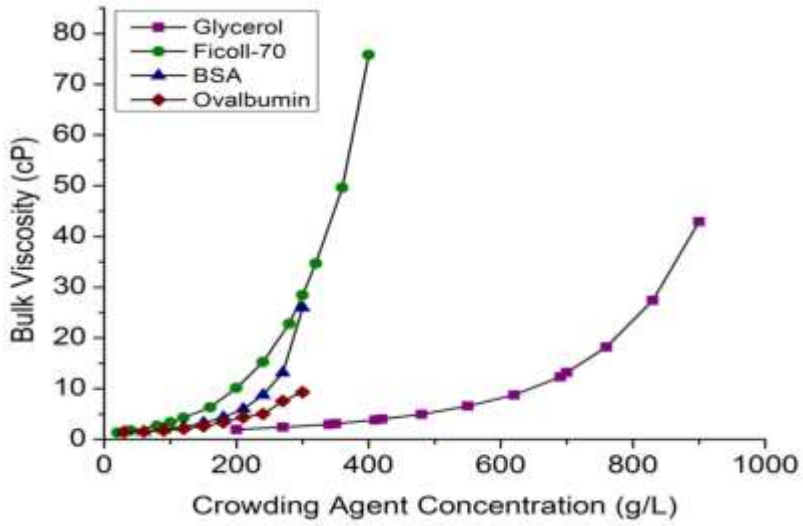

Figure 2.5: The bulk viscosity of the solution depends nonlinearly on the concentration of a crowding agent or glycerol. These viscosity measurements were carried out using an Ubbelohde viscometer.

According to the Strickler-Berg equation, the radiative rate constant of a given fluorophore depends on the squared refractive index of the surrounding medium (*51*):

$$\tau_r^{-1} = k_r = 2.88 \times 10^{-9}\, n^2 \frac{\int_{\Delta\upsilon_e} F(\tilde{\upsilon})d\tilde{\upsilon}}{\int_{\Delta\upsilon_e} F(\tilde{\upsilon})\tilde{\upsilon}^{-3}d\tilde{\upsilon}} \int_{\Delta\upsilon_a} \varepsilon(\tilde{\upsilon})d(ln\,\tilde{\upsilon}) \quad (2.1)$$

The radiative rate constant is directly related to the fluorescence rate constant, or the inverse of the excited state fluorescence lifetime:

$$k_{fl} = \tau_{fl}^{-1} = k_r + k_{nr} \quad (2.2)$$

Where the excited state fluorescence lifetime is the average time a fluorophore remains in the excited state after excitation. Fluorescence lifetime measurements are dependent on the surrounding environment and give insight into structural and environmental changes. Time-resolved fluorescence anisotropy is used to investigate the rotational diffusion on the picosecond to nanosecond timescale, but this approach is limited to the excited state

fluorescence lifetime. As a result, we measured the refractive index of the crowded solutions using an Abbe refractometer (**Figure 2.6**). Our results show that the refractive index of solution depends linearly on the concentration of glycerol, Ficoll-70, BSA, and ovalbumin, which is in line with the Strickler-Berg equation (**Equation 2.1**).

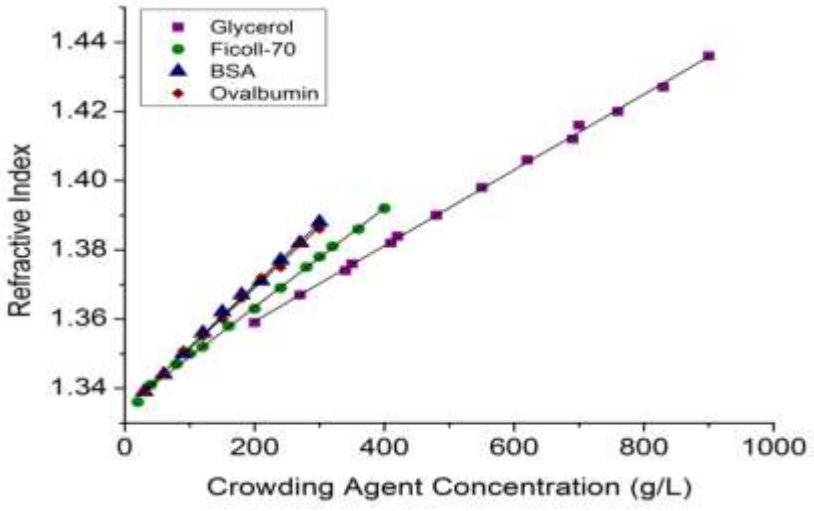

Figure 2.6: The refractive index of crowded solution depends linearly on the concentration of the crowding agents as well as glycerol. These measurements were carried out using an Abbe refractometer.

2.4 *Fluorescence correlation spectroscopy (FCS)*

For fluorescence fluctuation analysis, we used a home-built FCS system as described elsewhere (*52*); see **Figure 2.7**. Briefly, a fiber-coupled 488-nm laser (Coherent Sapphire 488-20) was steered towards an inverted microscope via the back exit port. A droplet of the fluorophore solution on a cover slip was excited using a 1.2NA microscope objective (60x) and the filtered fluorescence emission was focused on a 50-mm optical fiber that acted as a confocal pinhole. The fluorescence fluctuations were detected using an avalanche photodiode (APDs, SPCM CD-2969, Perkin-Elmer, Fremont, California) followed by amplification and autocorrelation using external multiple-tau-digital correlator (ALV/6010-160, Langen/Hessen, Germany). The FCS setup was calibrated daily using rhodamine green 110 (PBS, pH 7.4) with a diffusion coefficient of 3.0 x 10^{-6} cm^2/s (*45*, *46*, *52*). The autocorrelation, $G(\tau)$, of fluorescence fluctuation of a single

molecule diffusing through an open observation volume is given by (*45*, *53*):

$$G(\tau) = \frac{\langle \delta F(t) \otimes \delta F(t+\tau) \rangle}{\langle F \rangle^2} \tag{2.3}$$

Where $\delta F(t)$ is the fluorescence fluctuation at time t and τ is the correlation lag time. For a Gaussian (lateral) and Lorentzian (axial) observation volume, the 3D autocorrelation function depends on both the average number of molecules (N) residing in the observation volume and the diffusion time (τ_D) such that (*44, 45, 52, 54*):

$$G(\tau) = \frac{1}{N}\left(1 + {}^{\tau}/_{\tau_D}\right)^{-1}\left(1 + {}^{\tau}/_{\omega_0^2 \tau_D}\right)^{-\frac{1}{2}} \tag{2.4}$$

Where τ_D is the residence time of a molecule in the observation volume, and ω_0 is the structure parameter that describes the ratio of the axial (ω_z) to the lateral (ω_{xy}) extension of the observation volume. In the presence of a photophysical process (j^{th}) that cause an additional fluorescence fluctuation (e.g., triplet-state or blinking), the corresponding autocorrelation is given by (*55*):

$$G_J(t) = 1 - \frac{f_j}{(1-f_j)} \cdot exp\left(-\frac{t}{\tau_j}\right) \tag{2.5}$$

Where f_j is the population fraction of molecules undergoing intersystem crossing to the triplet state or fluorescence blinking with a characteristic time constant (τ_j). In this case, the overall autocorrelation function is given by:

$$G(t) = G_D(t) \times G_j(t) \tag{2.6}$$

The measured diffusion time is related to the lateral extension (ω_{xy}) of the observation and the translational diffusion coefficient (D) such that (*44, 45, 52, 54*):

$$\tau_D = \frac{\omega_{xy}^2}{4D} \tag{2.7}$$

In the Stokes-Einstein model, the translational diffusion coefficient (D_T, cm^2/sec) of a spherical molecule depends on temperature (T, Kelvin), viscosity (η, g/cm·sec), and the hydrodynamic radius (a) such that:

$$D_T = \frac{k_B T}{6\pi\eta a} \tag{2.8}$$

Where k_B is the Boltzmann constant ($k_B = 1.38 \times 10^{-16}$ g·cm^2/sec^2·K). The autocorrelation curves were analyzed using OriginPro software.

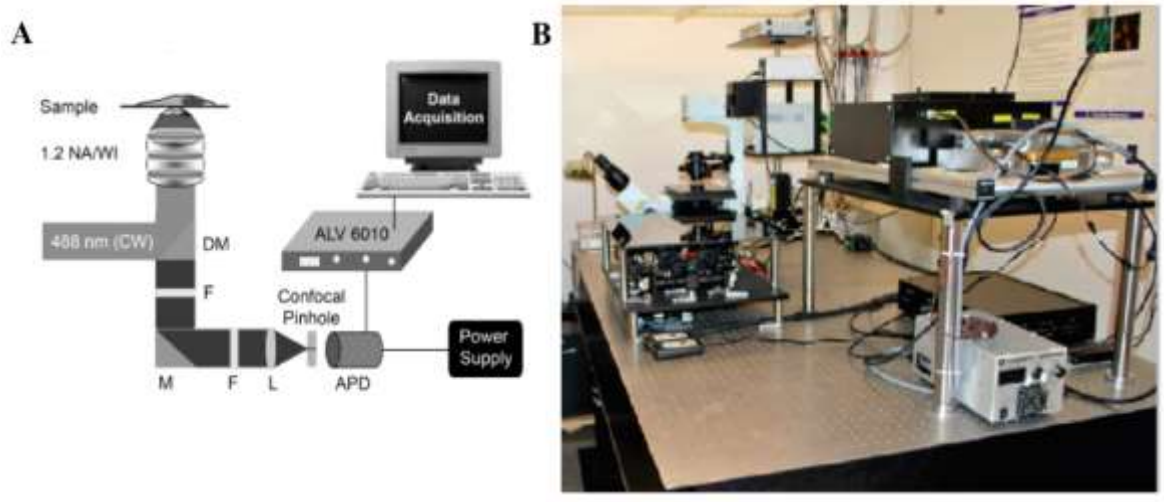

Figure 2.7: (**A**) Schematic representation of the FCS system used in these studies. DM: dichroic mirror, F: filter, M: mirror, L: lens, APD: avalanche photodiode (*54, 56, 57*). **(B**) A picture of the FCS system built around three fiber coupled laser systems, inverted microscope (widefield and TIRF) and a home built FCS.

2.5 *Time-resolved fluorescence and anisotropy*

Excited-state dynamics of our fluorescent probes was carried out using time-correlated single-photon counting technique and the experimental setup was described in details elsewhere (*52*); see **Figure 2.8**. Briefly, femtosecond infrared laser pulses (120 fs, 76 MHz, at 850 nm or 930 nm) were generated using a Titanium-Sapphire solid state laser system (Mira 900-F, Coherent). Pulse picking and second harmonic generator yielded,

one-photon laser pulses (425 and 465 nm) were generated at repetition rate of 4.2 MHz, which were used for both fluorescence lifetime and anisotropy measurements reported here. The one-photon laser pulses were conditioned and steered towards a droplet of the sample on a coverslip positioned on the microscope stage after the 1.2 NA objective. The filtered wavelength-dependent fluorescence was polarization-analyzed, detected by a microchannel plate (MCP) photomultiplier tube (R3809U, Hamamatsu), amplified and routed to a synchronized SPC-830 module (Becker & Hickl) for time-correlated single-photon counting measurements (*58, 59*). For fluorescence lifetime measurements, a Glan-Thompson polarizer was used for magic-angle detection and the acquired fluorescence decays were analyzed using the SPCImage software (Becker & Hickl), where the quality of the fit was judged using both χ^2 and the residual (*52, 58*). For anisotropy measurements, a polarizing beam splitter was used to isolate the parallel and perpendicular fluorescence polarizations (with respect to the laser polarization), which were detected simultaneously using two MCPs.

Generally, the fluorescence intensity, $F(t)$, of a given fluorophore can be described using a multiexponential decay model, depending on the chemical structure and the surrounding environment such that:

$$F(t) = \sum_{i=1}^{3} \alpha_i e^{-t/\tau_i} \tag{2.9}$$

Where α_i and τ_i are the amplitude fraction and fluorescence lifetime of the i^{th} fluorophore. The measured fluorescence decay was deconvoluted with a computer-generated system response function.

For time-resolved anisotropy, the measured parallel and perpendicular fluorescence decays were used to calculate using the anisotropy decay such that (*34*):

$$r(t) = \frac{I_{\parallel}(t) - GI_{\perp}(t)}{I_{\parallel}(t) + 2GI_{\perp}(t)} = \sum_i \beta_i e^{-t/\varphi_i} \tag{2.10}$$

The geometrical factor (G-factor) was also determined using a tail-matching approach (*32, 60*). The factor of two in the denominator of **Equation 2.10** depends on the

depolarization caused by high numerical aperture (NA) of the microscope objective (*58*). Since such depolarization does not affect the anisotropy decay time constant, we will use the traditional anisotropy decay **Equation 2.10**, especially with our under-filled 1.2 NA microscope objective. The anisotropy decays were analyzed using OriginPro software.

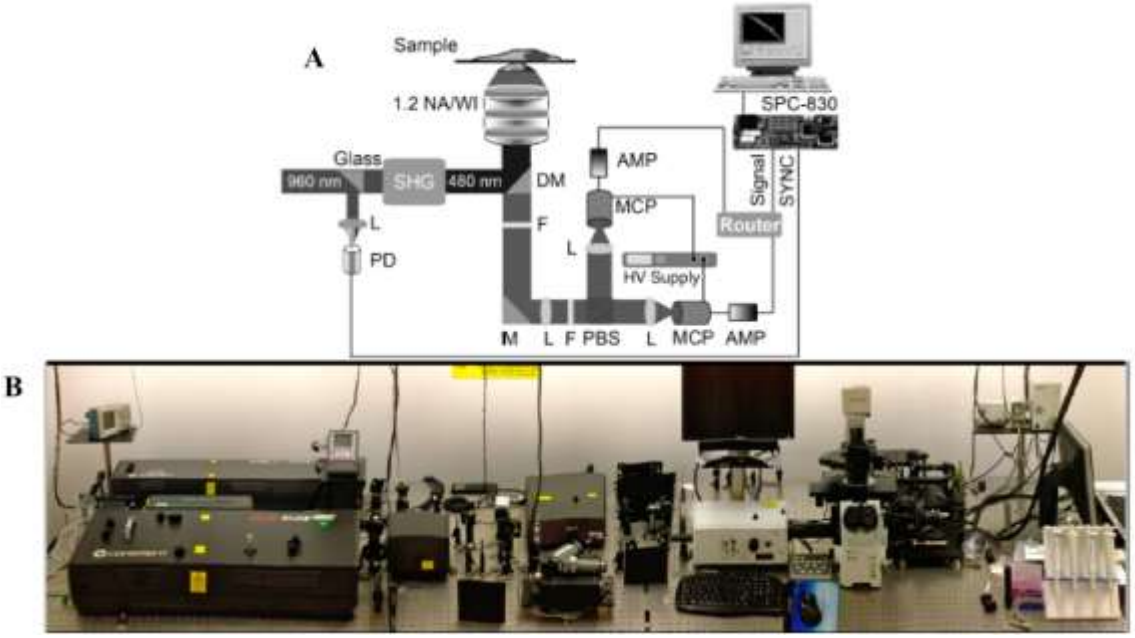

Figure 2.8: (**A**) Schematic representation of the time-resolved fluorescence anisotropy system. PD: fast photodiode, L: lens, DM: dichroic mirror, F: filter, PBS: polarizing beam splitter, MCP: microchannel plate, AMP: amplifier (*54, 56, 57*). (**B**) A picture of the time-resolved fluorescence and anisotropy system built around femtosecond laser system and a confocal microscope.

2.6 *FRET efficiency assessment using time-resolved fluorescence and anisotropy*

Fluorescence resonance energy transfer

Fluorescence resonance energy transfer (FRET) is a powerful tool (*38, 40-43*) for investigating conformational changes in biomolecules (*32*) and intermolecular interactions (*24-26*). The energy transfer efficiency between a donor and acceptor (i.e., FRET pair) depends on (*i*) the spectral overlap between the donor's emission and the acceptor's absorption, (*ii*) the intermolecular donor-acceptor distance, and (*iii*) the relative orientation of the dipole moments of the FRET pair (*33, 34*). FRET methods have been used successfully for intermolecular interactions in both solution and living cells

(*35*). The energy transfer efficiency in FRET studies can be determined using steady-state spectroscopy of a solution in a cuvette (*35*), multichannel confocal microscopy (*36*) or total-internal fluorescence (TIRF) microscopy (*37*) for intracellular investigations. Fluorescence lifetime measurements have also been used to quantify FRET in both controlled environments (*35*) and in living cells (*38, 39*).

FRET efficiency assessment

Excited-state dynamics of the FRET sensor was carried out using a time-correlated single-photon counting (TCSPC) technique and the experimental setup was described above (**see section 2.5**). This technique allows us to examine the effects of both the mutation and linker on the excited-state dynamics of the parent CFP and YFP in the FRET probe (*mCerulean—linker—mCitrine*). These measurements will also provide a means to assess the energy transfer efficiency of the FRET probe.

The measured fluorescence lifetime of the FRET probe was used to calculate the energy transfer efficiency (*E*), which is dependent on the donor-acceptor distance (R_{DA}^6) such that (*34*):

$$E = 1 - \frac{\tau_{DA}}{\tau_D} = \frac{R_0^6}{R_0^6 + R_{DA}^6} \tag{2.11}$$

Where τ_D and τ_{DA} are fluorescence lifetime of the donor alone and the donor-acceptor in the FRET pair, respectively. The Förster distance (R_0^6), is the distance at which transfer efficiency (*E*) is approximately 50%. This Förster distance depends on the spectral overlap ($J(\lambda)$), between the donor's emission and acceptor's absorption spectra the fluorescence quantum yield of the donor (ϕ_D^{fl}), the refractive index of the surrounding environment (n^4) as well as the orientation parameter between their dipole moments (κ^2). κ^2 is ~ $^2/_3$ for randomly oriented dipoles (*33, 34*):

$$R_0^6 = 8.785 \times 10^{-5} \frac{\kappa^2 \phi_D^{fl} J(\lambda)}{n^4} \tag{2.12}$$

To assess the conformational flexibility of the FRET probe, we carried out time-resolved

fluorescence anisotropy of the FRET probe as a function of excitation/detection wavelengths. Warren *et al* (*61*) have shown analytically how the energy transfer rate constant in homo-FRET of an oligomer of *N* fluorophores could be estimated using a biexponential anisotropy decay. Using the same analytical approach, assuming *N*=2 for our probe (*mCerulean—linker—mCitrine*), we can use the observed biexponential anisotropy decays of our FRET probe for an approximate estimate of the energy transfer rate (k_{ET}) using the following equation (*61*):

$$\varphi_1^{-1} = (\varphi_2^{-1} + Nk_{ET}) \tag{2.13}$$

In these calculations, we used the fast (φ_1) and slow (φ_2) rotational times in the biexponential anisotropy decays. It is worth noting that **Equation 2.13** was derived for homo-FRET which might not be applicable to our hetero-FRET structure here. However, it is a good approximation. Finally, using the fluorescence lifetime of the donor, the anisotropy-based energy transfer rate can be determined using the following equation (*34*):

$$E_{ET} = \frac{k_{ET}}{k_{ET} + (\tau_{fl}^{D})^{-1}} \tag{2.14}$$

2.7 Summary

In this thesis, **Chapter 3** will focus on the use of time-resolved fluorescence anisotropy methods to study the effects of crowding on rotational diffusion of our three size-dependent probes. In addition, fluorescence lifetime measurements will also be used as a means to assess the FRET efficiency of our FRET probe. Next, **Chapter 4** investigates the effects of crowding on the translational diffusion and fluorescence fluctuation using fluorescence correlation spectroscopy. Finally, **Chapter 5** will offer final conclusions and future outlooks for this project.

3. Chapter 3: Effects of crowding on rotational diffusion of size-dependent probes

Disclosure: This chapter has been published, in part, in the following:

(1): Currie, M., Thao, C., Timerman, R., Welty, R., Berry, B., Sheets, E.D., and Heikal, A.A. (2015) Multiscale diffusion of a molecular probe in a crowded environment: a concept. pp. 95840E-95840E-95816.
Currie, M., Leopold, H., Schwarz, J., Boersma, A., Sheets, E.D., Heikal, A.A. (2017) "Fluorescence Dynamics of a FRET Probe Designed for Crowding Studies" Journal of Physical Chemistry (B). (*In review*).

3.1 *Rationale*

To address the inherent complexity of diffusion in crowded environments, we are using laser-based fluorescence spectroscopy for both quantitative and noninvasive studies. Time-resolved fluorescence anisotropy is used in this thesis to assess fast (ps–ns) conformational changes, which would be reflected as changes in the rotational diffusion (*44*). In the context of crowding, we can determine whether crowding agents impose intermolecular interactions (e.g., specific or non-specific binding) upon the molecular probe of interest, which would decrease the corresponding rotational rate. For larger molecular tracers, however, crowding agents may induce a compaction of the molecule of interest and lead to faster rotational correlation times than those measured in the absence of crowding. In addition, for the FRET probe, we used a similar approach, by measuring the corresponding fluorescence lifetime as a means to determine the effects of crowding on the excited-state dynamics. The fluorescence lifetime of a given molecular tracer is on the same time scale as the rotational diffusion that is measured using anisotropy. Variations in the lifetime can reflect structural changes of the probe within its local microenvironment.

Our rationale for using time-resolved anisotropy measurements is to take advantage of the fast-time restriction imposed on a molecular ensemble in a crowded environment. Such temporal restrictions will limit slower processes such as translational diffusion, chemical reactions, and confined transport. As a result, time-resolved anisotropy measurements provide a snapshot of existing species such as free molecular probes in

buffer-like confined pockets among the population of crowding agents that form the excluded volume, the probe forming complexes with the crowding agent, and weak interactions between the probe and crowding agents (**Figure 1.2**). These molecular snapshots associated with rotational diffusion will serve as a guide for modeling the translational diffusion measured using FCS, which will be discussed in **Chapter 4** of this thesis.

According to the Stokes-Einstein model, the rotational diffusion coefficient (D_R) depends on both the hydrodynamic volume (V) and the viscosity (η) (*34, 62, 63*):

$$D_R = \frac{k_B T}{6\eta V} \tag{3.1}$$

Where the hydrodynamic volume (V), assuming a spherical shape, is equal to (*34*):

$$V = \frac{4}{3}\pi R^3 \tag{3.2}$$

Where (R) is the hydrodynamic radius of the molecule. The rotational diffusion time (φ) can then be related to the Stokes-Einstein equation by (*34*):

$$\varphi = \frac{\eta V}{k_B T} = \frac{1}{6D_R} \tag{3.3}$$

Accordingly, the model predicts that the ratio of the diffusion coefficient in buffer to that in a crowded environment $\left({}^{D_0}/_{D_c}\right)$ is equal to the ratio of the viscosity of the crowded environment to that of the buffer $\left({}^{\eta_c}/_{\eta_0}\right)$:

$$\frac{D_{buffer}}{D_{crowder}} = \frac{\eta_{crowder}}{\eta_{buffer}} \tag{3.4}$$

Therefore, if the rotational diffusion of a molecule deviates from the predications of the Stokes-Einstein model, we can elucidate how crowding is affecting the mechanism for rotational diffusion. Our hypothesis is that the validity of the Stokes-Einstein model for a diffusing spherical molecule in crowded environments will be limited by (*i*) the viscosity range in a homogeneously viscous environment, (*ii*) the concentration and type of the crowding agents, and (*iii*) the spatio-temporal resolution of the experimental technique used.

FRET efficiency assessment

Excited-state dynamics of the FRET sensor were carried out using time-correlated single-photon counting (TCSPC) technique and the experimental setup was described in **Chapter 2, section 2.5** of this thesis. This technique allows us to examine the effects of both the mutation and linker on the excited-state dynamics of the parent CFP and YFP in the FRET probe (*mCerulean—linker—mCitrine*). These measurements will also provide a means to assess the energy transfer efficiency of the FRET probe.

The measured fluorescence lifetime of the FRET probe was used to calculate the energy transfer efficiency (*E*), which is dependent on the donor-acceptor distance (R_{DA}^6) such that (*34*):

$$E = 1 - \frac{\tau_{DA}}{\tau_D} = \frac{R_0^6}{R_0^6 + R_{DA}^6} \tag{3.5}$$

Where τ_D and τ_{DA} are fluorescence lifetime of the donor alone and the donor-acceptor in the FRET pair, respectively. The Förster distance (R_0^6), is the distance at which transfer efficiency (*E*) is approximately 50%. This Förster distance depends on the spectral overlap ($J(\lambda)$), between the donor's emission and acceptor's absorption spectra, the fluorescence quantum yield of the donor (ϕ_D^{fl}), the refractive index of the surrounding environment (n^4) as well as the orientation parameter between their dipole moments (κ^2). κ^2 is ~ $^2/_3$ for randomly oriented dipoles (*33*, *34*):

$$R_0^6 = 8.785 \times 10^{-5} \frac{\kappa^2 \phi_D^{fl} J(\lambda)}{n^4} \tag{3.6}$$

To assess the conformational flexibility of the FRET probe, we carried out time-resolved fluorescence anisotropy of the FRET probe as a function of excitation/detection wavelengths. Warren *et al* (*61*) has shown analytically how the energy transfer rate constant in homo-FRET of an oligomer of *N* fluorophores could be estimated using biexponential anisotropy decay. Using the same analytical approach, assuming *N*=2 for our probe (*mCerulean—linker—mCitrine*), we can use the observed biexponential anisotropy decays of our FRET probe for an approximate estimate of the energy transfer

rate (k_{ET}) using the following equation(*61*):

$$\varphi_1^{-1} = (\varphi_2^{-1} + Nk_{ET}) \quad (3.7)$$

In these calculations, we used the fast (φ_1) and slow (φ_2) rotational times in the biexponential anisotropy decays. It is worth noting that **Equation 3.7** was derived for homo-FRET which might not be applicable to our hetero-FRET structure here. However, it is a good approximation. Finally, using the fluorescence lifetime of the donor, the anisotropy-based energy transfer rate can be determined using the following equation (*34*):

$$E_{ET} = \frac{k_{ET}}{k_{ET}+(\tau_{fl}^{D})^{-1}} \quad (3.8)$$

In this chapter, we investigated the effects that crowding has on the rotational diffusion of three size-dependent probes. RhG110, eGFP and a FRET sensor served as our fluorophores of varying sizes and time-resolved fluorescence anisotropy was used to monitor their rotational diffusion in various crowded environments. In addition, the FRET efficiency was assessed for the FRET sensor using TCSPC techniques. The synthetic polymer Ficoll-70 and proteins BSA and ovalbumin were used to mimic heterogeneous viscosity. These samples were prepared up to 400 g/L for Ficoll-70 and 270 g/L for BSA and ovalbumin to match the projected macromolecular crowding in living cells (*49, 50*). As a control for homogeneous viscosity, we used glycerol-enriched PBS extended up to 900 g/L to cover the wide range of viscosity that might be found in cellular compartments. As a reminder, the bulk viscosity measurements of all the crowding agents used in this chapter were measured independently with an Ubbelohde viscometer (**Appendix I**). The materials and methods used in this chapter are described in detail in **Chapter 2, sections 2.2 & 2.3 and 2.5 & 2.6** of this thesis.

3.2 *Effects of homogeneous viscosity on the rotational diffusion of size-dependent probes:* Pure buffer and glycerol-enriched buffer

Pure Buffer: RhG110 and eGFP

As a control, we conducted experiments with our three size-dependent probes in pure PBS buffer (pH 7.4) at room temperature. Typical anisotropy decays are shown in **Figure 3.1**. The rotational diffusion time of RhG110 in PBS can be satisfactorily described using a single exponential decay and was found to be (164 ± 13) ps. RhG110 was also used to determine the geometrical factor (G-Factor) based off a tail-matching approach (*34*). The anisotropy decay of eGFP also decays as a single exponential with a rotational diffusion time of (16.7 ± 3.2) ns, which is consistent with literature values that report a rotational diffusion time of ~17 ns (*64*). Using the Stokes-Einstein model (**Equation 3.1**) we calculated a hydrodynamic radius of 0.57 nm for RhG110 and 2.64 nm for eGFP. We can compare our experimental results to what is predicted by using the Stokes-Einstein model for rotational diffusion (**Equation 3.1**). We calculated the projected rotational times (φ) and hydrodynamic radii of RhG110 and eGFP in a buffer at room temperature. For RhG110 (507 Da), we calculated a rotational time of 175 ps and a hydrodynamic volume of 0.809 nm^3 (or 0.58 nm radius). These results are in agreement with our experimental results for RhG110 in PBS (**Table 3.1**). For eGFP (32.7 kDa), we calculated a rotational time of 11.3 ns and hydrodynamic volume of 52.2 nm^3 (or 2.32 nm radius). Experimentally, we observed a somewhat slower rotational time. However, the calculated hydrodynamic radius is only the minimum radius that could contain the given mass of a protein, and therefore only offers an estimation under the assumptions that the protein is a smooth, spherical shape (*34*, *65*).

Pure Buffer: FRET probe

To assess the conformational flexibility of the FRET probe, we carried out time-resolved anisotropy as a function of excitation/detection wavelengths in a buffer at room temperature. We based our excitation/detection wavelengths on the absorption, emission and spectral overlap of our donor and acceptor (**Figure 2.4**). For excitation and detection

of our donor, mCerulean, we excited at 425 nm and detected at 475/50 nm (i.e., center wavelength is 475 nm, with a bandwidth of 50 nm; 475 ± 25 nm). For excitation and detection of just the acceptor, mCitrine, we excited at 465 nm and detected at 530/40 nm. To assess the energy transfer between our donor and acceptor fluorophores, we will also excite the donor at 425 nm and detect the acceptor at 530/40 nm. Therefore, any fluorescence that we detect would have to be the result of an energy transfer from the donor to the acceptor, as we are not exciting our acceptor molecule at this wavelength.

Under 425 nm illumination, the polarization-analyzed fluorescence (475/50 nm) of the donor was detected and the corresponding anisotropy of the FRET probe decays as a single exponential with a rotational time of (18.2 ± 0.04) ns (**Figure 3.1**). As a comparison, we calculated a projected rotational time (φ) of 22.1 ns and hydrodynamic volume of 102.1 nm^3 (or 2.90 nm radius) for the FRET probe (64 kDa). Therefore the observed rotational time of the donor in the FRET probe is too fast to be assigned to the overall rotation of a 64 kDa molecule. As a result, we assign the observed rotational time to segmental mobility of the donor in the FRET probe due to the flexible linker with the acceptor. Using the Stokes-Einstein model again, we calculated the hydrodynamic radius of the rotating moiety of the donor to be 2.72 nm.

Under 425 nm illumination, the polarization-analyzed florescence (530/40 nm) of the FRET probe acceptor was detected and the corresponding anisotropy of the FRET probe decays as a biexponential with an apparent overall rotation time of (19.8 ± 0.8) ns (β_2 = 0.21) along with a faster rotational component (φ_1 = 2.0 ± 0.1 ns, β_1 = 0.066). The fast rotational time is too fast to be assigned as the tumbling motion of a 64 kDa size protein. As a result, we attribute the faster rotational time of the FRET probe under 425 nm illumination to energy transfer from the donor to the acceptor. Using the Stokes-Einstein model and the overall rotational time, we calculated a hydrodynamic radius of 2.80 nm.

Finally, under 465 nm excitation and 530/40 nm detection, the anisotropy of the FRET probe decays as a biexponential with an apparent overall rotational time of (18.3 ± 1.7) ns (β_2 = 0.24) along with a faster rotational component (φ_1 = 2.2 ± 0.8 ns, β_1 = 0.054) (**Figure 3.1**). Based on the steady state spectrum (**Figure 2.4**), both the donor and

acceptor can be excited at this wavelength, however the efficiency at which they are excited will be different. The fitting parameters for all molecules are summarized in (**Table 3.1**). Based on our time-resolved anisotropy results, we conclude that the linker in this FRET probe (*mCerulean—linker—mCitrine*) is rather long and flexible since the rotational time of either the donor or acceptor in this probe seems too fast for the overall tumbling motion of 64 kDa probe.

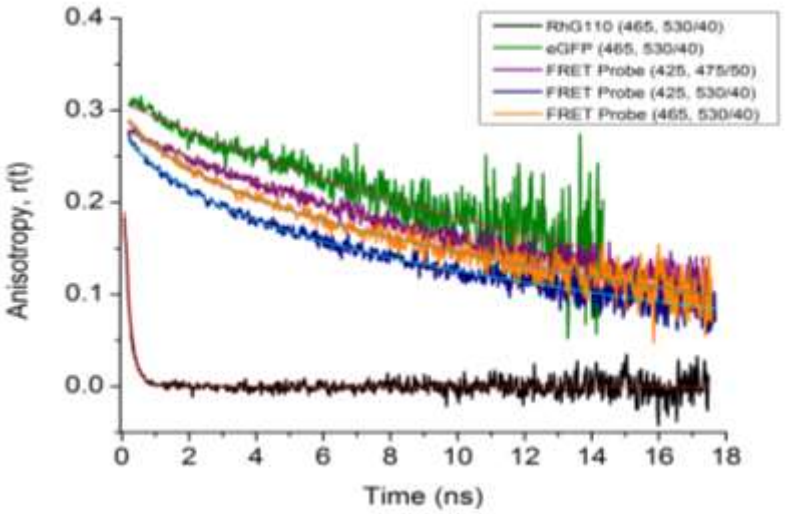

Figure 3.1: Time-resolved anisotropy of RhG110 (black), eGFP (green), the FRET probe (purple: 425/475 nm; blue: 425/530 nm; orange: 465/530 nm) in PBS buffer (pH 7.4) at room temperature.

The initial anisotropy of all the molecules used in this thesis seems to be smaller than the theoretical value (r_0 = 0.4) as shown in **Table 3.1**. Following the conventional interpretation of such deviation, we attribute this difference to the presence of ultrafast processes that compete with excited state relaxation via fluorescence pathways for all measurements in this chapter (*66*).

Table 3.1: The fitting parameters of time-resolved anisotropy of RhG110, eGFP and the FRET probe as measured using TCSPC technique with emission-polarization analysis. These measurements were carried out in a buffer (PBS, pH7.4) at room temperature as a function of excitation and detection wavelengths. The laser repetition rate was 4.2 MHz.

$\lambda_x - \lambda_{fl}$: Molecule	β_1	φ_1 (ns)	β_2	φ_2 (ns)	r_0	V_{rot} (nm^3)	R_{rot} (nm)
425 – 475/50:							
FRET Probe	--	--	0.276	18.3	0.276	84.6	2.72
425 – 530/40:							
FRET Probe	0.066	2.0	0.210	19.8	0.276	91.5	2.80
465 – 530/40:							
RhG	0.400	0.16	--	--	0.400	0.76	0.57
eGFP	--	--	0.310	16.7	0.310	77.2	2.64
FRET Probe	0.054	2.2	0.242	18.3	0.296	84.6	2.72

FRET Efficiency assessment

To assess the energy transfer efficiency of the FRET probe we carried out time-resolved fluorescence lifetime and anisotropy measurements using TCSPC technique. From these results we are able to calculate the donor-acceptor distance (R_{DA}^6), anisotropy-based energy transfer rate (k_{ET}) and estimate the energy transfer efficiency (E). For these measurements, we used a cleaved version of our FRET sensor in order to determine the fluorescence lifetime of the donor only (τ_D) (see **Chapter 2, section 2.2**). The intact FRET sensor was also measured and represents the lifetime of the donor in the presence of the acceptor (τ_{DA}). The donor (*mCerulean*) emission decays as a biexponential in the intact and cleaved FRET probe, with an average lifetime of 3.72 ns for the intact FRET probe and 3.90 ns for the cleaved FRET probe. There is a slight difference in the fluorescence lifetime of the intact probe as compared with the cleaved counterpart, which we attribute to energy transfer. The average fluorescence lifetime of the donor in the intact probe undergoes energy transfer to the tethered acceptor (*mCitrine*) at an estimated

efficiency of 5.4% in a buffer at room temperature (**Equation 3.5**). In contrast, the fast decay component of the lifetime decay for the donor in both the intact (3.27 ns) and cleaved probe (3.49 ns) yields an estimated energy transfer efficiency of 6.3%. Finally, the absorption and emission spectra of both the donor and acceptor of the FRET probe yield a Förster distance of 4.99 nm for this new FRET pair (**Equation 3.6**). Taken together, we estimate a *mCerulean—mCitrine* distance of 8.0 nm in a buffer at room temperature (**Equation 3.5**). Assuming N=2 for our probe (*mCerulean—linker—mCitrine*), we estimate an anisotropy-based energy transfer rate of 0.23 ± 0.02 ns^{-1} (**Equation 3.7**). In these calculations, we used the fast (φ_1) and slow (φ_2) rotational times of the biexponential anisotropy decays (**Table 3.1**). Assuming that the fluorescence lifetime of the donor alone is 3.9 ns, the anisotropy-based energy transfer rate yields ~47% energy transfer efficiency according to **Equation 3.8**. The difference between the estimated energy transfer efficiency using fluorescence lifetime and anisotropy approaches suggests that the homo-FRET approach developed by Warren et al (*61*) might not be directly applicable to hetero-FRET. As a means to account for the overestimated energy transfer efficiency (47%), we determined the amplitude fraction of the fast component (β_1) of the FRET probe using $\left(\frac{\beta_1}{\beta_1+\beta_2}\right)$ to be 0.24. Then, we used this as a correction factor for the energy transfer efficiency which we calculated previously. This resulted in an energy transfer efficiency of 11% which is in reasonable agreement with both our fluorescence lifetime-based approach (above) and the steady-state approximation approach by Boersma et al (*24*). It should be noted that, this correction factor technique was an approach we developed; as an anisotropy-based, hetero-FRET efficiency calculation does not exist.

Glycerol-enriched Buffer: RhG110 and eGFP

As a control for homogeneous viscosity, we did experiments with our three size-dependent probes in glycerol-enriched buffer. **Figure 3.2** shows typical anisotropy decays of RhG110 and eGFP as a function of glycerol (0-900 g/L). It is worth noting that the corresponding viscosity range associated with these glycerol concentrations spans the range of 1-43 cP. Time-resolved fluorescence anisotropy is used to investigate the

rotational diffusion on the picosecond to nanosecond timescale, but this approach is limited to the excited state fluorescence lifetime. As a result, we measured the refractive index of the crowded solutions using an Abbe refractometer (**Figure 2.6**). Our results show that the refractive index of solution depends linearly on the concentration of our crowding agents, which is in agreement with the Strickler-Berg model (*67*) and allows us to use these fluorescence methods for our experiments.

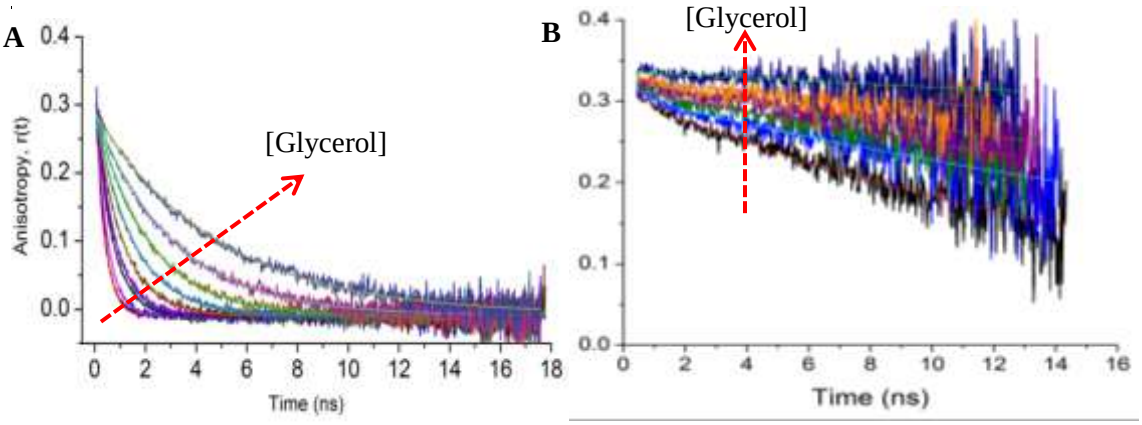

Figure 3.2: Time-resolved anisotropy of (**a**) RhG110 and (**b**) eGFP as a function of increasing glycerol concentration (0-900 g/L). Both RhG110 and eGFP decay as a single exponential over the range of glycerol concentrations.

RhG110 and eGFP were both fit to a single exponential decay over the span of glycerol concentrations. The results show an apparent increase in the rotational diffusion time of RhG110 and eGFP over the ps-ns timescale (**Table 3.2**). The results for RhG110 and eGFP confirm the existence of a single species in glycerol-enriched buffers, which is expected due to the homogeneity of the environment. The single exponential decay for eGFP is in agreement with other studies which conclude the protein as a whole undergoes rotational diffusion (*68*). This is consistent with the shape of the protein, and attests to the fact that the fluorophore is rigidly held within the β-barrel (*69*). From these results, we are able to use the rotational diffusion coefficient and the corresponding viscosity to test the validity of the Stokes-Einstein model (**Equation 3.2; Figure 3.3**).

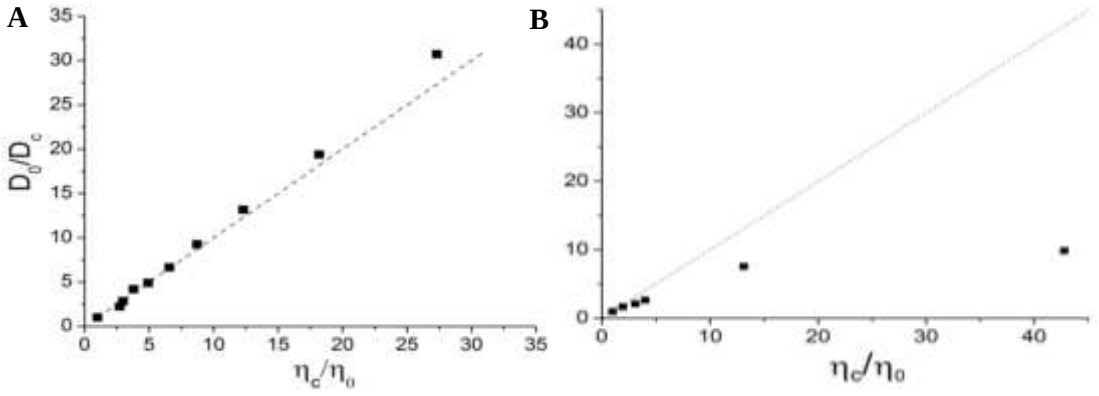

Figure 3.3: Diffusion coefficient analysis of (**a**) RhG110 and (**b**) eGFP in varying concentrations of glycerol. The dashed line represents what the Stokes-Einstein model predicts. Deviations from the model allow us to elucidate how the crowding agent affects the translational diffusion of our molecules.

Our results for RhG110 (**Figure 3.3a**) indicate that the molecule follows the predictions of the Stokes-Einstein model fairly closely, with some positive deviation seen at high concentrations. It is not surprising that the measured rotational diffusion coefficient deviates slightly from the predicted value using the Stokes-Einstein model. It is conceivable that a molecule undergoing fast rotational diffusion in a very viscous environment may not experience the same bulk viscosity perhaps due to additional factors such as sticking. Such deviations are likely be beyond the uncertainty of time-resolved fluorescence anisotropy because the rotational time at 830 g/L remains close enough to the excited state lifetime of RhG110 (~3.9 ns). This ratio of rotational time to the fluorescence lifetime seems reasonable for reliable usage of time-resolved anisotropy decays in crowding studies. Using the rotational diffusion time, we can use the Stokes-Einstein equation (**Equation 3.1**) to calculate the hydrodynamic volume and radius of RhG110 using **Equation 3.2**. We see that as we increase the concentration of glycerol, our hydrodynamic volumes and radii remain relatively the same (**Table 3.2**).

Our results for eGFP (**Figure 3.3b**) indicate that the molecule is moving faster than what is predicted by the Stokes-Einstein model at concentrations greater than 350 g/L. Using the rotational diffusion time, we can use the Stokes-Einstein equation (**Equation 3.1**) to calculate the hydrodynamic volume and radius of eGFP using **Equation 3.2**. We see that

as we increase the concentration of glycerol, our hydrodynamic volumes and corresponding hydrodynamic radii decrease for eGFP (**Table 3.2**). These results challenge the validity of the Stokes-Einstein model for molecules in highly viscous environments. Previous studies using NMR spectroscopy have shown a similar trend and have reported deviation from the model after 3.8 cP (~410 g/L) in glycerol-rich solutions (*70, 71*). Our results here seem to complement these findings.

Table 3.2: The fitting parameters of time-resolved anisotropy of RhG110 and eGFP as measured using TCSPC technique with emission-polarized analysis. These measurements were carried out in glycerol-enriched buffers (0-900 g/L) at room temperature.

$\lambda_x - \lambda_{fl}$: Molecule	r_0	φ_1 (ns)	V_{rot} (nm^3)	R_{rot} (nm)
465 – 530/40: **RhG110**				
270 g/L	0.35	0.36	0.61	0.53
340 g/L	0.34	0.45	0.62	0.53
410 g/L	0.32	0.67	0.72	0.56
690 g/L	0.31	2.12	0.71	0.55
830 g/L	0.30	4.94	0.74	0.56
465 – 530/40: eGFP				
200 g/L	0.31	32.4	68.0	2.53
350 g/L	0.32	40.7	53.7	2.34
420 g/L	0.32	50.5	51.5	2.31
700 g/L	0.32	112.5	35.1	2.03
900 g/L	0.33	189.7	18.2	1.63

Glycerol-enriched Buffer: FRET Probe

To assess the effects of viscosity on the conformational flexibility and energy transfer efficiency of the FRET probe we carried out time-resolved anisotropy as a function of excitation/detection wavelengths in glycerol-enriched buffer at room temperature. **Figure**

3.4 shows typical anisotropy decays of the FRET probe in varying concentrations of glycerol (0-900 g/L). Under 425 nm illumination, the polarization-analyzed fluorescence (475/50 nm) of the donor was detected and the corresponding anisotropy of the FRET probe decays as a single exponential over the range of glycerol concentrations (**Figure 3.4a**). Compared to our results in pure buffer, we see rotational diffusion times that are much longer, suggesting that the highly viscous environment limits the segmental mobility of the FRET probe. Using the Stokes-Einstein model, we calculated the hydrodynamic radii of the rotating moiety of the donor as a function of glycerol concentration and the results are summarized in **Table 3.3**. The results show that as our environment becomes more viscous, our molecule becomes more compact, further supporting our belief that the viscous environment is reducing mobility of the FRET probe.

Under 425 nm illumination, the polarization-analyzed fluorescence (530/40 nm) of the FRET probe decays as a biexponential with a fast rotational component (φ_1, β_1) and an apparent overall rotational component (φ_2, β_2) (**Figure 3.4b**). The fast component is too fast to be assigned to the tumbling motion of a 64 kDa protein, and therefore we attribute this component to energy transfer from the donor to the acceptor. Interestingly, the anisotropy decays provide visual differences between the excitation/detection of the donor and excitation of the donor and detection of the acceptor. As seen in **Figure 3.4b** there is now a pronounced fast decay component when detecting the acceptor that is not present in the detection of the donor, providing confirmation that under these conditions, energy transfer is occurring.

Finally, under 465 nm excitation and 530/40 nm detection, the anisotropy of the FRET probe decays as a biexponential with a fast rotational component (φ_1, β_1) and an apparent overall rotational component (φ_2, β_2) (**Figure 3.4c**). Again, this is not surprising as both the donor and acceptor can be excited at this wavelength due to spectral overlap of their emission. These results complement our results from above by allowing us to compare what the acceptor behaves like under direct excitation compared to indirect excitation via energy transfer from the donor. The results provide confirmation that the fluorescence

decay we see under 425 nm excitation is the acceptor as the anisotropy decays have similar features and rotational times under 465 nm excitation (**Table 3.3**). It should be noted that the overall rotational time in 900 g/L of glycerol had was on the order of 1.3 x 10^{119} ns, indicating that there is essentially no rotation of the molecule and therefore we assign this as residual anisotropy (r_∞).

Table 3.3: The fitting parameters of time-resolved anisotropy of the FRET probe measured as a function of excitation/detection wavelength using TCSPC technique with emission-polarized analysis. These measurements were carried out in glycerol-enriched buffers (0-900 g/L) at room temperature.

$\lambda_x - \lambda_{fl}$: Molecule	β_1	φ_1 (ns)	β_2	φ_2 (ns)	r_0	V_{rot} (nm^3)	R_{rot} (nm)
425 – 475/50: **FRET Probe**							
480 g/L	--	--	0.284	67.4	0.284	56.0	2.37
620 g/L	--	--	0.284	115.1	0.284	54.1	2.35
760 g/L	--	--	0.286	181.7	0.286	41.1	2.14
900 g/L	--	--	0.293	303.9	0.293	29.1	1.91
425 – 530/40: FRET Probe							
480 g/L	0.053	1.88	0.236	57.5	0.289	47.8	2.25
620 g/L	0.046	1.73	0.249	78.2	0.295	36.8	2.06
760 g/L	0.043	1.76	0.250	100.7	0.293	22.8	1.76
900 g/L	0.045	2.24	0.255	150.6	0.300	14.4	1.51
465 – 530/40: **FRET Probe**							
480 g/L	0.034	1.87	0.275	58.6	0.309	48.7	2.27
620 g/L	0.033	2.10	0.279	89.5	0.312	42.1	2.16
760 g/L	0.036	2.59	0.278	152.4	0.314	34.4	2.02
900 g/L	0.052	3.93	0.264	--	0.316	--	--

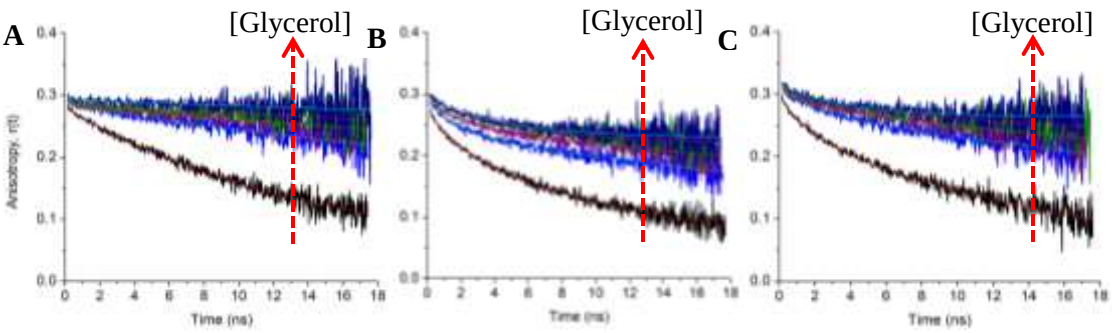

Figure 3.4: Time-resolved anisotropy of the FRET probe as a function of excitation/detection wavelengths in glycerol-enriched buffer (0-900 g/L). (**a**) Excitation of the donor (425 nm) and detection of the donor (475/50). (**b**) Excitation of the donor (425 nm) and detection of the acceptor (530/40 nm). (**c**) Excitation of the acceptor (465 nm) and detection of the acceptor (530/40).

FRET Efficiency assessment

To assess the energy transfer efficiency of the FRET probe, we carried out time-resolved fluorescence and anisotropy measurements using TCSPC technique as a function of glycerol (0-900 g/L). From these results we are able to calculate the donor-acceptor distance (R_{DA}^6), anisotropy-based energy transfer rate (k_{ET}) and estimate the energy transfer efficiency (E). For these measurements, we used a cleaved version of our FRET sensor in order to determine the fluorescence lifetime of the donor alone (τ_D) (see **Chapter 2, section 2.2**). The intact FRET sensor was also measured and represents the lifetime of the donor in the presence of the acceptor (τ_{DA}). The donor (*mCerulean*) emission decays as a biexponential in the intact and cleaved FRET probe, over the range of glycerol concentrations (0-900 g/L). There are slight differences in the fluorescence lifetimes of the intact probe as compared with the cleaved counterpart, which we again attribute to energy transfer. **Table 3.4** provides a summary of our FRET efficiency calculations as a function of increasing glycerol concentration (0-900 g/L). In general, the energy transfer efficiency (E) in glycerol is fairly low (4.3%-5.8%), which complement our findings from the time-resolved anisotropy of the FRET probe in glycerol-enriched buffer. The anisotropy results suggested that the viscous environment created a more compact structure, which we can confirm with our calculations of the donor-acceptor distance. As we increase our glycerol concentration, the donor-acceptor distance becomes

smaller. However, this shorter distance does not translate to higher FRET efficiency; in fact, we observe a decrease in efficiency as we increase the concentration of glycerol, thereby increasing the viscosity. Taken together, it is likely that the limited segmental mobility created by the high viscosity range (1-43 cP), reduces conformational fluctuations, and therefore reduces the FRET efficiency of this sensor. As a note, the corrected anisotropy-based energy transfer efficiency values (E_{ET}), were calculated using the weighted amplitude fraction of the fast component $\left(\frac{\beta_1}{\beta_1+\beta_2}\right)$ and the E_{ET} calculated using **Equation 3.8**.

Table 3.4: Summary of the FRET efficiency calculations of the FRET probe measured in glycerol-enriched buffers (0-900 g/L) calculated from time-resolved fluorescence and anisotropy data.

$\lambda_x - \lambda_{fl}$: FRET Probe	τ_{DA} (ns)	τ_D (ns)	E	R_0^6 (nm)	R_{DA}^6 (nm)	k_{ET} (ns^{-1})	E_{ET} (corrected)
425 – 475/50: **Glycerol**							
PBS	3.71	3.92	5.4%	4.99	8.00	0.23	11%
480 g/L	3.40	3.61	5.8%	4.18	6.65	0.26	9.0%
620 g/L	3.33	3.48	4.3%	4.00	6.71	0.28	7.6%
760 g/L	3.11	3.29	5.5%	3.84	6.17	0.28	7.0%
900 g/L	2.95	3.09	4.5%	3.67	6.11	0.22	6.2%

3.3 *Effects of heterogeneous viscosity on the rotational diffusion of size-dependent probes:* Polymers and protein crowded environments

Ficoll-70 crowded solutions: RhG110 and eGFP

To assess the effects that heterogeneous viscosity has on the rotational diffusion of our molecules, we used the synthetic polymer Ficoll-70 to create heterogeneously crowded environments. We can think of Ficoll-70 as creating hard spheres or excluded volume, which may impose conformational changes on the molecule, which would be reflected as changes in the rotational diffusion (*44*). In the context of crowding, we can determine whether crowding agents impose intermolecular interactions (e.g., specific or non-

specific binding) upon the molecular probe of interest, which would decrease the corresponding rotational time. For larger molecular tracers, however, crowding agents may induce a compaction of the molecule of interest and lead to faster rotational times than those measured in the absence of crowding.

For these experiments, RhG110 and eGFP were tested in varying concentrations of Ficoll-70 enriched buffer at room temperature. Typical anisotropy decays are shown in **Figure 3.5**.

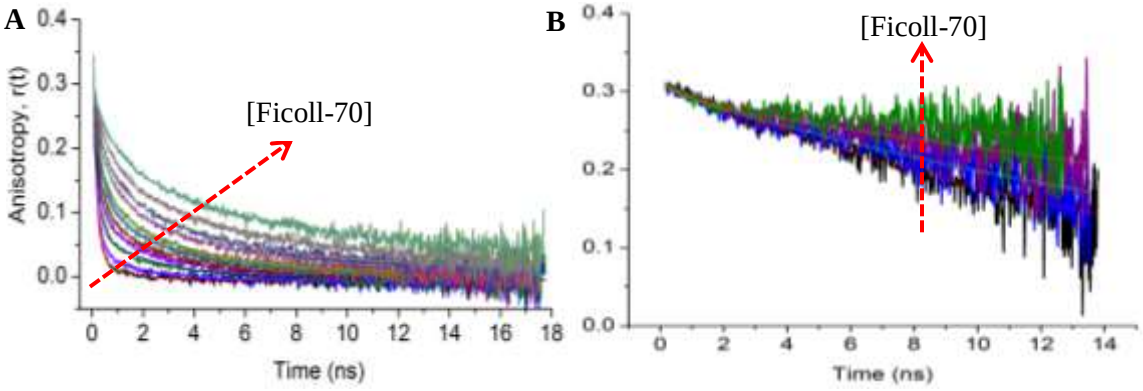

Figure 3.5: Time-resolved anisotropy of (**a**) RhG110 and (**b**) eGFP as a function of increasing Ficoll-70 concentration (0-400 g/L). RhG110 was fit to a biexponential decay, while eGFP decays as a single exponential.

RhG110 was fit to a biexponential decay over the span of the Ficoll-70 concentrations used (0-400g/L), as compared to a single exponential decay in pure buffer. The results show an apparent increase in the rotational time for RhG110 over the ps-ns time scale (**Table 3.5**). From these results, we are able to use the rotational diffusion coefficient and the corresponding viscosity to test the validity of the Stokes-Einstein model (**Equation 3.2**). For the biexponential decay of RhG110, we calculated the diffusion coefficient ratio ($^{D_0}/_{D_c}$), for both the fast rotational time (φ_1) and the slow or overall rotational time (φ_2), along with the average rotational time (φ_{ave}) (**Figure 3.6**). Our results of $\left(^{D_0}/_{D_c}\right)$ as a function of $(^{\eta_c}/_{\eta_0})$ show that the corresponding diffusion coefficient associated with faster rotational decay component (φ_1) has a negative deviation from the Stokes-Einstein model indicating the fluorophore is diffusing faster than what is predicted at the

corresponding bulk/homogeneous viscosity (**Figure 3.6a**). The threshold for such deviation is at a Ficoll-70 concentration of 120 g/L (~4.3 cP). The observed faster than predicted diffusion of RhG110 in the crowded environment is attributed to a rotational diffusion of the free probe in a buffer-like environment created by gaps in between the hard spheres in the Ficoll-crowded solution. The relatively slow rotational component (φ_2) shows positive deviation from the predictions of the Stokes-Einstein model (**Figure 3.6a**). The observed deviation in this case is attributed to weak or non-specific interactions between Ficoll-70 and RhG110 and not complex formation [i.e., Ficoll$(RhG)_n$], as rotational diffusion of 5-10 ns is much too fast to be attributed to rotation of a 70 kDa molecule, which would be ~24 ns. For a significant comparison, the corresponding average rotational diffusion coefficient ratio was also plotted as a function of (η_c/η_0) and the results are shown in **Figure 3.6b**. Based on the population fractions of species 1 and species 2 in the crowded environment, the rotational diffusion behavior is likely to be the average of both trends observed above for the two decay components. Initially, the trend shows diffusion that is slower than predicted, but at the highest three concentrations (320, 360 & 400 g/L) there is a shift to a faster than predicted trend in the diffusion. It might seem counterintuitive to imagine the highest concentrations diffusing faster than predicted, but at concentrations greater than 100 g/L, Ficoll-70 molecules are known to collapse to form a mesh-like network of polymers (*71*, *72*). This mesh-like environment likely allows for rotational diffusion that is more closely related to how RhG110 behaves in a buffer-like environment.

Table 3.5: The fitting parameters of time-resolved anisotropy of RhG110 measured using TCSPC technique with emission-polarized analysis. These measurements were carried out in Ficoll-70-enriched buffers (0-400 g/L) at room temperature.

$\lambda_x - \lambda_{fl}$: Molecule	β_1	φ_1 (ns)	V_{rot} (nm^3)	R_{rot} (nm)	β_2	φ_2 (ns)	V_{rot} (nm^3)	R_{rot} (nm)
465 – 530/40: RhG110								
120 g/L	0.238	0.373	0.35	0.44	0.066	5.36	5.09	1.07
200 g/L	0.207	0.563	0.23	0.38	0.083	6.43	2.57	0.85
320 g/L	0.173	1.05	0.13	0.32	0.110	10.01	1.17	0.65
400 g/L	0.145	1.62	0.088	0.28	0.143	16.44	0.89	0.60

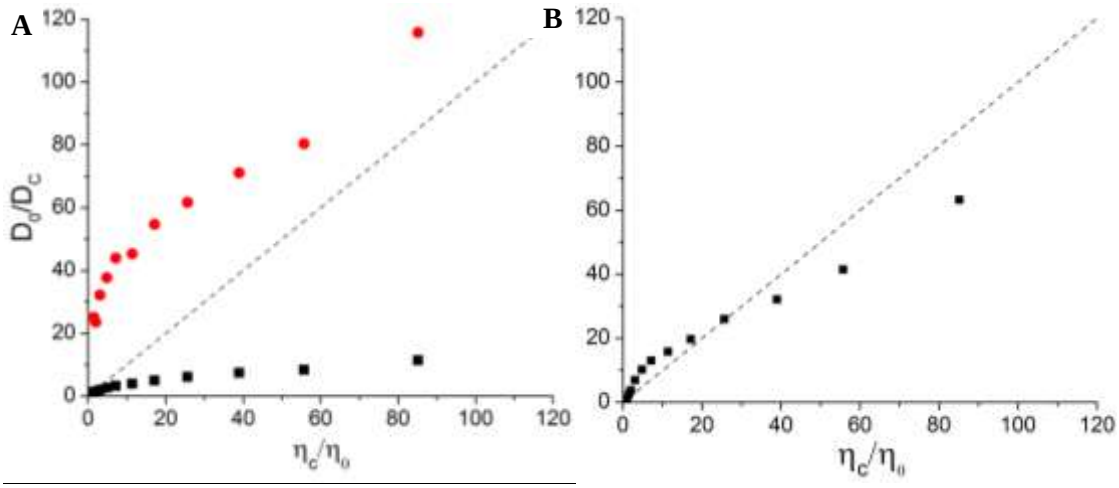

Figure 3.6: Diffusion coefficient analysis of RhG110 in varying concentrations of Ficoll-70 (0-400g/L). The dashed line represents the predictions from the Stokes-Einstein model. (**a**) Shows both the fast rotational component (φ_1, black squares) and the slow rotational component (φ_2, red circles). (**b**) Shows the average rotational time (φ_{ave}).

The anisotropy decay of eGFP was fit to a single exponential decay in Ficoll-70 concentrations of 0, 100, 200, and 300 g/L. The results show an apparent increase in the rotational time for eGFP over the ps-ns time scale (**Table 3.6**). From these results, we are able to use the rotational diffusion coefficient and the corresponding viscosity to test the

validity of the Stokes-Einstein model (**Equation 3.2**). For eGFP, we see a negative deviation from the Stokes-Einstein model, indicating the fluorophore is diffusing faster than what is predicted (**Figure 3.7**). This might seem counterintuitive to think of the fluorophore diffusing faster and not slower, but it is not entirely surprising given the results from RhG110 in Ficoll-70. As seen with RhG110, the fast rotational component was attributed to RhG110 diffusing in a buffer-like environment. The same can be said for eGFP in the Ficoll-70 crowded environment. Comparing the size of eGFP (32.7 kDa) to that of Ficoll (70 kDa), we see that our fluorophore is approximately half the size. This allows the eGFP molecules to diffuse in the gaps created by the hard spheres of the Ficoll-70 molecules. It is also known that Ficoll-70 molecules can collapse to form a mesh-like network (*71, 72*). On the ps-ns time scale of rotational diffusion, this mesh-like network is likely to affect rotational diffusion less than it would translational diffusion as it is expected that rotation in a mesh should be easier than translation through a mesh (*71*). The inherent blinking that eGFP is known to undergo (*73*) is likely not the cause of the fast rotational diffusion of this molecule either. Anisotropy can be thought of as a snapshot of how the molecule is behaving, unlike FCS measurements in which the molecule is moving randomly under constant illumination. This snapshot is on a very fast timescale, which allows us to rule out the possibility that a photophysical process, like the blinking behavior of eGFP, could be causing the appearance of a fast rotational diffusion time.

Table 3.6: The fitting parameters of time-resolved anisotropy of eGFP measured using TCSPC technique with emission-polarized analysis. These measurements were carried out in Ficoll-70-enriched buffers (0-300 g/L) at room temperature.

$\lambda_x - \lambda_{fl}$: Molecule	r_0	φ_1 (ns)	V_{rot} (nm^3)	R_{rot} (nm)
465 – 530/40: **eGFP**				
100 g/L	0.303	23.7	28.6	1.90
200 g/L	0.295	38.3	15.3	1.54
300 g/L	0.294	61.0	8.68	1.27

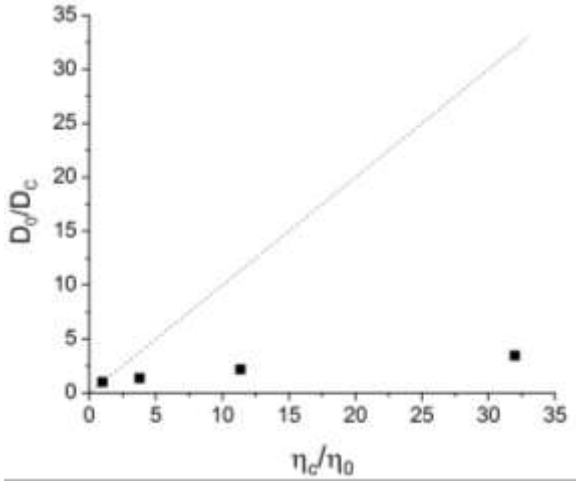

Figure 3.7: Diffusion coefficient analysis of eGFP in varying concentrations of Ficoll-70 (0-300g/L). The dashed line represents the predictions from the Stokes-Einstein model.

Ficoll-70 crowded solutions: FRET probe

To assess the effects of heterogeneous crowding on the conformational flexibility and energy transfer efficiency of the FRET probe we carried out time-resolved anisotropy as a function of excitation/detection wavelengths in Ficoll-70 enriched buffer at room temperature. **Figure 3.8** shows typical anisotropy decays of the FRET probe in Ficoll-70 concentrations of 0, 100, 200, and 300 g/L. Under 425 nm illumination, the polarization-analyzed fluorescence (475/50 nm) of the donor was detected and the corresponding anisotropy of the FRET probe decays as a single exponential over the range of Ficoll-70 concentrations (**Figure 3.8a**). The rotational times associated with the range of Ficoll-70 concentrations are much faster than what would be predicted of a 64 kDa molecule over a viscosity range of 3.4-28.5 cP (100-300 g/L), therefore we attribute this fast rotation time to the segmental mobility of the donor in the FRET probe due to the flexible linker with the acceptor. Using the Stokes-Einstein model, we calculated the hydrodynamic radii of the rotating moiety of the donor as a function of Ficoll-70 concentration and the results are summarized in **Table 3.7**. Our results show that as we increase the concentration of Ficoll-70, the hydrodynamic radius of the donor gets smaller.

Under 425 nm illumination, the polarization-analyzed fluorescence (530/40 nm) of the FRET probe decays as a biexponential with a fast rotational component (φ_1, β_1) and an apparent overall rotational component (φ_2, β_2) (**Figure 3.8b**). The fast component is too fast to be assigned to the tumbling motion of a 64 kDa protein; therefore we attribute this component to energy transfer from the donor to the acceptor. As seen in **Figure 3.8b**, there is now a pronounced fast decay component when we excite the donor and detect the acceptor. Even more interesting, is that the results show that, as we increase our Ficoll-70 concentration (thereby increasing the crowding) we see the amplitude fraction of the fast decay component increase as well. This is an important trend, and supports our hypothesis that as we increase the level of crowding in the surrounding environment, we increase the FRET between our donor and acceptor. Another important comparison can be made between our results in homogeneous and heterogeneous crowding. For example, looking at 620 g/L of glycerol, which corresponds to a viscosity of ~9 cP, the overall rotational time (φ_2) is ~78 ns (**Table 3.3**). Comparing this to the rotational time of the FRET probe in Ficoll-70 200 g/L, which has a viscosity of ~ 10 cP, the rotational time, is now only ~36 ns (**Table 3.7**). It appears as though the viscous environment of glycerol has a much greater effect on the segmental mobility of the FRET probe. Or taken another way, the excluded volume created by the Ficoll-70 enriched buffer favors a smaller, more compact probe. This is an important result in support of our hypothesis that crowding induces a more compact structure, which increases the ability for energy to be transferred from the donor to the acceptor. Finally, this also distinguishes between viscosity and crowding affects, as our results in similar levels of viscosity imply that the crowding, not the viscosity, is inducing higher FRET between the pair.

Under 465 nm illumination, the polarization-analyzed fluorescence (530/40 nm) of the FRET probe decays as a biexponential with a fast rotational component (φ_1, β_1) and an apparent overall rotational component (φ_2, β_2) (**Figure 3.8c**). Again, we see the same trend as we did in glycerol-enriched buffer, and attribute this to the fact that both the donor and acceptor can be excited at this wavelength due to spectral overlap of their emission. These results complement our results from indirect excitation of the acceptor,

and provide a comparison as to how the acceptor decays under direct excitation at 465 nm.

Table 3.7: The fitting parameters of time-resolved anisotropy of the FRET probe measured as a function of excitation/detection wavelength using TCSPC technique with emission-polarized analysis. These measurements were carried out in Ficoll-70 enriched buffers (0-300 g/L) at room temperature. Hydrodynamic volume and radii were calculated based on (φ_2).

$\lambda_x - \lambda_{fl}$: Molecule	β_1	φ_1 (ns)	β_2	φ_2 (ns)	r_0	V_{rot} (nm^3)	R_{rot} (nm)
425 – 475/50: **FRET Probe**							
100 g/L	--	--	0.275	23.4	0.275	28.6	1.90
200 g/L	--	--	0.276	34.2	0.276	13.9	1.49
300 g/L	--	--	0.276	54.5	0.276	7.87	1.23
425 – 530/40: FRET Probe							
100 g/L	0.060	1.57	0.215	22.1	0.275	27.1	1.86
200 g/L	0.067	1.48	0.201	36.1	0.268	14.7	1.52
300 g/L	0.072	0.99	0.197	41.4	0.269	5.98	1.13
465 – 530/40: **FRET Probe**							
100 g/L	0.057	2.06	0.233	26.8	0.290	32.7	1.98
200 g/L	0.054	1.53	0.233	37.6	0.287	15.3	1.54
300 g/L	0.057	1.17	0.231	51.1	0.288	7.38	1.21

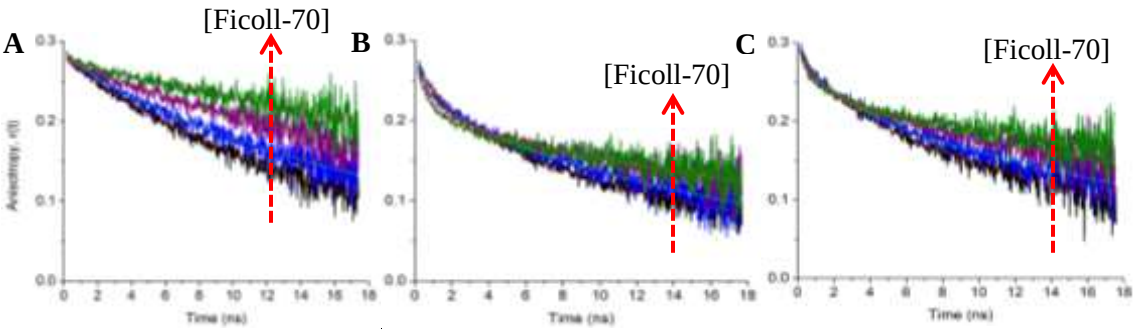

Figure 3.8: Time-resolved anisotropy of the FRET probe as a function of excitation/detection wavelengths in Ficoll-70 enriched buffer (0-300 g/L). (**a**) Excitation of the donor (425 nm) and detection of the donor (475/50). (**b**) Excitation of the donor (425 nm) and detection of the acceptor (530/40 nm). (**c**) Excitation of the acceptor (465 nm) and detection of the acceptor (530/40).

FRET Efficiency assessment

To assess the energy transfer efficiency of the FRET probe we carried out time-resolved fluorescence and anisotropy measurements using TCSPC technique as a function of Ficoll-70 (0-300 g/L). From these results we are able to calculate the donor-acceptor distance (R_{DA}^6), anisotropy-based energy transfer rate (k_{ET}) and estimate the energy transfer efficiency (E). For these measurements, we used a cleaved version of our FRET sensor in order to determine the fluorescence lifetime of the donor only (τ_D) (see **Chapter 2, section 2.2**). The intact FRET sensor was also measured and represents the lifetime of the donor in the presence of the acceptor (τ_{DA}). The donor (*mCerulean*) emission decays as a biexponential in the intact and cleaved FRET probe, over the range of Ficoll-70 concentrations (0-300 g/L). There are slight differences in the fluorescence lifetimes of the intact probe as compared with the cleaved counterpart, which we again attribute to energy transfer. **Table 3.8** provides a summary of our FRET efficiency calculations as a function of increasing Ficoll-70 concentration (0-300 g/L). In general, the energy transfer efficiency (E) in Ficoll-70 is still fairly low (2.4%-6.7%), however, we observed higher FRET efficiency at larger donor-accepter distances as compared to our results in glycerol-enriched buffers. From the time-resolved anisotropy of the FRET probe in Ficoll-70, we observed an increase in the fast component of the biexponential decay of the FRET probe when exciting the donor and detecting the acceptor. We attributed this to an excluded volume effect from the Ficoll-70 molecules inducing a more compact FRET structure, thereby increasing the energy transfer between our FRET

pair. The measurements of the fluorescence lifetime of the FRET probe and corresponding donor-acceptor distance calculations do not fully support this hypothesis, as our Ficoll-70 300 g/L donor-acceptor distance is the greatest of the three concentrations. Although they might be farther apart, there are other factors that affect/increase the FRET efficiency. Looking at the anisotropy-based energy transfer efficiency calculations, which include a correction for the amplitude of the fast decay component, our interpretations from the anisotropy data follow what we predict, as we see an increase in the energy transfer efficiency from 12-17% as we increase our Ficoll-70 concentrations. The somewhat contradictory results seen here attest to the fact that there is a need to develop a way to quantify hetero-FRET using the excited-state dynamics approach.

Table 3.8: Summary of the FRET efficiency calculations of the FRET probe measured in Ficoll-70 enriched buffers (0-300 g/L) calculated from time-resolved fluorescence and anisotropy data.

$\lambda_x - \lambda_{fl}$: FRET Probe	τ_{DA} (ns)	τ_D (ns)	E	R_0^6 (nm)	R_{DA}^6 (nm)	k_{ET} (ns^{-1})	E_{ET} (corrected)
425 – 475/50: **Ficoll-70**							
PBS	3.71	3.92	5.4%	4.99	8.00	0.23	11%
100 g/L	3.60	3.83	6.0%	4.70	7.43	0.30	12%
200 g/L	3.46	3.71	6.7%	4.52	7.01	0.32	14%
300 g/L	3.30	3.38	2.4%	4.33	8.02	0.49	17%

Protein crowded solutions: RhG110 and eGFP

To assess the effects that heterogeneous viscosity has on the rotational diffusion of our molecules we used the globular proteins bovine serum albumin (BSA) and ovalbumin to create heterogeneously crowded environments. This allows us to compare the behavior of our fluorophores in synthetic and protein-enriched crowded environments, which may impose conformational changes on the molecule, which would be reflected as changes in the rotational diffusion (*44*). Using a protein as a crowding agent allows us to elucidate if

there is any interaction or binding events that occur between the fluorophore and crowding agent. This would be reflected in rotational diffusion times which are slower than predicted for a molecule of a certain size.

For these experiments, RhG110 and eGFP were tested in varying concentrations of BSA and ovalbumin enriched buffer at room temperature. Typical anisotropy decays of BSA (**Figure 3.9**) and ovalbumin (**Figure 3.10**) are shown below.

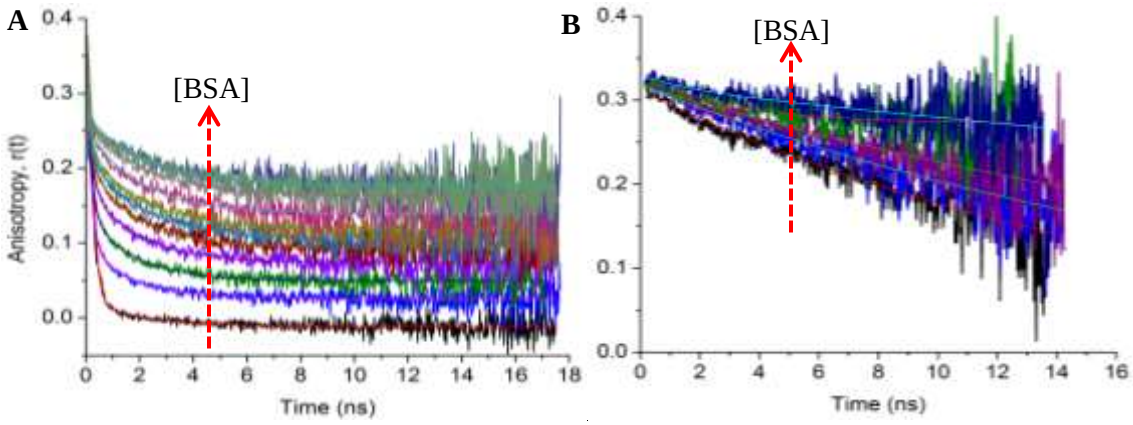

Figure 3.9: Time-resolved anisotropy of (**a**) RhG110 and (**b**) eGFP as a function of increasing BSA concentration (0-270 g/L). RhG110 was fit to a biexponential decay, while eGFP decays as a single exponential.

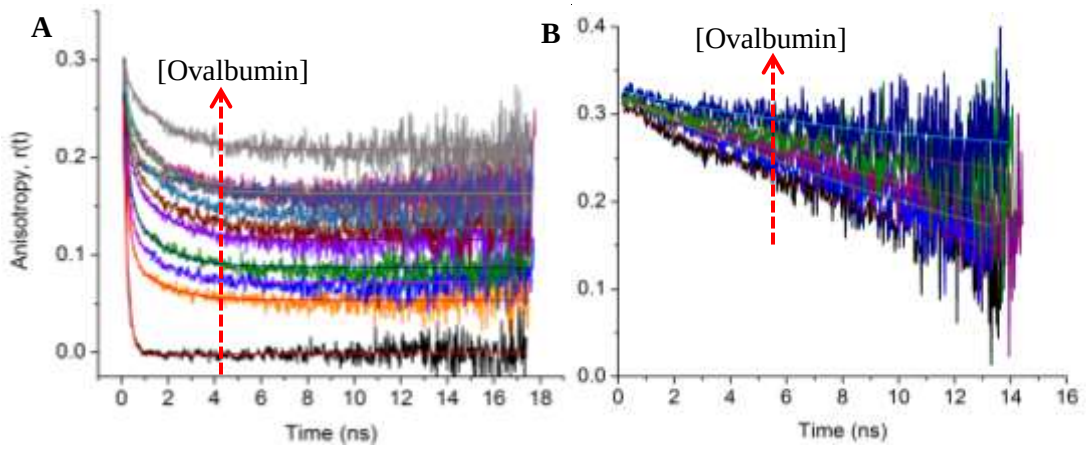

Figure 3.10: Time-resolved anisotropy of (**a**) RhG110 and (**b**) eGFP as a function of increasing ovalbumin concentration (0-270 g/L). RhG110 was fit to a biexponential decay, while eGFP decays as a single exponential.

RhG110 was fit to a biexponential decay and a residual anisotropy (r_∞) component over the span of the BSA concentrations used (0-270g/L). The results show an apparent increase in the rotational time for RhG110 over the ps-ns time scale (**Table 3.9**). The residual anisotropy component suggests an immobile fraction of the crowded population on the nanosecond timescale, which is likely due to binding between RhG110 and the BSA. It is worth mentioning that the anisotropy of pure BSA was measured and found to be significantly different from those of RhG110 in BSA enriched solution. This suggests that, although there is background signal from BSA, it does not interfere significantly with the measured anisotropy of RhG110 in the results reported here. From these results, we are able to use the rotational diffusion coefficient and the corresponding viscosity to test the validity of the Stokes-Einstein model (**Equation 3.2**). For the biexponential decay of RhG110 in BSA, we calculated the diffusion coefficient ratio ($^{D_0}/_{D_c}$), for both the fast rotational time (φ_1) and the slow or overall rotational time (φ_2), along with the average rotational time (φ_{ave}) (**Figure 3.11**). In the average rotational time calculations, the residual anisotropy was excluded from the overall amplitude fraction. Our rational here is to examine whether BSA crowding affects each rotational diffusion component (i.e., species of different hydrodynamic size) differently from that of the corresponding average rotational diffusion. In another way, we wanted to ensure averaging does not washout valuable mechanistic information. Our results of $\left(^{D_0}/_{D_c}\right)$ as a function of $\left(^{\eta_c}/_{\eta_0}\right)$ show that the corresponding diffusion coefficient associated with the faster rotational decay component (φ_1) has a negative deviation from the Stokes-Einstein model indicating the fluorophore is diffusing faster than what is predicted at the corresponding bulk/homogeneous viscosity (**Figure 3.11a**). The threshold for such deviation is at a BSA concentration of ~120 g/L. The observed faster than predicted diffusion coefficient of RhG110 in the crowded environment is attributed to a rotational diffusion of the free probe in a buffer-like environment in the BSA-crowded solution. As for the relatively slow component (φ_2), we attribute this to nonspecific or weak interactions that may be transient or long-lived between RhG110 and BSA. We do not attribute this slow component to complex formation between RhG110 and BSA [i.e.,

$BSA(RhG)_n$] however, as the rotational times observed are much too fast to be assigned to a ~66 kDa protein, which would be ~23 ns. For significant comparison, the corresponding average rotational diffusion coefficient ratio was also plotted as a function of (η_c/η_0) and the results are also shown in **Figure 3.11b**. Based on the population fractions of species 1 and species 2 in the crowded environment, the rotational diffusion behavior is likely to be averaging both trends observed above for the two decay components. It is worth mentioning that the two highest BSA concentration (240 & 270 g/L) indicate a faster than predicted diffusion behavior. While this is counterintuitive, the result might suggest a potential denaturation of BSA at higher concentrations. However, this speculative interpretation would need further experimental testing.

Table 3.9: The fitting parameters of time-resolved anisotropy of RhG110 measured using TCSPC technique with emission-polarized analysis. These measurements were carried out in BSA and ovalbumin-enriched buffers (0-270 g/L) at room temperature.

$\lambda_x - \lambda_{fl}$: Molecule	β_1	φ_1 (ns)	V_{rot} (nm^3)	R_{rot} (nm)	β_2	φ_2 (ns)	V_{rot} (nm^3)	R_{rot} (nm)
465 – 530/40: **RhG110 BSA**								
60 g/L	0.062	0.22	0.53	0.50	0.244	2.02	5.36	1.09
120 g/L	0.094	0.28	0.46	0.48	0.126	2.05	3.39	0.93
210 g/L	0.067	0.30	0.21	0.37	0.094	2.28	1.56	0.72
270 g/L	0.040	0.13	0.041	0.21	0.081	2.37	0.74	0.56
465 – 530/40: **RhG110 Ovalbumin**								
60 g/L	0.056	0.18	0.48	0.49	0.262	1.44	3.85	0.97
120 g/L	0.079	0.19	0.37	0.45	0.180	1.38	2.71	0.86
210 g/L	0.086	0.19	0.18	0.35	0.094	1.48	1.40	0.69
270 g/L	0.054	0.20	0.088	0.28	0.093	1.42	0.63	0.53

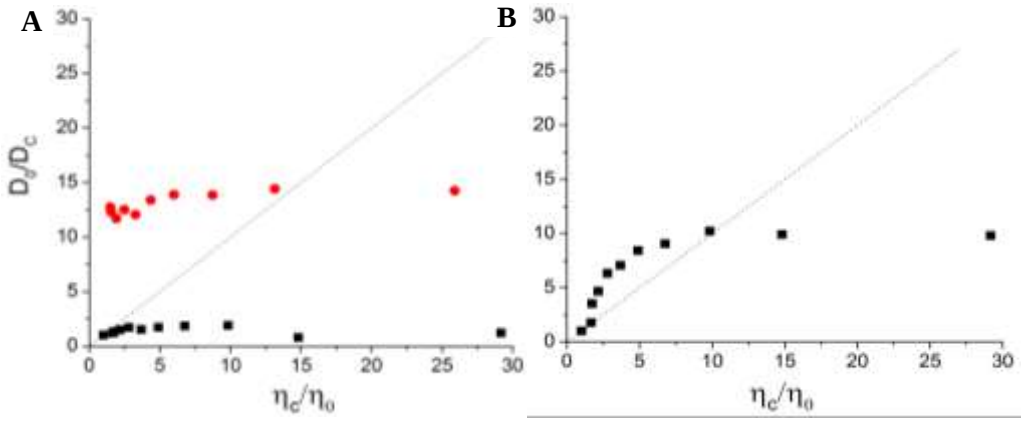

Figure 3.11: Diffusion coefficient analysis of RhG110 in varying concentrations of BSA (0-270g/L). The dashed line represents the predictions from the Stokes-Einstein model. (**a**) Shows both the fast rotational component (φ_1, black squares) and the slow rotational component (φ_2, red circles). (**b**) Shows the average rotational time (φ_{ave}).

In the presence of ovalbumin, the anisotropy of RhG110 decays as a biexponential. The results show an apparent increase in the rotational time for RhG110 over the ps-ns time scale over the span of ovalbumin concentrations (0-270 g/L) (**Table 3.9**). In comparison with BSA, a similar protein, we did not see a large residual decay component. This could likely be due to the fact that the viscosity range of ovalbumin is significantly smaller than that of BSA. Ovalbumin ranges from 1.54 – 9.33 cP, whereas BSA ranges from 1.50 – 25.90 cP. This increased viscosity, especially at high concentrations of BSA, appears to slow the diffusion of the fluorophore to a time where it is basically not diffusing at all. It is also worth mentioning that the anisotropy decay of pure ovalbumin was measured and was found to be significantly different from those of RhG110 in ovalbumin enriched solution. This suggests that, although there is background signal from ovalbumin, it does not interfere significantly with the measured RhG110 anisotropy results reported here. For the biexponential decay of RhG110 in ovalbumin, we calculated the diffusion coefficient ratio ($^{D_0}/_{D_c}$), for both the fast rotational time (φ_1) and the slow or overall rotational time (φ_2), along with the average rotational time (φ_{ave}) to examine whether the rotational diffusion of RhG110 follows the predictions of the Stokes-Einstein model (**Figure 3.12**). Our results of

$\left({}^{D_0}/_{D_c}\right)$ as a function of $\left({}^{\eta_c}/_{\eta_0}\right)$ show that the corresponding diffusion coefficient associated with the faster rotational decay component (φ_1) has a negative deviation from the Stokes-Einstein model indicating the fluorophore is diffusing faster than what is predicted at the corresponding bulk/homogeneous viscosity (**Figure 3.12a**). The observed faster than predicted diffusion coefficient of RhG110 in the crowded environment is attributed to a rotational diffusion of the free probe in buffer-like environment in the ovalbumin-crowded solution. As for the relatively slow component (φ_2), we attribute this to nonspecific or weak interactions that may be transient or long-lived between RhG110 and ovalbumin. We do not attribute this slow component to complex formation between RhG110 and ovalbumin [i.e., ovalbumin$(RhG)_n$] however, as the rotational times observed are much too fast to be assigned to a ~45 kDa protein, which would be ~16 ns. For significant comparison, the corresponding average rotational diffusion coefficient ratio was also plotted as a function of $\left({}^{\eta_c}/_{\eta_0}\right)$ and the results are also shown in **Figure 3.12b**. Based on the population fractions of species 1 and species 2 in the crowded environment, the rotational diffusion behavior is likely to be averaging both trends observed above for the two decay components. It is worth mentioning that the highest two ovalbumin concentrations (240 & 270 g/L) indicate a faster than predicted diffusion behavior, just as we observed with our BSA results. The result might suggest a potential denaturation of ovalbumin at higher concentrations. But again, this is speculative interpretation and would need further experimental testing.

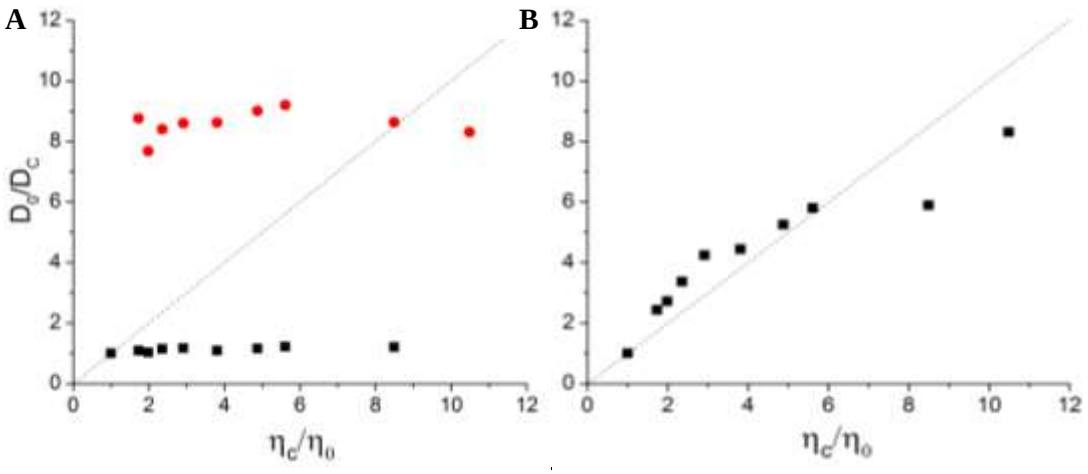

Figure 3.12: Diffusion coefficient analysis of RhG110 in varying concentrations of ovalbumin (0-270g/L). The dashed line represents the predictions from the Stokes-Einstein model. (**a**) Shows both the fast rotational component (φ_1, black squares) and the slow rotational component (φ_2, red circles). (**b**) Shows the average rotational time (φ_{ave}).

Interestingly, when we compare our results of the rotational diffusion of RhG110 in synthetic polymers vs. proteins, we see somewhat of a similar trend, where we have a fast component and overall slow component to our rotational diffusion of RhG110 indicating our fluorophore is interacting in some form with the crowding agent. However, it appears as though the proteins have a much more pronounced effect on the slow component. This could be due to nonspecific or weak chemical interactions between our fluorophore and protein. Similar trends have been observed in NMR studies on the rotational and translational diffusion of chymotrypsin inhibitor 2, a 7.4 kDa test protein (*71*). The authors highlight the differences between the effects of synthetic polymers and proteins and suggest that the use of proteins as crowding agents is a better assessment for modeling the complicated intracellular environment (*71*). While I would agree with this, I would attest to the fact that the use of synthetic polymers provides a reasonable assessment for studying the effects that excluded volume has on the diffusion of the molecule of interest.

The anisotropy decay of eGFP in both BSA and ovalbumin enriched buffers (0-300 g/L) can be satisfactorily described using a single exponential decay. The results show an apparent increase in the rotational time for eGFP over the ps-ns time scale (**Table**

3.10). From these results, we are able to use the rotational diffusion coefficient and the corresponding viscosity to test the validity of the Stokes-Einstein model (**Equation 3.2**). For eGFP, we see a negative deviation from the Stokes-Einstein model, indicating the fluorophore is diffusing faster than what is predicted in both BSA (**Figure 3.13a**) and ovalbumin (**Figure 3.13b**). It should be noted that the data point at a concentration of 200 g/L of BSA was removed from the diffusion coefficient analysis as the data does not appear to be reliable; however it is included in **Table 3.10** for comparison. The rotational diffusion of eGFP in these protein-enriched buffers appears to be less affected by nonspecific interactions with proteins, as we only see a single anisotropy decay component. The faster than predicted rotational component, along with the single exponential decay, indicates that the eGFP molecules are not interacting with the proteins and are behaving as if in a buffered-like environment. Previous studies have found that as the crowding agent becomes much larger than the fluorophore, the diffusion tends to become independent of the bulk viscosity, indicating the molecules are behaving as if in a pure solvent (*74*). Comparing the anisotropy of eGFP in BSA to that of ovalbumin, we see more of an effect on the rotational diffusion in BSA, which is approximately twice the size of eGFP (66 kDa vs. 32.7 kDa). Whereas with ovalbumin, the effects are less pronounced as the size difference between eGFP and ovalbumin is much smaller (45 kDa vs. 32.7 kDa).

Table 3.10: The fitting parameters of time-resolved anisotropy of eGFP measured using TCSPC technique with emission-polarized analysis. These measurements were carried out in BSA and ovalbumin enriched buffers (0-300 g/L) at room temperature.

$\lambda_x - \lambda_{fl}$: Molecule	r_0	φ_1 (ns)	V_{rot} (nm^3)	R_{rot} (nm)
465 – 530/40: **eGFP** **BSA**				
50 g/L	0.319	22.5	66.1	2.51
100 g/L	0.318	29.6	54.1	2.35
200 g/L	0.307	85.6	65.9	2.51
300 g/L	0.322	70.8	11.2	1.39
465 – 530/40: **eGFP** **Ovalbumin**				
50 g/L	0.322	21.3	58.8	2.41
100 g/L	0.318	27.7	56.3	2.38
200 g/L	0.313	48.5	48.3	2.26
300 g/L	0.321	70.6	31.1	1.95

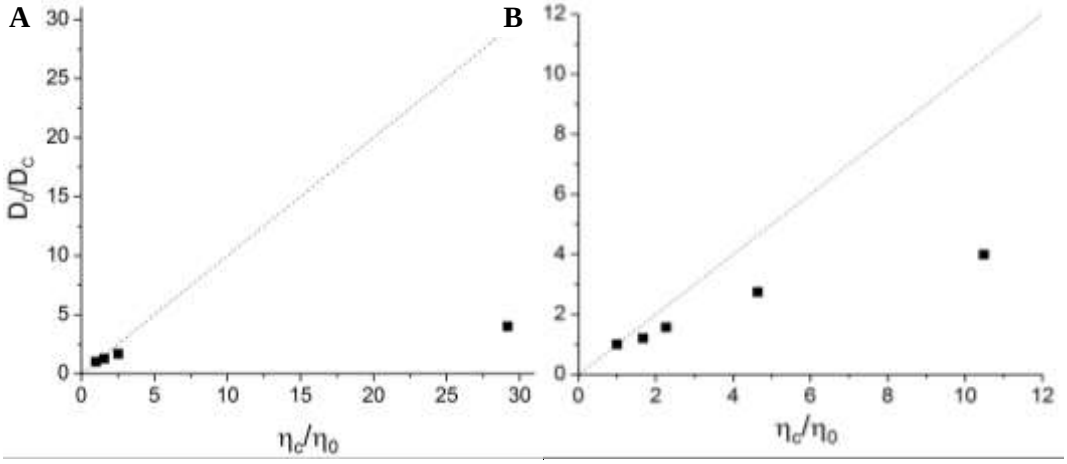

Figure 3.13: Diffusion coefficient analysis of eGFP in varying concentrations of (**a**) BSA and (**b**) ovalbumin (0-300g/L). The dashed line represents the predictions from the Stokes-Einstein model.

3.4 *Conclusions*

In summary, we used time-resolved fluorescence anisotropy to investigate the effects of macromolecular crowding on the rotational diffusion of three size-dependent probes. We did control experiments in PBS buffer and glycerol-enriched buffer in order to examine the effects of homogeneous viscosity on rotational diffusion. We then mimicked heterogeneously crowded environments with varying concentrations of Ficoll-70, a synthetic polymer, and the globular proteins BSA and ovalbumin and compared those results with the glycerol-enriched buffer in order to differentiate between viscosity and crowding effects. We saw in all environments, an apparent increase in the rotational diffusion time of our probes as we increased the concentration of our crowding agents, thereby increasing the viscosity.

For RhG110 and eGFP we used the Stokes-Einstein model, to compare the ratio of the diffusion coefficient in buffer to that in a crowded environment $\left({}^{D_0}/_{D_c}\right)$ with the ratio of the viscosity of the crowded environment to that of the buffer $\left({}^{\eta_c}/_{\eta_0}\right)$ to test the limits of the model. In Ficoll-70, BSA and ovalbumin, RhG110 undergoes a biexponential decay, whereas in pure and glycerol-enriched buffers it can be described as a single exponential decay, indicating that the crowding agents are nonspecifically interacting with the RhG110 molecules. However, we determined these interactions are not likely to be the result of complex formation, as the rotational times are much too fast to be attributed to rotation of molecules on the size order of our crowding agents. Previous studies have shown that a significantly large size difference between the crowding agent and fluorophore tends to show that the diffusion of the fluorophore acts independently of the bulk viscosity and behaves as if in pure solvent (*74*). Our data supports this finding as the fast rotational component of RhG110 is diffusing much faster than predicted, and the size difference between RhG110 (507 Da) and the crowding agents (45-70 kDa) is significant.

The anisotropy of eGFP in glycerol, Ficoll-70, BSA and ovalbumin can be described as a single exponential decay, indicating that eGFP is likely not interacting with the crowding agents. In all environments, we observed a negative deviation from the predications of

the Stokes-Einstein model, indicating a faster than predicated rotational diffusion. As stated above, the size difference between eGFP and the crowding agents might be the cause of this trend. Interestingly, as we increased the size of our crowding agent from ovalbumin (45 kDa) to BSA (66 kDa) to Ficoll-70 (70 kDa), the deviation from the Stokes-Einstein model became more significant, further supporting this hypothesis. It might also be the case that the crowding agents are inducing a compaction of the fluorophore, giving the appearance of a faster than predicted diffusion time.

For the FRET probe, we carried out time-resolved anisotropy as a function of excitation/detection wavelengths to assess the effects of homogeneous and heterogeneous crowding on the conformational flexibility and energy transfer efficiency of the FRET probe. We used glycerol-enriched buffer as a control for homogeneous viscosity and the crowding agent Ficoll-70 to mimic heterogeneous viscosity or excluded volume. Our results suggest that homogeneously viscous environment (e.g., glycerol-enriched buffer) reduces conformational fluctuations and therefore resulted in reduced FRET efficiency. In contrast, the excluded volume and confinement in the crowded environments (e.g., Ficoll-70 enriched buffer) seems to favor smaller donor-acceptor distance and therefore resulted in enhanced FRET efficiency when measured with time-resolved anisotropy. Fluorescence lifetime was also used as a means to assess the FRET efficiency, but showed an opposite trend than what was observed with the time-resolved anisotropy measurements. These results are somewhat convoluted and require imaginative thinking to try to decipher the affects that crowding has on our FRET sensor. In the future, more experiments with different FRET sensors (i.e., varying linker lengths/structures) will be useful for understanding how the excited-state dynamics of this FRET pair is affected by crowding.

3.5 *Implications and future directions*

The results for RhG110 and eGFP provide a snap shot of how the molecules are behaving in the diverse environments in which we conducted experiments. These results can be used to model our results for translational diffusion, which will be discussed in **Chapter 4** of this thesis. The size difference between the crowding agent and the fluorophore

resulted in the observed negative deviation seen for both molecular probes, giving the appearance that the molecule is diffusing as if in a pure solvent. Critically, these measurements will be useful towards rotational diffusion studies of biomolecules in living cells aimed at quantitative analysis of association reactions and conformational changes using similar techniques. For the FRET probe, we have established a technique to assess the degree of crowding using an excited-state dynamics technique. Our results reveal enhanced energy transfer efficiency with a pronounced effect on the excited state dynamics of the FRET sensor. This work builds on previous steady-state spectroscopy measurements by Boersma *et al.* (*24*) and our results serve as a point of reference for this FRET probe towards its full potential as a sensor for macromolecular crowding in living cells and tissues.

In the future, experiments in protein-crowded environments with the FRET sensor will be invaluable. We attempted to conduct these studies, but unfortunately the background fluorescence from BSA and ovalbumin resulted in a poor signal to noise ratio. It is unclear as to what the cause of this might be, so further investigation is essential. Ultimately, being able to encode this sensor into living cells will provide an understanding of the multidimensional nature of crowding effects experienced in the intracellular environment.

4. Chapter 4: Effects of crowding on translational diffusion and fluctuation analysis of size-dependent probes

Disclosure: This chapter has been published, in part, in the following:

(*1*): Currie, M., Thao, C., Timerman, R., Welty, R., Berry, B., Sheets, E.D., and Heikal, A.A. (2015) Multiscale diffusion of a molecular probe in a crowded environment: a concept. pp. 95840E-95840E-95816.
(*2*): Currie, M., Leopold, H., Schwarz, J., Boersma, A., Sheets, E.D., Heikal, A.A. (2017) "Fluorescence Dynamics of a FRET Probe Designed for Crowding Studies" *Journal of Physical Chemistry (B)*. (*In review*).

4.1 *Rationale*

Macromolecular crowding consists of both physical and chemical interactions between the crowding agents and the molecule of interest (*16-19*). This spatio-temporal complexity requires multiscale information on the single-molecule level, along with bulk studies, in order to understand the length- and time-scale dependence of crowding effects on cellular processes. To address such crowding effects at the single molecule level and on the μs–s time scale, we use fluorescence correlation spectroscopy (FCS) to quantify the translational diffusion of single molecules on longer spatio-temporal scales (*45*). We use FCS to monitor the time-dependent fluorescence fluctuation of single molecules diffusing in and out of an open observation volume. These fluctuations are then autocorrelated to give the average number of molecules residing in the observation volume, the diffusion time, and the time constant associated with photophysical processes such as triplet state or blinking, or chemical kinetics such as binding between the probe and crowding agent. At sufficiently high concentrations of crowding agent, the translational diffusion of the tracer will be impeded due to excluded volumes, and is expected to slow down the diffusion as compared with the absence of crowding agents.

According to the Stokes-Einstein model, the translational diffusion coefficient (D_T) depends on both the viscosity of the surrounding environment (η) and the hydrodynamic radius of the molecule (a) (*34*, *62*):

$$D_T = \frac{k_B T}{6\pi\eta a} \tag{4.1}$$

The model describes the diffusion of a spherical particle in a homogeneous environment undergoing Brownian motion. Accordingly, the model predicts that the ratio of the diffusion coefficient in buffer to that in a crowded environment $\left({}^{D_0}/_{D_c}\right)$ is equal to the ratio of the viscosity of the crowded environment to that of the buffer $\left({}^{\eta_c}/_{\eta_0}\right)$:

$$\frac{D_{buffer}}{D_{crowder}} = \frac{\eta_{crowder}}{\eta_{buffer}} \tag{4.2}$$

Therefore, if the translational diffusion of a molecule deviates from the Stokes-Einstein model, there will be a deviation from linearity, indicating that the molecule is either diffusing slower or faster than what is predicted. Any observed deviation would allow us to elucidate how crowding affects the mechanism of translational diffusion at the single molecule level. Our hypothesis is that the validity of the Stokes-Einstein model for a diffusing spherical molecule in crowded environments will be limited by (*i*) the viscosity range in a homogeneously viscous environment, (*ii*) the concentration and type of the crowding agents, and (*iii*) the spatio-temporal resolution of the experimental technique used.

In this chapter, we investigated the effects of crowding on the translational diffusion of the size-dependent fluorescent probes: RhG110, eGFP and a FRET sensor. The synthetic polymer Ficoll-70 and the protein BSA was used to mimic heterogeneous viscosity. These samples were prepared up to 320 g/L to match the projected macromolecular crowding in living cells (*49, 50*). As a control for homogeneous viscosity, we used glycerol-enriched PBS extended from 0-900 g/L to cover the wide range of viscosity that exists in cellular compartments. As a reminder, the bulk viscosity measurements of all the crowding agents used in this chapter were measured independently with an Ubbelohde viscometer (**Appendix I**). The materials and methods used in this chapter are described in detail in **Chapter 2, sections 2.3-2.4** of this thesis.

4.2 *Effects of homogeneous viscosity on the translational diffusion of size-dependent probes:* Pure buffer and glycerol-enriched buffer

Pure Buffer

In order to provide baseline measurements for our probes, we conducted experiments with RhG110 (507 Da), eGFP (32.7 kDa) and a FRET probe (64 kDa) in pure PBS buffer (pH 7.4). These measurements serve as a reference point for helping us to understand the translational diffusion mechanism associated with these probes in crowded environments. RhG110 was used to calibrate our FCS system, as the translational diffusion coefficient is well documented in literature (*46*, *75*). In pure buffer at room temperature, the translational diffusion of RhG110 is 3.0 x 10^{-6} cm^2/s (*46*), which corresponds to a measured diffusion time of ~0.07 ms in our FCS setup. From this we can also estimate the radial extension of the observation volume as ~288 nm using **Equation 2.7**. **Figure 4.1** shows typical autocorrelation curves for RhG110, eGFP and a FRET probe in PBS buffer.

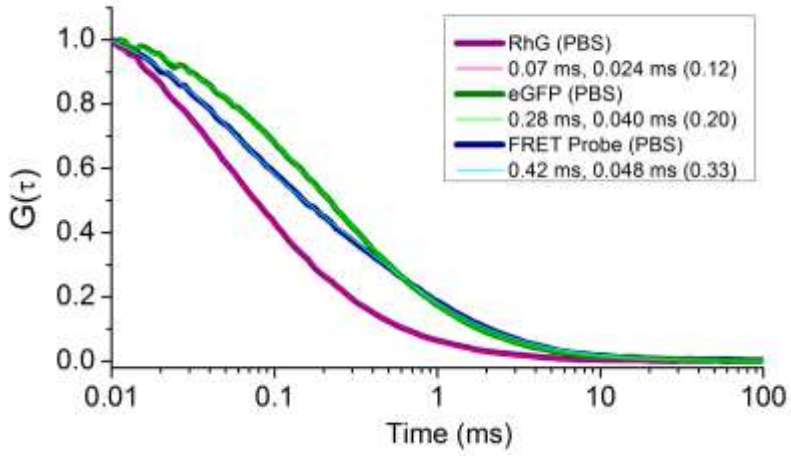

Figure 4.1: Normalized FCS autocorrelation curves of RhG110, eGFP and a FRET probe in PBS buffer as a function of correlation time (shown here on a logarithmic scale). The diffusion time, and to some extent photophysical processes such as intersystem crossing to the triplet state (RhG110), blinking (eGFP, FRET probe) and energy transfer (FRET probe) are responsible for the observed fluctuations. These photophysical processes represent between 12-33% of the observed fluctuations with estimated lifetimes of tens of microseconds.

Our results indicate under 488 nm illumination, the FRET probe diffuses slower (0.42 ± 0.05 ms) than both eGFP (0.28 ± 0.05 ms) and RhG110 (0.07 ± 0.01 ms) in a buffer at room temperature (**Figure 4.1, Table 4.1**). Based on these autocorrelation curves, we estimated a diffusion coefficient of the FRET probe to be (5.1 ± 0.7) × 10^{-7} cm^2/s as compared with (7.7 ± 1.3) × 10^{-7} cm^2/s for eGFP and 3.0 × 10^{-6} cm^2/s for RhG110. These results show that, as the size of the molecule increases, the translational diffusion coefficient decreases. Using the Stokes-Einstein model, the measured diffusion coefficient of the FRET probe yields a hydrodynamic radius of 4.82 nm as compared with 3.20 nm for eGFP and 0.82 nm for RhG110. Based on the molecular weight and hydration of a given protein; we calculated the hydrodynamic radius of each probe using the following equation:

$$\sqrt[3]{\frac{3}{4\pi} \times \frac{\left[\left(0.73\ {cm^3}/{g}\right) + \left(0.23\ {cm^3 H_2O}/{g\ protein}\right)\right] \times \left(10^{21}\ {nm^3}/{cm^3}\right) \times MW}{N_A}} \tag{4.3}$$

Using **Equation 4.3** and assuming a hydration of 0.23 g of H_2O per gram of protein, we used the molecular weight of RhG110 (507 Da), eGFP (32.7 kDa) and the FRET probe (64 kDa) to calculate the corresponding hydrodynamic radius. For RhG110, we calculated a hydrodynamic radius of 0.57 nm as compared with 2.29 nm for eGFP and 2.87 nm for the FRET probe. It is important to note that this is the minimum radius that could contain the given mass of a protein and therefore only offers an estimation for the radius assuming a smooth, spherical shape (*34*, *65*). Due to the irregular surfaces on proteins, the average radius is likely to be larger than the calculated radius using **Equation 4.3**. These results and trends are in agreement with our FCS estimated radii. We then used the calculated minimum radius and the Stokes-Einstein model to calculate expected translational diffusion coefficients for the three molecules. Based on the calculations, one would expect a translational diffusion coefficient of 4.3×10^{-6} cm^2/s for RhG110, 1.07 ×10^{-6} cm^2/s for eGFP and 8.54 ×10^{-7} cm^2/s for the FRET probe. These

estimates are again in general agreement with the measured translational diffusion coefficient in pure buffer at room temperature.

The measurements of our three molecules in pure buffer at room temperature serve as a control for measurements in crowded environments. In buffer, the molecules are free to move without obstacles, allowing us determine the diffusion time and translational diffusion coefficient of each. As expected, as the size of the molecule increases, the diffusion time becomes slower and the translational diffusion coefficient decreases.

Table 4.1: The fitting parameters of fluorescence fluctuation autocorrelation of RhG110, eGFP and the FRET probe as measured using FCS. These measurements were carried out in a buffer (PBS, pH7.4) at room temperature using a 488-nm laser, 1.2NA objective (water immersion), and 50-mm confocal pinhole.

$\lambda_x - \lambda_{fl}$ (nm): Molecule	τ_D (ms)	f_j*	τ_j (ms)	D_T (cm^2/s)	a_{FCS} (nm)	a_{cal} (nm)
488 – 530/40:						
RhG 110 (507 Da)	0.07 ± 0.01	0.12 ± 0.03	0.024 ± 0.01	3.0×10^{-6}	0.82	0.57
eGFP (32.7 kDa)	0.28 ± 0.05	0.20 ± 0.13	0.040 ± 0.01	$(7.7 \pm 1.3) \times 10^{-7}$	3.20	2.29
FRET Probe (64 kDa)	0.42 ± 0.05	0.33 ± 0.01	0.048 ± 0.001	$(5.1 \pm 0.7) \times 10^{-7}$	4.82	2.87

Glycerol-enriched Buffer

To differentiate between homogeneous viscosity and heterogeneous crowding, we did control experiments in glycerol-enriched buffer. This control allows us to distinguish among diffusion in viscous solution, confinement in a cage created by the hard-sphere crowding agents, weak interactions, and association reactions (long-lived or transient) that a molecular probe may experience in the crowded milieu of living cells. **Figure 4.2** shows typical autocorrelation curves of RhG110, eGFP and the FRET probe as a function of glycerol (0-900 g/L). According to the Stokes-Einstein model, the diffusion coefficient of a spherical molecule depends inversely on the viscosity of the surrounding medium. As shown in **Figure 2.5** the viscosity depends nonlinearly on the concentration of the

crowding agents. Therefore, the concentration and viscosity range allow us to use fluorescence spectroscopy methods to determine whether diffusion in crowded environments follows the Stokes-Einstein model.

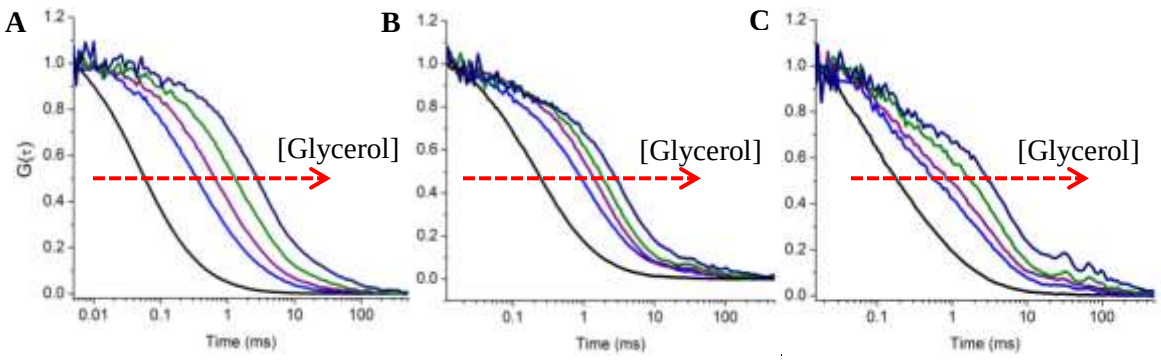

Figure 4.2: Normalized fluorescence fluctuation autocorrelation function of (**a**) RhG110, (**b**) eGFP and (**c**) the FRET probe described using a diffusion and intersystem crossing model. In these measurements, the concentration of glycerol ranged from 0-900 g/L (0-43 cP). As the concentration of glycerol increased, the translational diffusion time increased as well.

RhG110, eGFP and the FRET probe were all fit to a diffusion and intersystem crossing model as shown in **Equation 4.4**:

$$G(t) = \frac{1}{N} \times \left(\frac{1}{1+{}^{t}/_{\tau_D}}\right) \times \left(\frac{1}{\sqrt{1+{}^{t}/_{\left[\left(\frac{\omega_z}{\omega_{xy}}\right)^2 \tau_D\right]}}}\right) \times \left(1 + \frac{f_T}{1-f_T} \times e^{-{}^{t}/_{\tau_T}}\right) \tag{4.4}$$

Where $\left(\frac{1}{N}\right)$ is the number of molecules residing in the observation volume, (τ_D) is the diffusion time of a molecule crossing through the observation volume, $\left(\frac{\omega_z}{\omega_{xy}}\right)^2$ is the ratio of the axial-lateral extension to the observation volume, known as the structure parameter, (f_T) is the fraction of the molecular population undergoing intersystem crossing and finally (τ_T) is the triplet or blinking time associated with photophysical processes. This fitting function is able to satisfactorily describe the fluctuation autocorrelation of each of the three molecular probes over the viscosity range of 0-43 cP,

which corresponds to a concentration of 0-900 g/L of glycerol. The results show an apparent increase in the translational diffusion time of RhG110, eGFP and the FRET probe throughout the open observation volume as the glycerol concentration, and therefore the corresponding viscosity increases **(Table 4.2)**. From these results, we are able to use the translational diffusion coefficient and the corresponding viscosity to test the validity of the Stokes-Einstein model **(Equation 4.2; Figure 4.3)**.

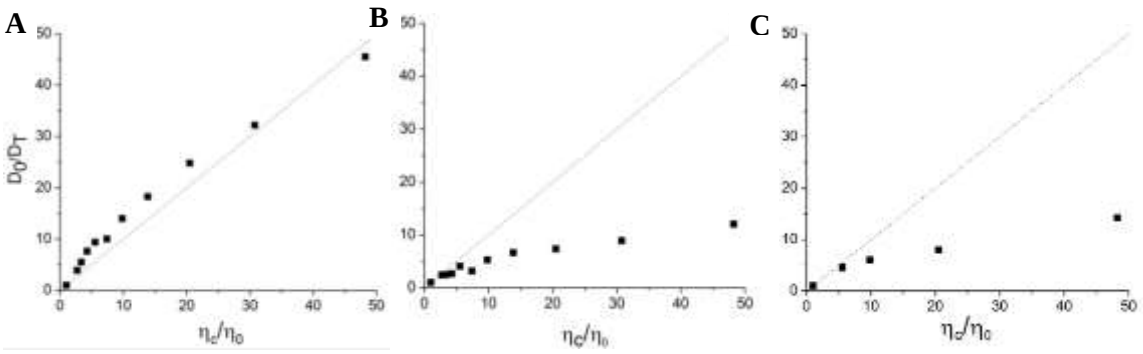

Figure 4.3: Diffusion coefficient analysis of (**a**) RhG110, (**b**) eGFP and (**c**) the FRET probe in varying concentrations of glycerol. The dashed line represents what the Stokes-Einstein model predicts. Deviations from the model allow us to elucidate how the crowding agent affects the translational diffusion of our molecules.

The comparison between the translational diffusion coefficient and highly viscous environments helps us test the limits of the Stokes-Einstein model using FCS methods. Our results indicate that RhG110 (**Figure 4.3a**) follows the predictions from the Stokes-Einstein model fairly closely. The slight positive deviation indicates that the molecule is diffusing slower than what is predicted by the Stokes-Einstein model. We attribute that deviation to "sticky" boundaries between RhG110 and the glycerol-enriched buffer; not slippery conditions as assumed by the Stokes-Einstein model. In contrast, eGFP (**Figure 4.3b**) and the FRET probe (**Figure 4.3c**), diffuse faster than what is predicted by the Stokes-Einstein model. This seems counterintuitive, as one would expect highly viscous environments would slow down the diffusion. Taking a closer look, we can see that as we increase the concentration past 480 g/L for eGFP, the negative deviation is more

dramatic. Using **Equation 4.1**, we can use the molecular weight of eGFP and the corresponding viscosity, to predict the diffusion coefficient in the Stokes-Einstein model (**Table 4.2**). As we increase the concentration of glycerol, the difference between experimental and calculated translational diffusion coefficients increases considerably. This data suggests that at higher concentrations of glycerol, eGFP is acting like a protein approximately one-sixth its size, which seems puzzling. However, it attests to the fact that the validity of the Stokes-Einstein model is limited in highly viscous environments for large molecules. We see similar trends with our FRET probe. After 480 g/L, we again see our molecule is diffusing faster than what the Stokes-Einstein model predicts. We can again use the molecular weight of the FRET probe and the corresponding viscosity to calculate the predicted translational diffusion coefficient in the Stokes-Einstein model (**Table 4.2**). As we increase the concentration of glycerol, the difference between experimental and calculated translational diffusion coefficients increases considerably. These results further put into question the validity of the Stokes-Einstein model in highly viscous environments. Previous studies have shown that the Stokes-Einstein model is valid up to 3.8 cP (or 410 g/L) in glycerol-rich solutions using NMR spectroscopy (*44, 71*). Our results here seem to complement these findings.

Alternatively, eGFP and the FRET probe undergo enhanced fluorescence blinking (*73*) and energy transfer efficiency in a viscous environment in the observation volume. Such enhancement of blinking and FRET switches the molecule from fluorescent or bright state to a dark state, which then appears as a faster diffusion time.

Finally, we can compare our results from the rotational diffusion of our probes discussed in **Chapter 3** of this thesis and see that, generally speaking, the translational and rotational diffusion of RhG110 and eGFP are in agreement with each other regarding the deviations observed using the Stokes-Einstein model.

Taken together, the validity of the Stokes-Einstein model seems to suffer when the size of the molecule and the viscosity of the environment increase. While, it is a fairly reasonable model for small molecules like RhG110; for both eGFP and the FRET probe it greatly underestimates both the hydrodynamic radius and molecular weight after

approximately 480 g/L. Generally speaking, the crowded interior of cells is estimated to be up to 400 g/L (or 4 cP), however, estimates of the plasma membrane in living cells can reach as high as 100 cP in viscosity (*76, 77*).

Table 4.2: The average number of molecules, translational diffusion time and experimental and calculated translational diffusion coefficients of RhG110, eGFP and the FRET probe as measured using FCS. The viscosity (η) is shown as measured with an Ubbelohde viscometer. These measurements were carried out in a glycerol-enriched buffer at room temperature using a 488-nm laser, 1.2NA objective (water immersion), and 50-mm confocal pinhole.

$\lambda_x - \lambda_{fl}$ (nm): Molecule	**N**	**τ_D (ms)**	**D_T (cm^2/s) Experimental**	**D_T (cm^2/s) Calculated**	**a_{FCS} (nm)**
488 – 530/40:					
RhG 110					
480 g/L	34.4	0.65	3.19×10^{-7}	7.60×10^{-7}	1.38
620 g/L	34.9	0.97	2.15×10^{-7}	4.30×10^{-7}	1.16
760 g/L	39.0	1.71	1.21×10^{-7}	2.07×10^{-7}	0.99
900 g/L	42.1	3.14	6.59×10^{-8}	8.77×10^{-8}	0.77
eGFP					
480 g/L	2.8	0.99	1.75×10^{-7}	1.92×10^{-7}	2.52
620 g/L	3.6	1.29	1.35×10^{-7}	1.09×10^{-7}	1.85
760 g/L	2.2	1.80	9.67×10^{-8}	5.23×10^{-8}	1.24
900 g/L	2.7	2.95	5.90×10^{-8}	2.22×10^{-8}	0.86
FRET Probe					
480 g/L	28.2	1.63	1.36×10^{-7}	1.54×10^{-7}	3.24
620 g/L	62.9	2.16	1.03×10^{-7}	8.69×10^{-8}	2.42
760 g/L	39.7	2.86	7.76×10^{-8}	4.18×10^{-8}	1.54
900 g/L	58.1	5.09	4.36×10^{-8}	1.77×10^{-8}	1.16

4.3 *Effects of heterogeneous viscosity on the translational diffusion of size-dependent probes:* Polymers and protein-crowded environments

Ficoll-70 crowded solutions

To assess the effects of heterogeneous viscosity on the translational diffusion of our three size-dependent probes, we used the synthetic polymer Ficoll-70 to create heterogeneously crowded environments. We can think of Ficoll-70 creating hard spheres (or excluded volumes), which can impede the diffusion of our molecules through the open observation volume fitted with obstacles. As mentioned in **Chapter 1** of this thesis, in heterogeneous environments, the molecule may experience weak or soft interactions, be confined in a cage-like environment made of excluded volumes represented by the crowding agents. Ficoll-70 enriched buffer will help us elucidate the translational diffusion mechanism of our probes in such crowded environments. We are also able to compare these results with our control experiments in glycerol-enriched buffer to differentiate between crowding and viscosity effects. It is important to note that buffer-like microenvironments exist among the crowding agents.

For these experiments, RhG110, eGFP and the FRET probe were tested in varying concentrations of Ficoll-70 enriched buffer at room temperature. The autocorrelation fluctuations for eGFP and the FRET probe were fit to the diffusion and intersystem crossing model as shown in **Equation 4.4**. RhG110 was fit to a two diffusing species model as seen in **Equation 4.5**:

$$G(\tau) = \frac{1}{N}\left[(1-f)\times\left(\frac{1}{1+{}^{t}/_{\tau_{D_1}}}\right)\times\left(\frac{1}{\sqrt{1+{}^{t}/_{S^2\tau_{D1}}}}\right) + f\times\left(\frac{1}{1+{}^{t}/_{\tau_{D_2}}}\right)\times\left(\frac{1}{\sqrt{1+{}^{t}/_{S^2\tau_{D_2}}}}\right)\right] \qquad (4.5)$$

In **Equation 4.5**, $\left(\frac{1}{N}\right)$ is the number of molecules residing in the observation volume, (τ_D) is the diffusion time of a molecule crossing through the observation volume, (S) is the structure parameter, $\left(\frac{\omega_z}{\omega_{xy}}\right)$ which is the ratio of the axial-lateral extension to the observation volume, (f) is the fraction of molecules associated with (τ_{D_2}) and $(1-f)$ is

the fraction of molecules associated with (τ_{D_1}). Representative autocorrelation functions for RhG110, eGFP and the FRET probe as a function of Ficoll-70 (0-320 g/L) are shown in **Figure 4.4**.

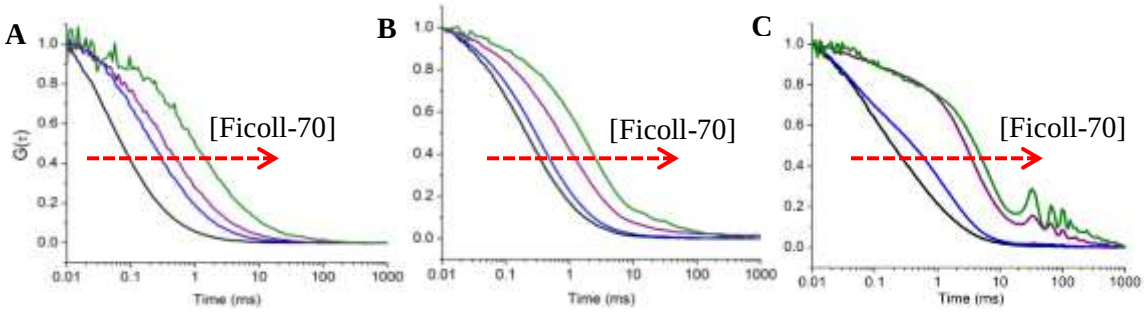

Figure 4.4: Normalized fluorescence fluctuation autocorrelation function of (**a**) RhG110, (**b**) eGFP and (**c**) the FRET probe described using a two diffusing species model. In these measurements, the concentration of Ficoll-70 ranged from 0-320 g/L. As the concentration of Ficoll-70 increased, the translational diffusion time increased as well.

The results show an apparent increase in the translational diffusion time of RhG110, eGFP and the FRET probe throughout the open observation volume as the Ficoll-70 concentration increased (**Table 4.3**). The autocorrelation curves for the FRET probe in Ficoll-70 concentrations of 200 and 300 g/L show very distinct fluctuations in the tail region (**Figure 4.4c**). These fluctuations can be attributed to a high concentration of molecules in the observation volume and are considered artifacts. From these results, we are able to use the translational diffusion coefficient and the corresponding viscosity to test the validity of the Stokes-Einstein model **(Equation 4.2; Figure 4.5)**.

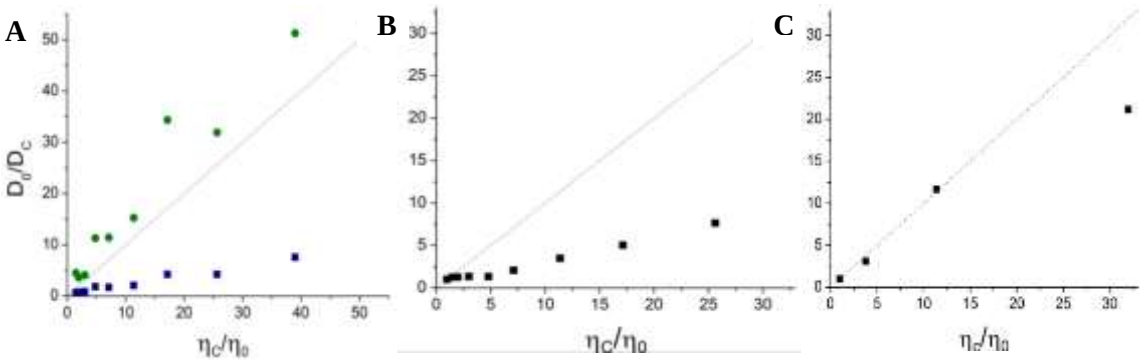

Figure 4.5: Diffusion coefficient analysis of (**a**) RhG110, (**b**) eGFP and (**c**) the FRET probe in varying concentrations of Ficoll-70. The dashed line represents what the Stokes-Einstein model predicts. For RhG110, (τ_{D_1}) (blue squares) and (τ_{D_2}) (green circles) are both shown. Deviations from the model allow us to elucidate how the crowding agent affects the translational diffusion of our molecules.

From our results for RhG110 (**Figure 4.5a**), we see a fast and slow component to the translational diffusion of RhG110 in Ficoll-70 enriched buffer. Looking first at (τ_{D_1}), which represents between 20-40% of the population of molecules and is deemed the fast component, we are able to attribute this to several factors. First, Ficoll-70, a 70 kDa polymer, can create an excluded volume, in which the much smaller RhG110 is likely to be able to diffuse as if it were in a buffer-like environment. This would give the impression that the molecule is diffusing much faster than what is predicted by the Stokes-Einstein model based on the bulk viscosity of this crowded environment. The diffusion times of RhG110, which correspond to(τ_{D_1}), are generally on the time scale of RhG110 in buffer, which is approximately 0.07 ms (**Table 4.3**). Secondly, RhG110 is known to undergo intersystem crossing to the triplet state (*78, 79*) and therefore this fast diffusion component could also be attributed to photophysical processes that are inherent in RhG110. Looking at (τ_{D_2}), which represents between 60-80% of the population, and can be described as the slow component, we attribute this to the overall diffusion of RhG110. Several factors could contribute to the slower than predicted diffusion time. As mentioned above, the size difference between RhG110 and Ficoll-70 is very large. If RhG110 and Ficoll-70 interact nonspecifically, the diffusion of RhG110 will slow considerably. This is likely the most plausible cause for the slower than predicted

diffusion of RhG110. It is important to note that while the translational diffusion is slowed considerably, it is not on the time scale of a diffusing 70 kDa molecule. Meaning, the diffusion seen is not the result of complex formation between RhG110 and Ficoll-70 [i.e., Ficoll$(RhG)_n$]. This further confirms the results of the rotational diffusion analysis of RhG110 seen in **Chapter 3**, where we observed a biexponential decay, but not on a time scale that could be associated with such a large molecule. It is also known that at concentrations greater than 100 g/L Ficoll-70 molecules collapse to form a mesh-like network of polymers (*71, 72*). This mesh-like environment would likely slow the translational diffusion of RhG110, as it would be more difficult to diffuse through. It might also cause the RhG110 molecules to aggregate, giving the impression of a larger molecule diffusing through the observation volume. Using **Equation 4.1** we can use the molecular weight and the calculated hydrodynamic radius to calculate the predicted translational diffusion coefficient (**Table 4.3**). We see in all cases, the model predicts a smaller diffusion coefficient and therefore slower diffusion time of RhG110. We can also use the Stokes-Einstein model and the experimental diffusion coefficient to determine the hydrodynamic radius and molecular weight of the molecule. For example, at 200 g/L, RhG110 has an experimental diffusion coefficient of 1.97×10^{-7} cm^2/s which translates to a hydrodynamic radius of 1.09 nm and a molecular weight of 3.5 kDa, as compared to the hydrodynamic radius in buffer of 0.58 nm and molecular mass of 507 Da. This information supports the fact that our molecule is interacting with the Ficoll-70 molecules in some fashion whether that be by nonspecific interactions or by RhG110 molecules clumping due to the mesh of Ficoll-70.

As we increase the size of our molecular probe to eGFP, we see the translational diffusion can now be described using a one diffusing species model with an exponential term (**Equation 4.4**). Based on our results from RhG110 in varying Ficoll concentrations, we would expect that the translational diffusion of eGFP would be slowed by the obstacles created by the Ficoll-70 molecules. However, our results indicate that eGFP is diffusing faster than what is predicted by the Stokes-Einstein model (**Figure 4.5b**). While it might seem counterintuitive to think of eGFP moving faster (and not slower) than predicted, this result is not entirely surprising. First, eGFP is approximately half the size

of Ficoll-70 molecules, meaning there are gaps in which eGFP can diffuse through as if it were in a buffer-like environment, leading to a faster diffusion time than anticipated. Secondly, eGFP is known to undergo blinking when exposed to laser intensity for a long period of time (*77, 80*). As mentioned above, Ficoll-70 can form a mesh-like environment at concentrations greater than 100 g/L (*71, 72*). This could result in eGFP essentially becoming entangled in the mesh created by the Ficoll-70 molecules. Once eGFP is essentially stuck in this mesh, it could undergo blinking or irreversible photobleaching, which would give the appearance as if the molecule had diffused faster through the observation volume. Third, GFP mutants which become immobilized and excited under 488 nm light can undergo repeated cycles of fluorescence emission also known as "blinking" (*73*). This blinking behavior is a switch from an anionic (or bright) state to a neutral (or dark) state. This blinking behavior gives the impression that eGFP molecules are diffusing in and out of the observation volume faster than they really are. As the concentration of Ficoll-70 increases however, the measured diffusion time of eGFP is slowed, which is expected. Comparing the results from the rotational diffusion of eGFP measured in **Chapter 3**, we see that a similar trend with negative deviation from the Stokes-Einstein model predictions. However, it appears as though the rotational diffusion is affected less by the increasing Ficoll concentrations and behaves as though it were in pure solvent (**Figure 3.7**).

Finally, looking at how the FRET probe behaves in Ficoll-70 concentrations, we would anticipate similar negative deviation from the Stokes-Einstein model as we observed with eGFP because the FRET probe is made of two GFP mutants that act as a donor and acceptor. However, we see that the FRET probe follows predications by the model closely with negative deviation only at the highest concentration of 300 g/L (**Figure 4.5c**). The size of the FRET probe compared to that of Ficoll-70 (64 kDa vs. 70 kDa) would be a factor at this point. The FRET probe is likely not able to diffuse through any gaps that might be created by the hard spheres of the Ficoll molecules, therefore we do not see the faster than predicted diffusion time we observed with RhG110 and eGFP, both of which are considerably smaller than Ficoll-70. Additionally, the structure of the FRET probe might be a factor in the translational diffusion of this molecule. Imagining

the two fluorescent molecules held together by a flexible linker, it might be plausible that they are acting independently from each other, which could slow the diffusion of the molecule. While we do not see a positive deviation from the Stokes-Einstein model that would indicate that the probe is moving slower than predicted, it is a factor to consider for this molecule. The negative deviation at 300 g/L is likely similar to what we observed with eGFP, as the CFP and YFP fluorescent molecules are mutants of wt GFP and can undergo enhanced blinking as observed in eGFP (*73, 81*).

Table 4.3: The average number of molecules, translational diffusion times and experimental and calculated translational diffusion coefficients of RhG110, eGFP and the FRET probe as measured using FCS. The diffusion coefficient for RhG110 was calculated using (τ_{D_2}). These measurements were carried out in a Ficol-70-enriched buffer at room temperature using a 488-nm laser, 1.2NA objective (water immersion), and 50-mm confocal pinhole.

$\lambda_x - \lambda_{fl}$ (nm): Molecule	**N**	**τ_{D1} (ms)**	**τ_{D2} (ms)**	**D_T (cm^2/s) Experimental**	**D_T (cm^2/s) Calculated**	**a_{FCS} (nm)**
488 – 530/40:						
RhG 110						
120 g/L	14.9	0.14	0.88	2.66×10^{-7}	8.81×10^{-7}	1.92
200 g/L	32.5	0.16	1.19	1.97×10^{-7}	3.72×10^{-7}	1.09
320 g/L	49.2	0.59	4.00	5.85×10^{-8}	1.08×10^{-7}	1.07
eGFP						
120 g/L	2.2	0.45	---	4.77×10^{-7}	2.23×10^{-7}	1.04
200 g/L	6.2	1.18	---	1.81×10^{-7}	9.41×10^{-8}	1.25
320 g/L	13.8	2.31	---	9.22×10^{-8}	2.75×10^{-8}	0.84
FRET Probe						
100 g/L	4.5	1.36	---	1.32×10^{-7}	2.26×10^{-7}	4.52
200 g/L	8.3	5.14	---	3.49×10^{-8}	7.51×10^{-8}	6.18
300 g/L	22.4	9.32	---	1.92×10^{-8}	2.67×10^{-8}	4.00

BSA crowded solutions

To assess the effects of heterogeneous viscosity on translational diffusion, we used the globular protein BSA to create heterogeneously crowded environments. Using a protein as a crowding agent allows us to elucidate if there is any interaction or binding events that occur between the fluorophore and crowding agent. This would be reflected in translational diffusion times which are slower than predicted for a molecule of a certain size. We are also able to compare these results with our control experiments in glycerol-enriched buffer to differentiate between crowding and viscosity affects. It is important to note that buffer-like microenvironments exist among the crowding agents.

For these experiments, RhG110 was tested in varying concentrations of BSA-enriched buffer at room temperature. The autocorrelation fluctuation of RhG110 was fit to a two diffusing species model as seen in **Equation 4.5**. Representative autocorrelation functions for RhG110 as a function of BSA (0-270 g/L) are shown in **Figure 4.6**.

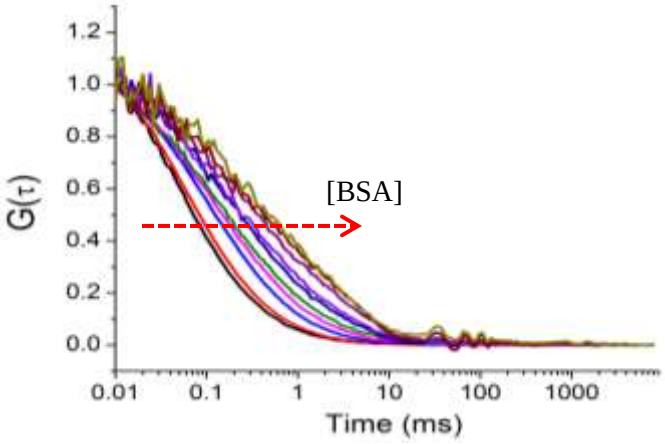

Figure 4.6: Normalized fluorescence fluctuation autocorrelation function of RhG110 described using a two diffusing species model. In these measurements, the concentration of BSA ranged from 0-270 g/L. As the concentration of BSA increased, the translational diffusion time increased as well.

The results show an apparent increase in the translational diffusion time of RhG110, throughout the open observation volume as the BSA concentration increased (**Table 4.4**). The autocorrelation curves at BSA concentrations of 240 and 270 g/L show fluctuations in the tail region (**Figure 4.6**), which can be attributed to a high concentration of

molecules in the observation volume. From these results, we are able to use the translational diffusion coefficient and the corresponding viscosity to test the validity of the Stokes-Einstein model **(Equation 4.2; Figure 4.7)**.

Table 4.4: The average number of molecules, translational diffusion times and experimental and calculated translational diffusion coefficients for RhG110 as measured using FCS. The diffusion coefficient for RhG110 was calculated using (τ_{D_2}). These measurements were carried out in BSA-enriched buffer at room temperature using a 488-nm laser, 1.2NA objective (water immersion), and 50-mm confocal pinhole.

$\lambda_x - \lambda_{fl}$ (nm): Molecule	N	τ_{D1} (ms)	τ_{D2} (ms)	D_T (cm^2/s) Experimental	D_T (cm^2/s) Calculated	a_{FCS} (nm)
488 – 530/40: RhG 110						
60 g/L	7.9	0.017	0.169	1.15×10^{-6}	2.46×10^{-6}	1.22
120 g/L	30.8	0.038	0.413	4.72×10^{-7}	1.51×10^{-6}	1.86
210 g/L	98.9	0.097	1.35	1.44×10^{-7}	6.25×10^{-7}	2.52
270 g/L	122.4	0.207	1.95	1.00×10^{-7}	2.85×10^{-7}	1.79

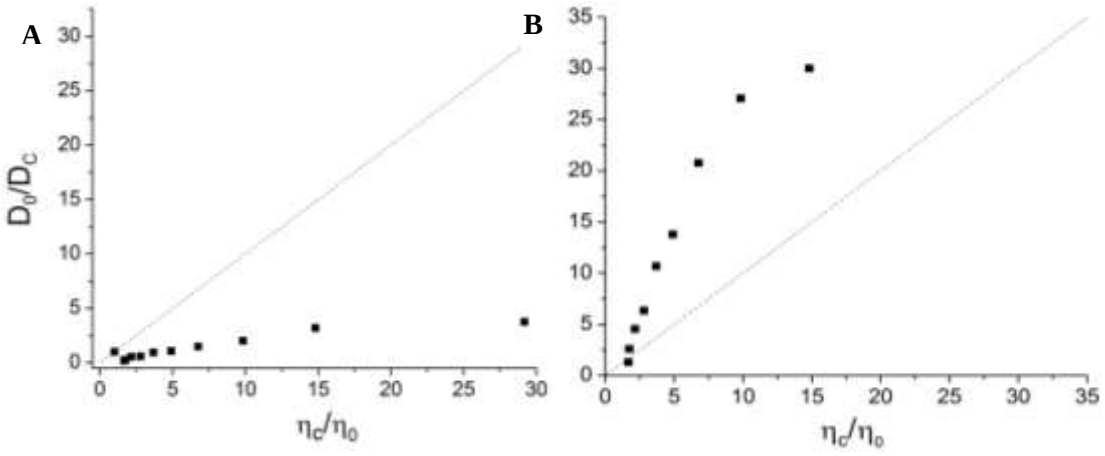

Figure 4.7: Diffusion coefficient analysis of RhG110 in varying concentrations of BSA. The dashed line represents what the Stokes-Einstein model predicts. (**a**) Represents (τ_{D_1}) and (**b**) represents (τ_{D_2}). Deviations from the model allow us to elucidate how the crowding agent affects the translational diffusion of our molecules.

From our results for RhG110 (**Figure 4.7**), we see a fast and slow component to the translational diffusion of RhG110 in BSA-enriched buffer. The fast component, (τ_{D_1}), is too fast to be assigned to the diffusion of RhG110, as RhG110 in pure buffer has a translational diffusion time of ~0.07 ms. In this case, we attribute this fast component to photophysical processes, as RhG110 is known to undergo intersystem crossing to the triplet state (*78, 79*). Looking at (τ_{D_2}), which can be described as the slow component, we attribute this to the overall diffusion of RhG110 in BSA-enriched buffer. The diffusion is much slower than predicted by the Stokes-Einstein model and is likely the result of nonspecific and electrostatic interactions between RhG110 and BSA. It is important to mention that, while the diffusion is slowed significantly, it is not on the time scale that diffusion of a ~66 kDa protein would experience and therefore is not the result of complex formation between RhG and BSA [i.e., $BSA(RhG)_n$]. This result is further confirmed by our rotational diffusion analysis of RhG110 in BSA seen in **Chapter 3**. We observed a biexponential decay of RhG110 over the range of BSA concentrations, yet the rotational diffusion was not slowed to the point where it could be said that a complex was forming between the fluorophore and crowding agent.

4.4 *Conclusions*

In summary, we used fluorescence correlation spectroscopy (FCS) to investigate the effects of macromolecular crowding on the translational diffusion of three size-dependent probes. We did control experiments in PBS buffer and glycerol-enriched buffer in order to examine the effects of homogeneous viscosity on translational diffusion. We then mimicked heterogeneously crowded environments with varying concentrations of Ficoll-70, a synthetic polymer, and compared those results with the glycerol-enriched buffer in order to differentiate between viscosity and crowding effects. We saw in all environments, an apparent increase in the translational diffusion time of our probes as we increased the concentration of our crowding agents, thereby increasing the viscosity. Using the Stokes-Einstein model, we compared the ratio of the diffusion coefficient in

buffer to that in a crowded environment $\left({}^{D_0}/_{D_c}\right)$ with the ratio of the viscosity of the crowded environment to that of the buffer $\left({}^{\eta_c}/_{\eta_0}\right)$ to test the limits of the model. Generally speaking, RhG110 followed predictions fairly closely in both glycerol-enriched and Ficoll-enriched buffers. Interestingly, both eGFP and the FRET probe showed negative deviation from the model in glycerol-enriched buffer after approximately 480 g/L concentration (4.9 cP). This is consistent with previous studies using NMR, in which the validity of the model held to a viscosity of 3.8 cP (*44, 71*).

In Ficoll-70 environments, eGFP was shown to have negative deviation from predictions, thereby diffusing faster than anticipated by the model. This was explained by four theories: (*i*) an excluded volume effect of Ficoll molecules creating gaps in which eGFP diffuses as if in a buffer, (*ii*) the mesh-like environment of high concentration of Ficoll-70 essentially trapping molecules leading to, (*iii*) irreversible photobleaching of eGFP and (*iv*) blinking of eGFP molecules switching from bright to dark states thereby giving the appearance of molecules diffusing into and out of the observation volume. Our results from the FRET probe in Ficoll-70 enriched buffer indicate that the Stokes-Einstein model is fairly sufficient at describing the diffusion of our probe. A negative deviation is observed at the highest concentration of Ficoll-70, but we attribute this to enhanced blinking, as YFP is a mutant of wt GFP.

Additionally, the translational diffusion of RhG110 was measured in varying concentrations of the protein crowding agent, BSA. RhG110 was fit to a two diffusing species model, with a fast and slow component. These results complement rotational diffusion analysis discussed in **Chapter 3**.

4.5 *Implications and future directions*

The results challenge the validity of the Stokes-Einstein model in highly heterogeneously viscous environments. The estimations of the hydrodynamics of the molecules cause the greatest discrepancy between what the model predicts and what is experimentally observed. As stated previously, calculations for the hydrodynamic radius of a molecule only offer the minimum that could contain a given mass and assume a smooth, spherical

shape. Underrepresentation of the radius of the molecule then affects the calculated translational diffusion coefficient causing deviations from the model. Unfortunately there is no model to describe molecules of differing shapes like the FRET probe in crowded environments.

To further investigate the effects that crowding has on size dependent probes, experiments using different crowding agents would be beneficial. We attempted to use BSA and ovalbumin in our studies, but had inconsistent results with eGFP and the FRET probe due to background signal caused by BSA and ovalbumin. It is unclear as to what caused this result to occur, so investigating this further would be of interest. It has been reported that diffusion in protein-enriched buffers of BSA causes a positive deviation from the Stokes-Einstein model, indicating that there are likely nonspecific or electrostatic interactions between the fluorescent molecule and the protein crowder (*71*).

5. Chapter 5: Conclusions and future outlook

In the extensive work described in this thesis, we have looked at the effects that macromolecular crowding has on three size-dependent probes: RhG110 (507 Da), eGFP (32.7 kDa) and a FRET probe (64 kDa). We used laser-based fluorescence spectroscopy for both quantitative and noninvasive studies to elucidate how the diffusion mechanisms of our probes are affected by the various crowded environments. Our results allowed us to examine the effects of crowding as a function of concentration, length scale, homogeneous versus heterogeneous viscosity, size, and surface structure.

On the ps-ns time scale, we used time-resolved anisotropy to assess the rotational diffusion of RhG110 and eGFP. We used the corresponding ratio of the diffusion coefficient in buffer to that in a crowded environment $\left({}^{D_0}/_{D_c}\right)$ with the ratio of the viscosity of the crowded environment to that of the buffer $\left({}^{\eta_c}/_{\eta_0}\right)$ to test the limits of the Stokes-Einstein model. We found as we increased the crowding, thereby increasing the viscosity, the model failed to describe the rotational diffusion of our probes. This is not entirely surprising for heterogeneously crowded environments, as the Stokes-Einstein model is based on the assumption of homogeneous bulk viscosity. The deviation from the model, however, allowed us to elucidate how crowding affects the rotational diffusion mechanism of our probes. These experimental approaches are promising for use to distinguish between the longer-range and shorter-range effects of crowding on a tracer. In the future, these measurements will be useful towards understanding the rotational diffusion of biomolecules in living cells that are aimed at quantitative analysis of association reactions and conformational changes using similar techniques.

At the single-molecule level, fluorescence fluctuation analysis using FCS allowed us to assess the translational diffusion of RhG110 and eGFP on longer time scales than those measured using time-resolved anisotropy. Again we used the corresponding ratio of the diffusion coefficient in buffer to that in a crowded environment $\left({}^{D_0}/_{D_c}\right)$ with the ratio of the viscosity of the crowded environment to that of the buffer $\left({}^{\eta_c}/_{\eta_0}\right)$ to test the limits of

the Stokes-Einstein model. Our results from time-resolved anisotropy studies served as a model for understanding the diffusion mechanism of these probes on this longer time scale. The ability to compare rotational and translational diffusion under the same experimental conditions is an extremely valuable tool, as it gives us a more complete picture of the effects of crowding on our molecules of interest.

We are the first group to investigate the excited-state dynamics of the FRET sensor used in this study. On the nanosecond time scale, time-resolved anisotropy indicated a fast rotational decay component that we attributed to energy transfer in the FRET probe. Importantly, these fast rotational dynamics indicate that both the donor and acceptor in the FRET probe undergo segmental mobility that is faster that the overall rotation of a 64 kDa probe. Both the efficiency and rate constant of energy transfer of this FRET probe determined by the lifetime measurements seem in a general agreement with that determined by the anisotropy measurements. At the single-molecule level, fluorescence fluctuation analysis using FCS seems to support our ensemble findings on the nanosecond timescale concerning the flexible, extended structure of the FRET probe. In addition to translational diffusion, energy transfer in the FRET probe provides an additional mechanism for enhancing fluorescence blinking, which is known to occur in a wide range of GFP mutants. Taken together, our results provide complementary information for this genetically encoded FRET probe to make accessible to fluorescence lifetime and polarization imaging microscopy towards the ultimate site-specific crowding studies in living cells.

This project has great implications for future studies. In regards to the work done with RhG110 and eGFP, investigating the rotational and translational diffusion using different crowding scenarios would help to further understand the role that crowding has on the diffusion mechanism of proteins. The intracellular environment is extremely complex; therefore it would be interesting to attempt to mix heterogeneous crowding agents with a viscosity agent like glycerol to try to create an environment that might more closely mimic the interior of a cell.

The greatest potential for this project surrounds work with the FRET probe. The construct described here is the parent FRET sensor (GE) in a group of five different derivatives of which have altered linker regions (**Figure 5.1**).

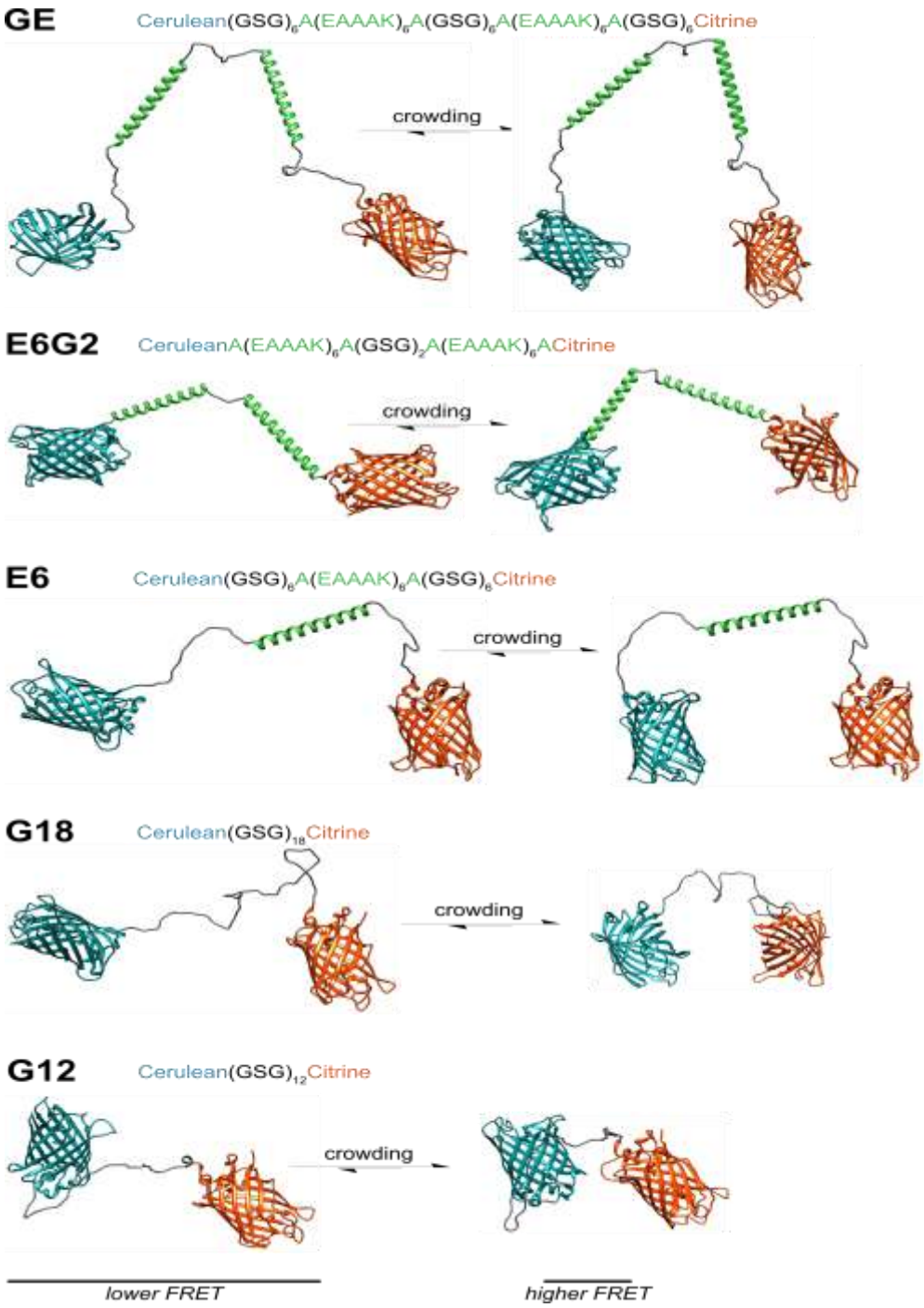

Figure 5.1: The five variations of the FRET sensor with altered linker regions.

Characterization of these new constructs will provide valuable information on the effects of the linker region as it relates to the energy transfer efficiency of the FRET pair. We need to investigate how macromolecular crowding might influence the multiscale molecular dynamics of the other derivatives of FRET probe as well. Characterizing the different derivatives will allow us to determine which of the five sensors has the greatest potential for energy transfer for future use *in vivo*. The ultimate goal with the FRET sensor project is to genetically encode our sensor to allow for a greater understanding of the multidimensional nature of crowding effects on cellular process.

References

(1) Currie, M., Thao, C., Timerman, R., Welty, R., Berry, B., Sheets, E.D., and Heikal, A.A. (2015) Multiscale diffusion of a molecular probe in a crowded environment: a concept. pp. 95840E-95840E-95816.

(2) Currie, M., Leopold, H., Schwarz, J., Boersma, A.J., Sheets, E.D., and Heikal, A.A. (2017) Fluorescence dynamics of a FRET probe designed for crowding studies. *Journal of Physical Chemistry (B)*.

(3) Ellis, R.J. (2001) Macromolecular crowding: obvious but underappreciated. *Trends in Biochemical Sciences*. **26**, 597-604

(4) Ellis, R.J., and Minton, A.P. (2003) Cell biology: Join the crowd. *Nature*. **425**, 27-28

(5) Minton, A.P. (2005) Influence of macromolecular crowding upon the stability and state of association of proteins: Predictions and observations. *Journal of Pharmaceutical Sciences*. **94**, 1668-1675

(6) Tokuriki, N., Kinjo, M., Negi, S., Hoshino, M., Goto, Y., Urabe, I., and Yomo, T. (2004) Protein folding by the effects of macromolecular crowding. *Protein Science : A Publication of the Protein Society*. **13**, 125-133

(7) Dauty, E., and Verkman, A.S. (2004) Molecular crowding reduces to a similar extent the diffusion of small solutes and macromolecules: measurement by fluorescence correlation spectroscopy. *Journal of Molecular Recognition : JMR*. **17**, 441-447

(8) Dix, J.A., and Verkman, A.S. (2008) Crowding effects on diffusion in solutions and cells. *Annual Review of Biophysics*. **37**, 247-263

(9) Minton, A.P. (1992) Confinement as a determinant of macromolecular structure and reactivity. *Biophysical Journal*. **63**, 1090-1100

(10) Minton, A.P. (2001) The influence of macromolecular crowding and macromolecular confinement on biochemical reactions in physiological media. *The Journal of Biological Chemistry*. **276**, 10577-10580

(11) Minton, A.P., Zhou, X.H., and Rivas, G. (2008) Macromolecular crowding and confinement: biochemical, biophysical, and potential physiological consequences. *Annu. Rev. Biophys.* **37**, 375-397

(12) Zhou, H.X. (2013) Influence of crowded cellular environments on protein folding, binding, and oligomerization: biological consequences and potentials of atomistic modeling. *FEBS Lett.* **587**, 1053-1061

(13) Ellis, R.J. (2001) Macromolecular crowding: an important but neglected aspect of the intracellular environment. *Curr. Opin. Struct. Biol.* **11**, 114-119

(14) Sharp, K.A. (2015) Analysis of the size dependence of macromolecular crowding shows that smaller is better. *Proc. Natl. Acad. Sci. USA.* **112**, 7990-7995

(15) Weiss, M. (2014) Crowding, diffusion, and biochemical reactions. *Int. Rev. Cell Molec. Biol.* **307**, 383-417

(16) Ferreira, L., Madeira, P.P., Breydo, L., Reichardt, C., Uversky, V.N., and Zaslavsky, B.Y. (2015) Role of solvent properties of aqueous media in macromolecular crowding effects. *J. Biomol. Struct. Dynam.*, 1-12

(17) Politou, A., and Temussi, P.A. (2015) Revisiting a dogma: the effect of volume exclusion in molecular crowding. *Curr. Opin. Struct. Biol.* **30**, 1-6

(18) Wang, Y., Benton, L.A., Singh, V., and Pielak, G.J. (2012) Disordered protein diffusion under crowded conditions. *The Journal of Physical Chemistry Letters*. **3**, 2703-2706

(19) Wang, Y., Sarkar, M., Smith, A.E., Krois, A.S., and Pielak, G.J. (2012) Macromolecular crowding and protein stability. *J. Am. Chem. Soc.* **134**, 16641-16618

(20) Breydo, L., Sales, A.E., Ferreira, L., Fedotoff, O., Shevelyova, M.P., Permyakov, S.E., Kroeck, K.G., Permyakov, E.A., Zaslavsky, B.Y., and Uversky, V.N. (2015) Effects of osmolytes on protein-solvent interactions in crowded environment: analyzing the effect of TMAO on proteins in crowded solutions. *Arch. Biochem. Biophys.* **570**, 66-74
(21) Strulson, C.A., Molden, R.C., Keating, C.D., and Bevilacqua, P.C. (2012) RNA catalysis through compartmentalization. *Nat. Chem.* **4**, 941-946
(22) Freedberg, D.I., and Selenko, P. (2014) Live cell NMR. *Annu. Rev. Biophys.* **43**, 171-192
(23) Smith, A.E., Zhou, Z., and Pielak, G.J. (2015) Hydrogen exchange of disordered proteins in Escherichia coli. *Protein Sci.* **doi: 10.1002/pro.2643**,
(24) Boersma, A.J., Zuhorn, I.S., and Poolman, B. (2015) A sensor for quantification of macromolecular crowding in living cells. *Nature Methods*. **12**, 227-229
(25) Gnutt, D., Gao, M., Brylski, O., Heyden, M., and Ebbinghaus, S. (2015) Excluded-volume effects in living cells. *Angew. Chem. Int. Ed.* **54**, 2548-2551
(26) Biswas, S., and Chowdhury, P.K. (2015) Unusual domain movement in a multidomain protein in the presence of macromolecular crowders. *Phys. Chem. Chem. Phys.* **17**, 19820-19833
(27) Lavalette, D., Tetreau, C., Tourbez, M., and Blouquit, Y. (1999) Microscopic viscosity and rotational diffusion of proteins in a macromolecular environment. *Biophysical Journal*. **76**, 2744-2751
(28) Zorrilla, S., Rivas, G., Acuna, A.U., and Lillo, M.P. (2004) Protein self-association in crowded protein solutions: a time-resolved fluorescence polarization study. *Protein Science : A Publication of the Protein Society*. **13**, 2960-2969
(29) Zorrilla, S., Rivas, G., and Lillo, M.P. (2004) Fluorescence anisotropy as a probe to study tracer proteins in crowded solutions. *Journal of Molecular Recognition : JMR*. **17**, 408-416
(30) Zorrilla, S., Hink, M.A., Visser, A.J.W.G., and Lillo, M.P. (2007) Translational and rotational motions of proteins in a protein crowded environment. *Biophysical Chemistry*. **125**, 298-305
(31) Ranjit, S., Lanzano, L., and Gratton, E. (2014) Mapping diffusion in a living cell via the phasor approach. *Biophys. J.* **107**, 2775-2785
(32) Davey, A.M., Krise, K.M., Sheets, E.D., and Heikal, A.A. (2008) Molecular perspective of antigen-mediated mast cell signaling. *J. Biol. Chem.* **283**, 7117-7127
(33) Forster, T. (1948) Intermolecular energy migration and fluorescence. *Ann. der Physik.* **2**, 55-75
(34) Lakowicz, J.R. (2006) *Principles of Fluorescence Spectroscopy*, New York: Springer
(35) Wu, P.G., and Brand, L. (1994) Resonance energy transfer: Methods and applications. *Analytical Biochemistry*. **218**, 1-13
(36) Biskup, C., Zimmer, T., Kelbauskas, L., Hoffmann, B., Klöcker, N., Becker, W., Bergmann, A., and Benndorf, K. (2007) Multi-dimensional fluorescence lifetime and FRET measurements. *Microscopy Research and Technique*. **70**, 442-451
(37) Hildebrandt, L.L., Preus, S., and Birkedal, V. (2015) Quantitative single molecule FRET efficiencies using TIRF microscopy. *Faraday Discussions*. **184**, 131-142
(38) Koushik, S.V., and Vogel, S.S. (2008) Energy migration alters the fluorescence lifetime of Cerulean: implications for fluorescence lifetime imaging Forster resonance energy transfer measurements. *BIOMEDO*. **13**, 031204-031204-031209
(39) Thaler, C., Koushik, S.V., Puhl, H.L., Blank, P.S., and Vogel, S.S. (2009) Structural rearrangement of CaMKIIα catalytic domains encodes activation. *Proceedings of the National Academy of Sciences*. **106**, 6369-6374

(40) Müller, S., Galliardt, H., Schneider, J., Barisas, B., and Seidel, T. (2013) Quantification of Förster resonance energy transfer by monitoring sensitized emission in living plant cells. *Frontiers in Plant Science*. **4**,
(41) Majoul, I., Straub, M., Duden, R., Hell, S.W., and Söling, H.-D. (2002) Fluorescence resonance energy transfer analysis of protein–protein interactions in single living cells by multifocal multiphoton microscopy. *Reviews in Molecular Biotechnology*. **82**, 267-277
(42) Jares-Erijman, E.A., and Jovin, T.M. (2003) FRET imaging. *Nat Biotech*. **21**, 1387-1395
(43) Day, R.N., Tao, W., and Dunn, K.W. (2016) A simple approach for measuring FRET in fluorescent biosensors using two-photon microscopy. *Nat. Protocols*. **11**, 2066-2080
(44) Heikal, A.A. (2014) Time-resolved fluorescence anisotropy and fluctuation correlation analysis of major histocompatibility complex class I proteins in fibroblast cells. *Methods*. **66**, 283-291
(45) Hess, S.T., Huang, S., Heikal, A.A., and Webb, W.W. (2002) Biological and chemical applications of fluorescence correlation spectroscopy: a review. *Biochemistry*. **41**, 697-705
(46) Müller, J.D., and Gratton, E. (2003) High-pressure fluorescence correlation spectroscopy. *Biophysical Journal*. **85**, 2711-2719
(47) Arpino, J.A.J., Rizkallah, P.J., and Jones, D.D. (2012) Crystal structure of enhanced green fluorescent protein to 1.35 Å resolution reveals alternative conformations for Glu222. *PLoS ONE*. **7**, e47132
(48) Royant, A., and Noirclerc-Savoye, M. (2011) Stabilizing role of glutamic acid 222 in the structure of enhanced green fluorescent protein. *Journal of Structural Biology*. **174**, 385-390
(49) Luby-Phelps, K. (2013) The physical chemistry of cytoplasm and its influence on cell function: an update. *Mol. Biol. Cell*. **24**, 2593-2596
(50) Mittal, S., Chowdan, R.K., and Singh, L.R. (2015) Macromolecular crowding: macromolecules friend or foe. *Biochim. Biophys. Acta*. **1850**, 1822-1831
(51) Stickler, S.J., and Berg, R.A. (1962) Relationship between absorption intensity and fluorescence lifetime of molecules. *J. Chem. Phys.* **37**, 814-822
(52) Yu, Q., Proia, M., and Heikal, A.A. (2008) Integrated biophotonics approach for noninvasive and multiscale studies of biomolecular and cellular biophysics. *J. Biomed. Optics*. **13**, 041315
(53) Kubin, R.F., and Fletcher, A.N. (1982) Fluorescence quantum yields of some rhodamine dyes. *Journal of Luminescence*. **27**, 455-462
(54) Heikal, A.A. (2011) A multiparametric fluorescence approach for biomembrane studies. in *Advances in Planar Lipid Bilayers and Liposomes* (Iglic, A., ed.)^eds.), pp. 169-197, Elsevier
(55) Schwille, P., Haupts, U., Maiti, S., and Webb, W.W. (1999) Molecular dynamics in living cells observed by fluorescence correlation spectroscopy with one- and two-photon excitation. *Biophysical Journal*. **77**, 2251-2265
(56) Heikal, A.A. (2010) Intracellular coenzymes as natural biomarkers for metabolic activities and mitochondrial anomalies. *Biomark Med*. **4**, 241-263
(57) Vishwasrao, H.D., Yu, Q., Hewawasam, K., and Heikal, A.A. (2014) Polarization imaging of cellular autofluorescence. in *Natural Biomarkers for Cellular Metabolism: Biology, Techniques, and Applications* (Ghukasyan, V., and Heikal, A.A., ed.)^eds.), Taylor & Francis
(58) Becker, W. (2005) *Advanced Time-Correlated Single-Photon Counting Techniques*: Springer

(59) O'Connor, D.V., and Phillips, D. (1984) *Time-Correlated Single Photon Counting*: Academic Press
(60) Davey, A.M., Walvick, R.P., Liu, Y., Heikal, A.A., and Sheets, E.D. (2007) Membrane order and molecular dynamics associated with IgE receptor cross-linking in mast cells. *Biophys. J.* **92**, 343-355
(61) Warren, S.C., Margineanu, A., Katan, M., Dunsby, C., and French, P.M.W. (2015) Homo-FRET based biosensors and their application to multiplexed imaging of signalling events in live cells. *International Journal of Molecular Sciences*. **16**, 14695-14716
(62) Einstein, A. (1905) The theory of the Brownian movement. *Ann. der Physik*. **17**, 549
(63) Debye, P.J.W. (1929) Polar Molecules. 172
(64) Hess, S.T., Sheets, E.D., Wagenknecht-Wiesner, A., and Heikal, A.A. (2003) Quantitative analysis of the fluorescence properties of intrinsically fluorescent proteins in living cells. *Biophysical Journal*. **85**, 2566-2580
(65) Erickson, H.P. (2009) Size and shape of protein molecules at the nanometer level determined by sedimentation, gel filtration, and electron microscopy. *Biological Procedures Online*. **11**, 32-51
(66) Heikal, A.A., Hess, S.T., and Webb, W.W. (2001) Multiphoton molecular spectroscopy and excited-state dynamics of enhanced green fluorescent protein (EGFP): acid–base specificity. *Chemical Physics*. **274**, 37-55
(67) Strickler, S.J., and Berg, R.A. (1962) Relationship between absorption intensity and fluorescence lifetime of molecules. *The Journal of Chemical Physics*. **37**, 814-822
(68) Suhling, K., Davis, D.M., and Phillips, D. (2002) The influence of solvent viscosity on the fluorescence decay and time-resolved anisotropy of green fluorescent protein. *Journal of Fluorescence*. **12**, 91-95
(69) Ormö, M., Cubitt, A.B., Kallio, K., Gross, L.A., Tsien, R.Y., and Remington, S.J. (1996) Crystal structure of the Aequorea victoria green fluorescent protein. *Science*. **273**, 1392-1395
(70) Li, C., Wang, Y., and Pielak, G.J. (2009) Translational and rotational diffusion of a small globular protein under crowded conditions. *The Journal of Physical Chemistry. B*. **113**, 13390-13392
(71) Wang, Y., Li, C., and Pielak, G.J. (2010) Effects of proteins on protein diffusion. *Journal of the American Chemical Society*. **132**, 9392-9397
(72) Rubinstein, M., and Colby, R.H. (2003) *Polymer Physics*, Oxford: Oxford University Press
(73) Dickson, R.M., Cubitt, A.B., Tsien, R.Y., and Moerner, W.E. (1997) On/off blinking and switching behaviour of single molecules of green fluorescent protein. *Nature*. **388**, 355-358
(74) Lavalette, D., Hink, M.A., Tourbez, M., Tétreau, C., and Visser, A.J. (2006) Proteins as micro viscosimeters: Brownian motion revisited. *Eur Biophys J*. **35**, 517-522
(75) Gendron, P.-O., Avaltroni, F., and Wilkinson, K.J. (2008) Diffusion coefficients of several rhodamine derivatives as determined by pulsed field gradient–nuclear magnetic resonance and fluorescence correlation spectroscopy. *Journal of Fluorescence*. **18**, 1093
(76) Marguet, D., Spiliotis, E.T., Pentcheva, T., Lebowitz, M., Schneck, J., and Edidin, M. (1999) Lateral diffusion of GFP-Tagged H2Ld molecules and of GFP-TAP1 reports on the assembly and retention of these molecules in the endoplasmic reticulum. *Immunity*. **11**, 231-240
(77) Swaminathan, R., Hoang, C.P., and Verkman, A.S. (1997) Photobleaching recovery and anisotropy decay of green fluorescent protein GFP-S65T in solution and cells:

cytoplasmic viscosity probed by green fluorescent protein translational and rotational diffusion. *Biophysical Journal*. **72**, 1900-1907

(78) Blom, H., Chmyrov, A., Hassler, K., Davis, L.M., and Widengren, J. (2009) Triplet-state investigations of fluorescent dyes at dielectric interfaces using total internal reflection fluorescence correlation spectroscopy. *The Journal of Physical Chemistry A*. **113**, 5554-5566

(79) Widengren, J., and Rigler, R. (1996) Mechanisms of photobleaching investigated by fluorescence correlation spectroscopy. *Bioimaging*. **4**, 149-157

(80) White, J., and Stelzer, E. (1999) Photobleaching GFP reveals protein dynamics inside live cells. *Trends in Cell Biology*. **9**, 61-65

(81) McAnaney, T.B., Zeng, W., Doe, C.F.E., Bhanji, N., Wakelin, S., Pearson, D.S., Abbyad, P., Shi, X., Boxer, S.G., and Bagshaw, C.R. (2005) Protonation, photobleaching, and photoactivation of yellow fluorescent protein (YFP 10C): A unifying mechanism. *Biochemistry*. **44**, 5510-5524

(82) Ma, J.K.H., Hadzija, B. (2013) *Basic Physical Pharamcy*, Burlington, MA: Jones & Bartlett Learning

(83) Sojoudi, A., Saha, S.C. (2012) Shear thinning and shear thickening non-Newtonian confined fluid flow over rotating cylinder. *American Journal of Fluid Dynamics*. **2**, 117-121

Appendix I: Bulk Viscosity and Refractive Index Measurements

According to the Stokes-Einstein model, the diffusion coefficient of a spherical molecule depends inversely on the viscosity of the surrounding medium. Here we independently measured the bulk viscosity of crowded solutions using an Ubbelohde viscometer. The results show that the viscosity depends nonlinearly on the concentration of the crowding agents (**Figure A1.1a**). In contrast with glycerol and protein crowding agents, the polymer Ficoll-70 exhibits a more pronounced effect on the bulk viscosity over the concentration range investigated here. The concentration and viscosity range investigated allows us to use fluorescence spectroscopy methods to determine whether diffusion in crowded environments follows the Stokes-Einstein model.

According to the Strickler-Berg equation, the radiative rate constant of a given fluorophore depends on the squared refractive index of the surrounding medium (*51*). The radiative rate constant is directly related to the fluorescence rate constant, or the inverse of the excited state fluorescence lifetime. Time-resolved fluorescence anisotropy is used to investigate the rotational diffusion on picosecond to nanosecond timescale, but this approach is limited to the excited state fluorescence lifetime. As a result, we measured the refractive index of the crowded solutions using an Abbe refractometer. Our results show that the refractive index of solution depends linearly on the concentration of glycerol, Ficoll-70, BSA and ovalbumin (**Figure A1.1b**). The results for all crowding agents and glycerol are shown in **Tables A1.1-A1.4**.

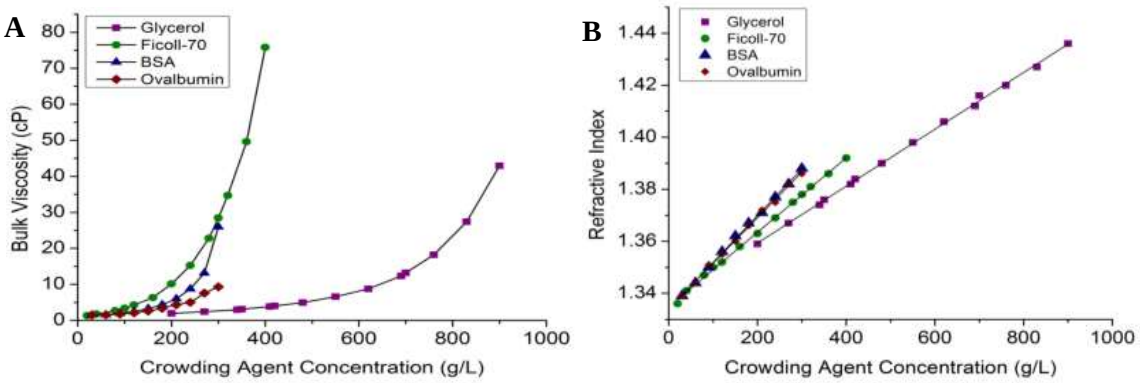

Figure A1.1: (**a**) The bulk viscosity, measured with Ubbelohde viscometers, depends nonlinearly on the concentration of the crowding agents. (**b**) The refractive index of crowded solution depends linearly on the concentration of the crowding agents as well as glycerol. These measurements were carried out using an Abbe refractometer.

Table A1.1: Viscosity and refractive index measurement for glycerol (200-900 g/L). 25 mL samples were prepared for viscosity measurements. The viscosity value is an average of three trials.

Glycerol Concentration (g/L)	Glycerol added (g)	PBS Buffer added (mL)	% Glycerol	Viscosity (cP)	Standard Deviation	Refractive Index
200	5.0	21.0	19.3	1.96	0.0053	1.359
270	6.75	19.7	25.6	2.42	0.038	1.367
340	8.5	18.2	31.8	2.98	0.050	1.374
350	8.75	18.1	32.7	3.12	0.016	1.376
410	10.25	16.9	37.8	3.81	0.022	1.382
420	10.5	16.7	38.7	4.04	0.028	1.384
480	12.0	15.5	43.7	4.95	0.015	1.390
550	13.75	10.9	49.4	6.59	0.019	1.398
620	15.5	12.7	55.0	8.75	0.022	1.406
690	17.25	11.3	60.4	12.33	0.106	1.412
700	17.5	11.1	61.2	13.19	0.041	1.416
760	19.0	9.9	65.7	18.24	0.095	1.420
830	20.75	8.5	70.9	27.40	0.044	1.427
900	22.5	7.1	76.0	42.93	0.273	1.436

Table A1.2: Viscosity and refractive index measurement for Ficoll-70 (20-400 g/L). 35 mL of a 400 g/L stock was prepared and then diluted to prepare 25 mL samples for viscosity measrements. The viscosity value is an average of three trials.

Ficoll-70 Concentration (g/L)	Ficoll-70 added (mL)	PBS Buffer added (mL)	% Ficoll-70	Viscosity (cP)	Standard Deviation	Refractive Index
20	1.25	23.75	7.2	1.34	0.0072	1.336
40	2.5	22.5	14.1	1.75	0.014	1.341
80	5.0	20.0	26.9	2.68	0.022	1.347
100	6.25	18.75	32.9	3.36	0.0029	1.350
120	7.5	17.5	38.7	4.27	0.023	1.352
160	10.0	15.0	49.6	6.33	0.042	1.358
200	12.5	12.5	59.6	10.12	0.164	1.363
240	15.0	10.0	68.9	15.27	0.093	1.369
280	17.5	7.5	77.5	22.81	0.105	1.375
300	18.75	6.25	81.6	28.47	0.130	1.378
320	20.0	5.0	85.5	34.70	0.115	1.381
360	22.5	2.5	93.0	49.60	0.248	1.386
400	25.0	0	100	75.80	0.346	1.392

Table A1.3: Viscosity and refractive index measurement for ovalbumin (30-300 g/L). 15 mL samples were prepared for viscosity measurements. The viscosity value is an average of three trials.

Ovalbumin Concentration (g/L)	Ovalbumin added (g)	PBS Buffer added (mL)	% Ovalbumin	Viscosity (cP)	Standard Deviation	Refractive Index
30	0.45	14.55	3.02	1.46	0.011	1.339
60	0.92	14.10	6.14	1.54	0.076	1.344
90	1.36	13.68	9.04	1.76	0.0053	1.351
120	1.82	13.25	12.05	2.10	0.0043	1.355
150	2.26	12.83	14.97	2.59	0.0077	1.360
180	2.70	12.43	17.85	3.39	0.013	1.366
210	3.15	12.03	20.78	4.34	0.0040	1.372
240	3.62	11.60	23.75	4.99	0.0056	1.375
270	4.06	11.24	26.53	7.56	0.020	1.382
300	4.51	10.83	29.39	9.33	0.042	1.386

Table A1.4: Viscosity and refractive index measurement for BSA (30-300 g/L). 15 mL samples were prepared for viscosity measurements. The viscosity value is an average of three trials.

BSA Concentration (g/L)	BSA added (g)	PBS Buffer added (mL)	% BSA	Viscosity (cP)	Standard Deviation	Refractive Index
30	0.45	14.54	3.07	1.49	0.0029	1.339
60	0.90	14.11	6.00	1.55	0.0030	1.344
90	1.35	13.68	9.04	1.92	0.0038	1.350
120	1.80	13.25	12.03	2.49	0.0082	1.356
150	2.25	12.83	14.96	3.28	0.028	1.362
180	2.70	12.41	17.99	4.36	0.0053	1.367
210	3.15	12.03	20.75	6.02	0.015	1.371
240	3.60	11.60	23.79	8.76	0.020	1.377
270	4.05	11.22	26.53	12.18	0.0059	1.382
300	4.5	10.81	29.51	25.97	0.014	1.388

Appendix II: Rheology Measurements of Viscosity

Bulk viscosity measurements are required for the Stokes-Einstein model for translational and rotational diffusion. The independent measurements of the bulk viscosity are used to model multi-scale diffusion of small probes in crowded environments. In addition to measurements conducted with viscometers (**Appendix I**), we also conducted bulk viscosity measurements using rheology techniques. By definition, rheology is the study of flow and deformation of matter and consists of three key parts: shear stress, shear rate and viscosity (*82*). Viscosity of a fluid depends on the shear rate, temperature, pressure, time and physical or chemical properties of the fluid.

The study of rheology involves an in-depth understanding of the properties of the fluid in which you are investigating. Fluids can be described as ideally viscous if they have irreversible deformation and flow. If the viscosity of the fluid is constant, it is considered a Newtonian fluid and can be described by the following equation (*82*):

$$\tau = \eta D \tag{A2.1}$$

Where (τ) is the shear stress, (D) is the shear rate and (η) is the proportionality constant called viscosity. However, most fluids do not follow ideal behavior and are therefore described as non-Newtonian fluids and are a combination of plastic, viscous and elastic properties. These fluids depend on the structure of the material and their viscosity will vary depending on shear rate or stress. Non-Newtonian fluids can undergo shear-thinning or shear-thickening depending on the structure of the material and will deviate from linearity (**Figure A2.1**) (*82, 83*).

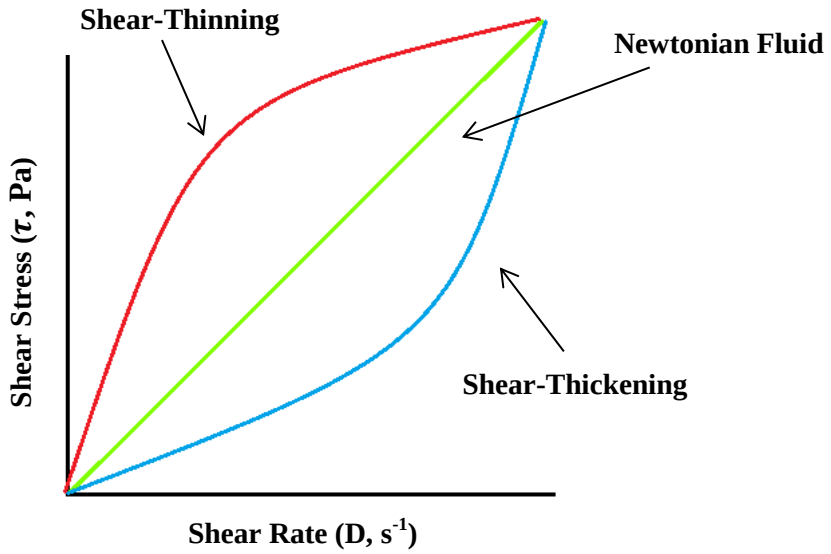

Figure A2.1: Newtonian fluids (green) have linear relationship between shear stress and shear rate. Non-Newtonian fluids can undergo shear-thinning (red) or shear-thickening (blue) based on the structure of the material.

These rheology measurements were carried out at the University of Minnesota, Twin Cities campus with the help of David Giles. The TA-AR G2 Rheology unit was used with both parallel plate and concentric cylinder geometry measurements. For parallel plate geometry, a 40 mm steel plate (987154) was used with a gap of 470 microns. The time constant was set at 6 seconds and the temperature was held constant at 23ºC. Samples of 0.6 mL of ovalbumin (30-300 g/L; **Table A2.1, Figure A2.2a**), BSA (30-300 g/L; **Table A2.2, Figure A2.2b**), Ficoll-70 (20-400 g/L; **Table A2.3, Figure A2.3**) and glycerol (270-900 g/L; **Table A2.4, Figure A2.4a**) were all measured using parallel plate geometry. For concentric cylinder geometry, a standard size conical cylinder (988221) was used with a gap set at 5000 microns. The time constant was set at 6 seconds and the temperature was held constant at 23ºC. 15 mL samples of glycerol (270-900 g/L; **Table A2.4, Figure A2.5b**) were measured using concentric cylinder geometry. By plotting the shear stress (Pa) vs. the shear rate (s^{-1}), we were able to independently measure the viscosity of our crowding agents. TA Rheology Advantage software was used for all data analysis.

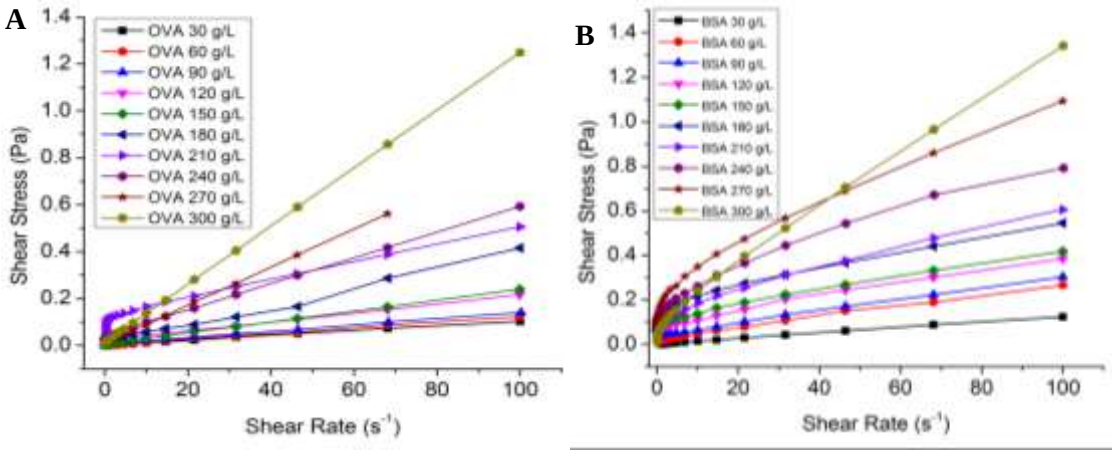

Figure A2.2: (**a**) The bulk viscosity of ovalbumin (30-300 g/L) measured with parallel plate geometry rheology. (**b**) The bulk viscosity of BSA (30-300 g/L) measured with parallel plate geometry rheology.

Table A2.1: Parallel plate geometry rheology measurements for ovalbumin (30-300 g/L). All trials were conducted a minimum of two times. Viscosity is shear stress (Pa) vs. shear rate (s^{-1}).

Ovalbumin Concentration (g/L)	**Viscosity (cP)**	**Standard Deviation**
30	1.06	0.00
60	1.18	0.063
90	1.54	0.024
120	2.28	0.43
150	2.34	0.086
180	3.46	0.46
210	6.31	0.56
240	6.64	0.81
270	8.59	0.44
300	13.38	1.05

Table A2.2: Parallel plate geometry rheology measurements for BSA (30-300 g/L). All trials were conducted a minimum of two times. Viscosity is shear stress (Pa) vs. shear rate (s^{-1}).

BSA Concentration (g/L)	Viscosity (cP)	Standard Deviation
30	1.75	0.81
60	3.07	0.28
90	3.56	0.24
120	4.61	0.11
150	5.09	0.060
180	6.99	0.26
210	6.42	0.65
240	9.64	0.21
270	12.26	1.10
300	14.71	0.13

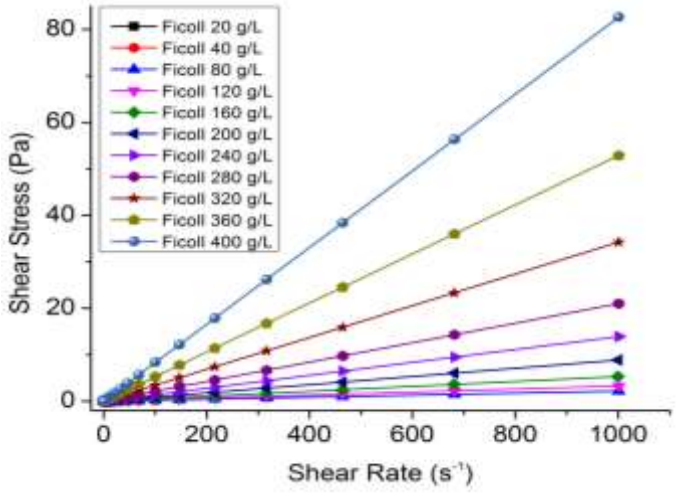

Figure A2.3: The bulk viscosity of Ficoll-70 (20-400 g/L) measured with parallel plate geometry rheology.

Table A2.3: Parallel plate geometry rheology measurements for Ficoll-70 (20-400 g/L). All trials were conducted a minimum of two times. Viscosity is shear stress (Pa) vs. shear rate (s^{-1}).

Ficoll-70 Concentration (g/L)	Viscosity (cP)	Standard Deviation
20	2.62	0.47
40	1.98	0.79
80	2.01	0.047
120	3.17	0.028
160	5.22	0.025
200	9.24	0.64
240	14.03	0.13
280	21.78	0.18
320	34.64	0.17
360	56.09	0.16
400	84.44	0.43

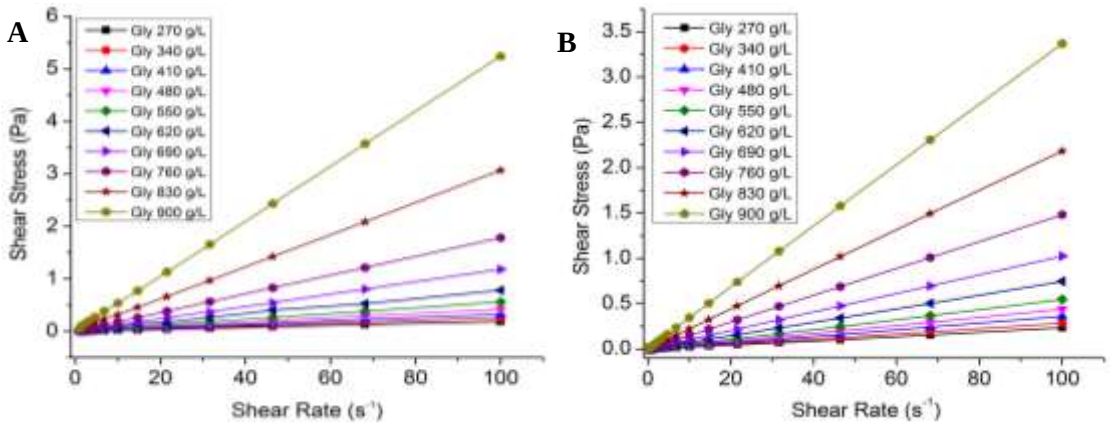

Figure A2.4: (**a**) The bulk viscosity of glycerol (270-900 g/L) measured with parallel plate geometry rheology. (**b**) The bulk viscosity, measured concentric cylinder geometry rheology for glycerol (270-900 g/L).

Table A2.4: Parallel plate geometry rheology measurements for glycerol (270-900 g/L). All trials were conducted a minimum of two times. Viscosity is shear stress (Pa) vs. shear rate (s^{-1}).

Glycerol Concentration (g/L)	Viscosity (cP)	Standard Deviation
270	1.86	0.067
340	2.52	0.011
410	3.22	0.014
480	4.17	0.005
550	5.62	0.012
620	7.94	0.062
690	11.81	0.000
760	17.86	0.000
830	30.68	0.000
900	52.43	0.042

Table A2.5: Concentric cylinder geometry rheology measurements for glycerol (270-900 g/L). All trials were conducted a minimum of two times. Viscosity is shear stress (Pa) vs. shear rate (s^{-1}).

Glycerol Concentration (g/L)	Viscosity (cP)	Standard Deviation
270	2.27	0.061
340	2.79	0.048
410	3.55	0.025
480	4.36	0.050
550	5.43	0.050
620	8.01	0.82
690	10.33	0.16
760	14.99	0.26
830	22.28	0.47
900	34.91	0.97